0 0 0 4 4 0 3 3 0

To be published as a Chapter in book
"Advances in Nuclear Physics,"
Erik Voight, Editor, Voight and
Berenger

LBL-4620 c.1

RADIATIVE PION CAPTURE IN NUCLEI

Helmut W. Baer, Kenneth M. Crowe, and Peter Truöl

November 1975

Prepared for the U. S. Energy Research and
Development Administration under Contract W-7405-ENG-48

For Reference

Not to be taken from this room

LAWRENCE BERKELEY LABORATORY
UNIVERSITY OF CALIFORNIA
BERKELEY

LBL-4620 c.1

DISCLAIMER

This document was prepared as an account of work sponsored by the United States Government. While this document is believed to contain correct information, neither the United States Government nor any agency thereof, nor the Regents of the University of California, nor any of their employees, makes any warranty, express or implied, or assumes any legal responsibility for the accuracy, completeness, or usefulness of any information, apparatus, product, or process disclosed, or represents that its use would not infringe privately owned rights. Reference herein to any specific commercial product, process, or service by its trade name, trademark, manufacturer, or otherwise, does not necessarily constitute or imply its endorsement, recommendation, or favoring by the United States Government or any agency thereof, or the Regents of the University of California. The views and opinions of authors expressed herein do not necessarily state or reflect those of the United States Government or any agency thereof or the Regents of the University of California.

0 0 0 0 4 4 0 8 5 5 1

RADIATIVE PION CAPTURE IN NUCLEI*

Helmut W. Baer
Department of Physics, Case Western Reserve University
Cleveland, Ohio

Kenneth M. Crowe
Department of Physics and Lawrence Berkeley Laboratory
University of California, Berkeley, California

Peter Truöl
Physik-Institut der Universität
Zürich, Switzerland

*This work was done under the auspices of the U. S. Energy Research and Development Administration.

0 0 0 0 4 4 0 8 5 5 2

TABLE OF CONTENTS

1. INTRODUCTION 1

2. EXPERIMENTAL METHODS 6

3. THE RADIATIVE BRANCHING RATIO AND RELATED PIONIC ATOM PHYSICS. . 13

4. THEORY OF PHOTOPRODUCTION OF PIONS NEAR THRESHOLD AND CALCULATION OF (π^-,γ) TRANSITION RATES 20

4.1 Impulse Approximation Hamiltonian 21

4.2 Radiative Capture on Protons 22

4.3 Calculation of 1s-Radiative Pion Capture in the "Elementary-Particle-Soft-Pion" Ansatz 29

5. RESULTS ON LIGHT NUCLEI, ISOTOPES OF HYDROGEN AND HELIUM . . . 33

5.1 Hydrogen. 33

5.2 Deuterium 34

5.3 Tritium 36

5.4 Helium-3 38

5.5 Helium-4 41

6. RESULTS ON 1p-SHELL NUCLEI 42

6.1 Overview of General Features 42

6.2 Pole Model for Quasi-Free Capture 44

6.3 $\pi^- + {}^6Li \rightarrow {}^6He(g.s.) + \gamma$ as Test Case of the Theory . . . 46

6.4 Analogs of Giant M1 States 51

6.5 Analogs of the Giant Dipole Resonance 55

7. RESULTS ON MEDIUM MASS AND HEAVY NUCLEI 63

7.1 ${}^{209}Bi(\pi^-,\gamma){}^{209}Pb$ and Observation of a New Collective State 64

8. CONCLUSIONS AND OUTLOOK 72

1. INTRODUCTION

The central question to be addressed in this article is: what can be learned about nuclear structure by stopping negatively charged pions in targets of nuclei from various regions of the periodic table and examining the emitted photon spectra between 50 and 150 MeV with a resolution of $\lesssim$ 2 MeV? The two processes which account for nearly all photons in this energy interval are radiative capture,

$$\pi^- + A_i \rightarrow A_f + \gamma \tag{1.1a}$$

$$\rightarrow (A-1)_f + n + \gamma \tag{1.1b}$$

$$\rightarrow (A-2)_f + n + n + \gamma \tag{1.1c}$$

$$\vdots$$

and charge exchange

$$\pi^- + A_i \rightarrow A_f + \pi^\circ \tag{1.2}$$

$$\hookrightarrow 2\gamma \ .$$

The latter has been observed only with hydrogen and ^{3}He targets. Measurements of the photon spectra from hydrogen and deuterium targets in the early 1950's helped determine basic properties of the pion, such as its mass, odd intrinsic parity, and the π-N coupling constant. In recent years targets ranging up to A = 209 have been studied and much of the interest has turned to the use of radiative pion capture as a probe of nuclear structure.

The study in 1965 by Davies, et al. (DMW 66) with a large NaI crystal

demonstrated that the branching ratios for reactions (1.1) for pions in bound atomic orbits of light and medium mass nuclei is 2-3%. A single measurement for heavy nuclei was performed by Petrukhin and Prokoshkin (PP65) who used a total absorption Čerenkov counter to detect "hard" γ-rays in coincidence with stopped pions in a target of natural lead. A branching ratio of 2.1±0.5% was measured. The observation of high energy photons from reactions (1.1) was strongly suggestive of a direct interaction of the π^- with a proton in the nucleus (rather than through formation of a compound nuclear state), with the fundamental process being $\pi^- + p \rightarrow n + \gamma$. Since photo production of pions on nucleons had been quite well studied, one had a reasonably good idea (BSW 51) about what transition operator to use in calculating transition rates in nuclei. Observing that the dominant term of the photo production operator near threshold, $A(\vec{\sigma}\cdot\hat{\varepsilon})\tau^+$, contains the nucleon spin, several authors (DE66, AE66, Mur+67) using the impulse approximation predicted strong and selective excitation of the spin-isospin components of the giant dipole resonance (GDR). For $T_z=0$ targets, such excitations are characterized by L=1, S=1, $J^\pi=0^-$, 1^-, 2^-, T=1 and $T_z=0,\pm1$ in the SU(4) classification of giant resonances (Wal 66). This prediction followed closely upon an early study of μ-capture by Foldy and Walecka (FW 64) who suggested that the excitation of spin-isospin states via the axial vector operator was necessary to account for total μ-capture rates. Particularly promising targets for both reactions were ^{12}C and ^{16}O, since electron scattering data and photo nuclear reaction studies indicated the presence of collective 1^- and 2^- states which could be interpreted as members of the SU(4) multiplet. Motivated by these predictions the group at Berkeley set up a high-resolution electron-positron pair spectrometer at the 184" cyclotron of the Lawrence Berkeley Laboratory and were able to observe (Bis + 70b) the predicted sharp lines in the $^{12}C(\pi^-,\gamma)^{12}B$ reaction (Fig. 1).

In the six years following, the field progressed considerably. Experimentally, high resolution photon spectra have been measured for nuclei ranging over the entire periodic table. These have revealed that there is selectivity to a second type of collective nuclear excitation—the giant magnetic dipole (M1) states which now have been clearly identified (Bae + 1975) with sharp lines in the (π^-,γ) photon spectrum of four 1p shell nuclei. The pionic x-ray data which play a crucial role in the comparison of theoretical transition rates to measured branching ratios have improved, especially for the test case of ^{6}Li. Theoretically, the importance of including momentum dependent terms in the effective interactions for p-state capture has been clarified. More realistic shell model wave functions are now being used. Also the validity of the impulse approximation and possible renormalizations of the elementary $\pi^- p \rightarrow n\gamma$ amplitude have been studied (DEF 75). These efforts, as will be seen, have shown radiative π^- capture to be a quantitative probe of nuclear structure.

In addition to nuclear structure investigations, the experimental π^- capture matrix elements are of interest in evaluating the theory which treats nuclei as elementary particles and low-energy pion reactions in the soft-pion limit ($m_\pi \rightarrow 0$). In this approach the impulse approximation is not made. Instead, one expresses various semi-leptonic and electromagnetic processes such as μ-capture, β-decay, electron and neutrino scattering, and radiative and charge-exchange π-capture in terms of invariant form factors of the vector and axial-vector weak hadronic currents of the nucleus taken as a single entity. By making use of the conserved vector current (CVC) and partially conserved axial vector current (PCAC) hypothesis, together with the soft pion limit, one can derive relationships (Sec. 4.3) between the rates for the various processes. For example, it is proved that radiative

π-capture from the 1s orbital is governed by the axial-vector form factor, also appearing in μ-capture and in allowed Gamow-Teller β-decay at lower momentum transfers. This type of study was initiated by Kim and Primokoff (KP 65) and has been advocated recently by numerous authors (a review is given by (ER 72)). At present only three transitions $^3He \rightarrow {}^3H$, $^6Li \rightarrow {}^6He$, and $^{14}N \rightarrow {}^{14}C$ have been studied in this manner and these will be discussed (Secs. 4, 6). Two facts have limited greater application of this approach to π-capture. In the interesting 1p shell nuclei, it appears that $\simeq$ 50% (A=5) to $\simeq$ 90% (A=16) of the captures occur from atomic p states. For these orbits the soft pion results do not obtain. Thus measured branching ratios cannot be compared directly to the theoretical 1s rates. Also, to predict accurate 1s rates, one needs good data on the other reactions involving the same states (or analogs) at similar momentum transfers ($\simeq$ 130 MeV/c). Only in a few cases have these been adequate.

Within the very recent past, both experimental (Deu + 74) and theoretical (e.g., KD 73, RE 73, SDU 74, Can + 74) studies of the inverse process—photo production of pions on nuclei with isolation of individual nuclear states—were initiated. The first experimental results were cross sections for the $^6Li(\gamma,\pi^+)^6He$(g.s.) reaction at 0.3 to 2 MeV above threshold. From these data and the lively theoretical interests (e.g., CLW 74, MPU 75), one can already appreciate the value of having data on the inverse reaction. Since radiative capture is from bound π^- atomic orbits and photoproduction results in an unbound π, an improved treatment of the strong interaction distortion of the pion wave function may result. Also, for the (γ,π) cross sections just above threshold the soft-pion results may apply directly. Although the data are still sparse, from the initial results of ^6Li, discussed in Sec. 6.3, it seems clear that in the future photoproduction will play an

important complementary role to radiative pion capture. One hopes that the two reactions taken together will provide an unusually precise evaluation of the theory on both points of nuclear structure and on the elementary-particle-soft-pion-treatment of low-energy π-nucleus interactions.

The organization of this article is as follows. In Sec. 2 we discuss the experimental methods for measuring the photon spectra, primarily with pair spectrometers, and the determination of the radiative branching ratio. The relationship between the measured branching ratios and theoretical absorption rates and the role of the pionic x-ray data is discussed in Sec. 3. In Sec. 4 we review the theory of the probe. Since calculations of transitions rates in complex nuclei are generally based on the nucleonic process $\pi N \rightleftarrows \gamma N$, the determination of the amplitudes of the latter from the data is discussed, and a numerical evaluation of the photoproduction multipoles near threshold is given. Such a discussion does not exist in the literature, and, in our view, is relevant to future, quantitative nuclear structure studies. In Sec. 5 the experimental results and interpretations for the hydrogen and helium isotopes are given. The nuclear structure aspects of this reaction are most clearly seen in the results on 1p shell nuclei which are reviewed in Sec. 6. In Sec. 7 we state the few results available on heavy nuclei and discuss the evidence for an interesting new collective excitation in ^{209}Bi. We conclude in Sec. 8 with a look towards new and exciting possibilities for the (π^-,γ) reaction at the meson physics facilities just coming into operation.

2. EXPERIMENTAL METHODS

The most direct investigation of radiative pion capture reactions is through detection of the primary photons. Transitions induced by pions at rest and producing two-body final states of a γ-ray and recoil nucleus give a sharp line in the γ-spectrum with an energy ($E\gamma$) uniquely related to the excitation energy (E_x) of the recoil nucleus,

$$E_\gamma = Q\ (1 - \frac{Q}{2M}) \qquad (2.1)$$

where $Q = M - (M_f + E_x)$, M_f is the ground state mass of the final state nucleus, and $M = M_i + m_\pi - B_\pi$ is the initial state mass consisting of the target nucleus mass (M_i) and the pion mass (m_π), less the pion atomic binding energy (B_π). Thus a precise measurement of the γ-ray energy identifies the final state of the recoil nucleus through its excitation energy. The spectroscopy of the outgoing photon has indeed been the most successful and informative experimental approach to date, although it is not easy to overcome the conflicting demands of high resolution and large acceptance required of the photon detector.

Other methods make use of nuclear transitions following π-capture: β- and γ-decay and neutron emission. In one case, $^3He(\pi^-,\gamma)^3H$,d,n, recoil nucleus spectroscopy was employed (Zai + 65). These methods have been reviewed previously (Tru 71). Since the quantitative information coming from such experiments which bears directly on radiative π-capture transition has been quite limited, they will not be discussed here. We mention only that there exists a large discrepancy in the radiative branching ratio for ^6Li and ^{12}C ground state transitions. Measurements of the induced β-activity differ by factors of 3.3 (Deu + 68) and 6.3 (Hil + 70), respectively, from

those done with a pair spectrometer (Sec. 6). Although this discrepancy has not been fully explained (see, e.g., discussion by Deutsch in (BC 73)), it is known that π-induced activation measurements are plagued by neutrons produced in the target or in the material used to degrade the incoming pion beam which can produce large backgrounds of the same activity via (n,p) reactions.

The detection of the high energy photon has been accomplished with NaI crystals, lead-glass Čerenkov counters, and electron-positron pair spectrometers. Since the energy resolution of total absorption Čerenkov counters is typically 35% (FWHM) at 130 MeV, they are not suitable for detailed γ-spectrum studies, but because of the large acceptance have been used in γ-n coincidence studies (Lam + 74). NaI crystals were used in measurements of the total radiative branching ratios by Davies et al. (DMW 66) and more recently by Bayer et al. (Bay + 75) in pion charge exchange experiments on the proton. Fig. 2b shows the photon spectrum for the 129.4 MeV line of the $\pi^- p \rightarrow n\gamma$ reaction as measured (Bay + 75) with a 27 cm diameter x 33 cm deep NaI crystal. The resolution is 6.3 MeV (FWHM) and its efficiency is 100%. This resolution is not adequate to resolve nuclear states in general, but quite satisfactory for study of the elementary interactions $\pi^- p \rightarrow \pi^0 n$, γn for pions at rest or in flight. Other possible applications of NaI detectors include measurement of the very weak $^{14}N(\pi^-,\gamma)^{14}C$(g.s.) transition (Bae + 75) which is separated by 6 MeV from the nearest line, and in coincidence measurements in which the 1s-capture contribution is separated from the total capture rate by requiring a coincidence with the $2p \rightarrow 1s$ pionic x-ray,

Pair-spectrometers have been employed in radiative capture work since the first observation of photons from the $\pi^- p \rightarrow n\gamma$ reaction by Panofsky et al. (PAH 51). Fig. 2a displays the resolution of this first spectrometer and

that of the improved version of Phillips and Crowe (PC 54). The latter was used to determine the pion mass and had a resolution of 2.3 MeV (FWHM). This is nearly the same as the 2 MeV of the Lawrence Berkeley Laboratory (LBL) instrument (Bis + 72, Bae + 73) used in the last six years for nuclear structure studies. The reason for this is not that 2 MeV represents an inherent lower limit on the resolution, but is in general a consequence of a compromise between improving resolution and reducing the already small acceptance. In fact, the spectrometer of Nicholson et al. (Nic+ 68) reached 0.6 MeV (FWHM) at 129.4 MeV (Fig. 1c) but with an acceptance an order of magnitude lower than the LBL spectrometer.

Pair Spectrometers. Most of the pair spectrometers employed in nuclear physics studies use a sufficiently high magnetic field (B) to bend the e^+-e^- pair through 180°. For a homogeneous field the separation distance (d) between the e^+-e^- trajectory is directly proportional to the photon energy

$$E_\gamma \text{ (MeV)} = 0.3 \text{ B (kG)} \frac{1}{2} \frac{d(\text{cm})}{\cos\theta \cos\phi} \qquad (2.2)$$

where θ and ϕ are the horizontal and vertical entrance angles with respect to the normal to the converter plane. Thus the 180° spectrometer is self-focusing in first order. The energy resolution depends on the spatial resolution of the e^+-e^- detection and on the ability to measure the entrance angles. The first requirement is easily met, e.g., B = 8 kG, d = 108 cm (E_γ = 130 MeV), and Δd = 1 cm gives $\Delta E_\gamma/E_\gamma$ = 1%. The second requirement has in the past been met by limiting the entrance angles and thus greatly sacrificing solid angle. In this mode, the uncertainties on the angle determination are due to the multiple scattering in the converter foil. If the magnetic

field is non-uniform, the dependence on the entrance angles is much more critical. Energy loss due to ionization and radiation in the converter is the other large contribution to the resolution. It increases, of course, with increasing converter thickness as does multiple scattering. One is limited to converter foils of about 1-3% radiation lengths if a resolution 1-2 MeV is desired. This limits the conversion probability to 0.7-2.3%.

The properties of the LBL spectrometer and the SIN spectrometer presently under construction (Tru + 71) are summarized in Table I. The LBL spectrometer and set-up at the 184" cyclotron are shown in Fig. 3. The spectrometer magnet consists of two 46 x 91 cm^2 C-magnets combined with a common pole tip to give an analyzing volume of 218 cm in length, 60 cm wide, with a 33 cm gap. The nominal field was 8 kG measured to an accuracy of ± .2%. The γ-rays were converted in a 3% radiation length fold foil (.010 cm) mounted on a styrofoam backing. The conversion probability is 2.3% and e^+/e^- momenta up to 110 MeV/c are bent through 180°. The field was chosen to yield maximum efficiency at E = 120 MeV. The directions of electron-positron pairs at entry and exit of the spectrometer were measured with two sets of detectors. In the first series of experiments, six arrays of four gap optical spark chambers were used. For the second series, three magnetostrictive readout wire spark chambers with four planes each were used. The wire spacing was 0.1 cm, and the wire angles relative to the horizontal midplane of the magnet were +12, -12, -12 and 0°. The 12° stereo view was employed to keep the magnetostrictive readout wires out of the high field region. This decreased the spatial resolution in the critical horizontal coordinate to ± 0.3 cm. A signal from two nonadjacent pairs of scintillation counters in coincidence with a stopped pion constituted the trigger. A typical percentage of good, analyzable pairs per trigger was 10-20%.

The majority of bad triggers were due to photon conversion in the lead wall with only one high-energy electron or positron track visible in the chamber (Bis + 72).

The acceptance and resolution of the spectrometer were calculated with a Monte Carlo code which incorporates the geometry of the spectrometer including the measured field map, calculates the pair-production cross-section, multiple scattering and energy loss in the converter and the wire chambers, and finally generates spark chamber wire addresses. The latter are processed through the same analysis codes as the real events, first through a pattern recognition program, then through the momentum determination routine based on a least-square interactive tracking method. The spectrometer acceptance (N_γ) as a function of photon energy and a hydrogen spectrum are shown in Fig. 4. For all of the LBL data runs, a liquid hydrogen target mounted on rails was used for checking the performance of the spectrometer. The $\pi^- p \rightarrow n\gamma$ line gives the resolution function employed in all the folding integrals for comparison of theory with experiment. The charge exchange reaction $\pi^- p \rightarrow \pi^\circ n$; $\pi^\circ \rightarrow 2\gamma$ provides a check on the acceptance between 55 and 83 via the Panofsky ratio.

Radiative Branching Ratio. This quantity represents the absolute normalization in a radiative capture experiment with stopped pions and requires a determination of the number of high energy photons produced per pion absorbed into the nucleus. The latter is equivalent to the number of pions coming to rest in the target, since in general nuclear absorption lifetimes ($\approx 10^{-12}$sec) are much shorter than the free pion mean lifetime (2.8×10^{-8}sec). The branching ratio can be defined for a single peak or the entire spectrum (total radiative branching ratio), and is related to the measured quantities

by the expression

$$R_\gamma = \frac{N_\gamma \cdot (1 - \ell) \cdot t \cdot e^{\mu x}}{\pi_{in} \cdot \varepsilon \cdot (1 - \delta) \cdot \eta(130)} \tag{2.3}$$

N_γ is the number of counts in the spectrum originating from captures in the target. (In measurements with the LBL spectrometer, the photon direction was reconstructed from the e^+-e^- trajectories, thereby permitting a cut of events originating outside the target.); ℓ represents the small fraction of counts resulting from radiative in-flight transitions; t is the unfolding factor which multiplies $N_\gamma(1 - \ell)$ to give the number of photons expected with a uniform spectrometer acceptance at the value $\eta(E_\gamma = 130 \text{ MeV})$. For a single peak, $t = \eta(130)/\eta(E_\gamma)$. For R_γ (total) it is determined by folding the pole-model distribution function (Sec. 6.2) with the spectrometer acceptance and line shape (Fig. 4) and comparing the result with the spectrum. The fraction of the photons with energies below 50 MeV, and thus not observed in the pair spectrometer, is 3-5% as given by the pole model; $e^{\mu x}$ corrects for the attenuation of photons in the target, scintillation counter, and spark chamber between the converter foil and origin. $\pi_{in} \cdot \varepsilon \cdot (1 - \delta)$ is the number of pionic atoms formed as determined from the telescope (π_{in}), the π-stopping fraction ε, and the small correction δ for nonradiative in-flight interactions in the target (estimated ~ 1%). The fraction ε of incident π's stopping in the target is determined from target in/out measurements. In this way π's stopping in the target walls as well as geometric and electronic inefficiencies are taken into account. As a check, ε can be calculated from the equivalent CH_2 stopping power of the targets and measured CH_2 range curves;

agreement to ± 10% with the in/out determination of ε was generally achieved.

Counting Rates. Typical counting rates for the LBL spectrometer and π^- channel were: $N_\gamma = (N_\pi/\text{sec}) \times (\eta_\gamma) \times (R_\gamma) = (10^5)(2\times10^{-5})(2\times10^{-2})$ = 144 events/hr. Targets of 2-5 g/cm^2 were used to achieve a π-stopping rates of 10^5/sec. Total branching ratios are typically 2% (Chap. 3). Significant increases in the singles counting rates and coincidence detection of x-rays and neutrons are expected in the near future at the meson factories. Some typical rates are given in Table II. From these one sees that some interesting coincidence experiments will be possible, e.g., the separation of the 1s and 2p state capture contributions in ^{6}Li. Also feasible will be the measurement of high resolution singles photon spectra with 10^5-10^6 events, compared to the typical 5×10^3 events of the Berkeley measurements.

3. THE RADIATIVE BRANCHING RATIO AND RELATED PIONIC ATOM PHYSICS

The total radiative branching ratios for the currently measured nuclei are listed in Table III. One sees that for $A > 3$, they are quite independent of nuclear mass and charge, varying from 1% (^{209}Bi) to 3.4% (^{6}Li). Charge exchange with stopped pions has been observed only in ^{1}H and ^{3}He, the only stable nuclei with $T_z < 0$ and thus the only possibilities for observing pure isospin flip in the (π^-,π°) reaction. In heavier nuclei ($A > 27$), the charge exchange reaction is generally Q-value allowed ($|Q| < 4.6$ MeV), but is greatly suppressed (Table III). The dominant capture orbitals are also given in the Table, and from these one can see that the average distance between the pion and proton when the interaction occurs does not vary greatly through the periodic table. For example, the Bohr radii ($r_B = 200\ n^2/Z$ F) and nuclear radii ($r_N = 1.3\ A^{1/3}$ F) are, respectively: for ^{3}He(1s), 100 and 2 F; for ^{40}Ca(3d), 90 and 4 F; for ^{209}Bi(4f), 60 and 8 F.

To relate the experimental branching ratios to theoretical radiative transition rates requires detailed knowledge of the pionic atom physics as deduced from the x-ray data. We discuss here only those aspects necessary to the quantitative comparison of measured branching ratios with theoretical (π^-,γ) transition rates. A comprehensive review of the field of pionic atom physics was given by Backenstoss (Bac 70) in which most of the currently existing data is tabulated and results of an optical model analysis of level widths and shifts are given. Discussions of the general features of pionic and muonic atoms may also be found in Refs. (Kim 71, AJ 74, DD 69). Descriptions of the initial formation and cascade are given by Leon and Seki (LS 74, LS 75). Molecular structure effects in the capture of pions in chemical compounds are reviewed by Gershtein and Ponomarev (GP 75). These effects will be important in future π-capture studies with enriched isotopes where the

use of chemical compounds is required; work discussed here was performed with targets of a single element.

The measured radiative branching ratio arises from a sum on the partial branching ratios over the active capture orbitals,

$$R_\gamma = \sum_{n\ell} \frac{\lambda_\gamma(n\ell)}{\lambda_a(n\ell)} \omega(n\ell) \tag{3.1}$$

The quantities $\lambda_\gamma(n\ell)$ [$\lambda_a(n\ell)$] are the radiative [total] absorption transition rates for capture from atomic orbitals $n\ell$. The $\omega(n\ell)$ are the probability per π-atom formed for absorption from orbitals $n\ell$. In general they are restricted by the condition $\sum_{n\ell} \omega(n\ell) = 1$ which expresses the fact that nuclear absorption lifetimes are much shorter than the free pion lifetime.+ The dominant capture probability can be deduced directly from the systematics (Bac 70) of pionic x-ray yields and widths; however, detailed cascade calculations (e.g., EK 61, LS 72) are required to get the complete $\omega(n\ell)$ distributions. In such calculations the populations $P(n\ell)$ for levels $n\ell$ (per π-atom formed) are obtained, and these are related to the capture probabilities by

$$\omega(n\ell) = P(n\ell) \frac{\lambda_a(n\ell)}{\lambda_a(n\ell) + \lambda^{em}(n\ell) + \lambda_A(n\ell)} \tag{3.2}$$

where $\lambda^{em}(n\ell)$ [$\lambda_A(n\ell)$] are the x-ray [Auger] transition rates for depopulating level $n\ell$. A complete specification of $\omega(n\ell)$ constitutes a capture schedule.

Capture schedules are not yet available for many nuclei; however, from those of ^{6}Li and ^{12}C (Table IV) the general trends for the light nuclei up to A ~ 20 can be seen. For these only s- and p- orbits contribute significantly, with 1s and 2p dominating. For heavier nuclei, it seems reasonable to expect a similar capture pattern of two ℓ-values, each with several n. The hydrogen isotopes (Table IV) are unique in π^- capture studies (LB 62).

+Decay of the π^- during the cascade in liquid ^{4}He has been observed (1.21± 0.8%, (BKS 65)) and is taken into account in the cascade calculations of (Bac + 74).

The π-H atom is neutral and so can pass freely through neighboring atoms where it experiences the strong electric field of protons. These perturb the pion cascade through Stark transitions among the n^2 states of a given n, forcing the π^- into s orbits with high n, from which capture then takes place. The specific capture schedule depends on the density of the target, which determines the average time between collisions. In Table IV, the capture schedules for a liquid hydrogen target are given. Similar capture schedules are expected (Leo 75) for liquid deuterium and tritium targets although the specific values of $\omega(ns)$ will differ somewhat due to the effect that different strong absorption rates $\lambda_a(ns)$ have on the branches in the cascade.

In addition to the $\omega(n\ell)$, the total absorption widths $\lambda_a(n\ell)$ must be extracted from the x-ray data to use Eq. (3.1) to test theoretical radiative rates. With present measurement techniques, at most two $\lambda_a(n\ell)$ can be obtained on any nucleus. One width can be measured directly with Ge and Si detectors from the broadening of the x-ray lines which terminate the cascade. The broadening of the $2p \rightarrow 1s$ line (K_α) is due entirely to the 1s strong absorption width

$$\Gamma(2p \rightarrow 1s) = \hbar\lambda_a(1s) = 6.58\text{x}10^{-16}\lambda_a(1s) \quad (\text{eV, sec}^{-1}) \qquad (3.3)$$

For increasing Z, the K series yield decreases, becoming undetectable at $Z \sim 11$. The L series ($nd \rightarrow 2p$) then terminates the cascade, and the directly measured ($12 \lesssim Z \lesssim 30$) broadening gives $\Lambda_a(2p)$. The electromagnetic contribution $\hbar\lambda^{em}(2p \rightarrow 1s)$ to the width of L series lines (0.1-10 eV) is negligibly small compared to the capture width (0.2-20 keV). Direct level width measurements have been made on M_α lines ($4f \rightarrow 3d$) for nuclei with $39 \leqslant Z \leqslant 59$, and on N_α lines ($5g \rightarrow 4f$) for nuclei with $73 \leqslant Z \leqslant 94$ (Bac 70).

The second capture width that can be obtained is that of the initial

level in the cascade-terminating-$K_\alpha, L_\alpha \ldots$, transition. These are comparable to the electromagnetic widths and therefore are too small to be measured directly. They can be determined by an indirect method (Bac 70) which relies on a cascade calculation for the initial level population and on one measured x-ray yield. For example, in a light nucleus these are related by

$$Y(2p \rightarrow 1s) = P(2p) \frac{\lambda^{em}(2p \rightarrow 1s)}{\lambda_a(2p) + \lambda^{em}(2p \rightarrow 1s) + \lambda_A(2p)} \tag{3.4}$$

Since electromagnetic rates can be calculated quite accurately, Eq. (3.4) can be used to obtain $\lambda_a(2p)$

$$\lambda_a(2p) = \lambda^{em}(2p \rightarrow 1s) \frac{P(2p) - Y(2p \rightarrow 1s)}{Y(2p \rightarrow 1s)} \tag{3.5}$$

(The Auger rate λ_A is much smaller than λ^{em} for the active capture orbitals and therefore has been dropped in Eq. (3.5).) The calculated $P(n\ell)$ can be checked in a few cases with direct measurements of yields for all x-rays feeding level $n\ell$. In general, however, a cascade calculation is required together with the measured $Y(2p \rightarrow 1s)$. At present, the latter are still quite uncertain, with some large discrepancies between the various groups (see, e.g., Sap + 72). Thus $\lambda_a(2p)$, as well as the $\lambda_a(3d)$, $\lambda_a(4f)$, and $\lambda_a(5g)$, when they are deduced from intensity measurements, generally are not precisely known. In many cases, optical potential values (e.g., KE 69, Bac 70, Sap 72), where the potential parameters have been determined by fits to large data sets of directly measured level widths, would appear to give more reliable values for use in Eq. (3.11).

Assuming that for a typical nucleus nearly all captures occur from orbits of two ℓ-values, Eq. (3.1) reduces to

$$R_\gamma = \sum_n \frac{\lambda_\gamma(n\ell)}{\lambda_a(n\ell)} \omega(n\ell) + \sum_n \frac{\lambda_\gamma(n,\ell+1)}{\lambda_\alpha(n,\ell+1)} \omega(n,\ell+1) \tag{3.6}$$

Since at most two $\lambda_a(n\ell)$ can be measured, and several $\omega(n\ell)$ for each ℓ are significantly greater than zero (Table IV), Eq. (3.6) can still not be used in a direct comparison with experiment. The crucial assumption made at this point is that $\lambda_\gamma(n\ell)/\lambda_a(n\ell)$ is independent of n for fixed ℓ. Most authors employ this approximation although little published work exists to demonstrate its validity, and some authors (RW 71) have questioned it for p-orbits. Its validity requires that the variations in *shape* inside the nucleus of the strongly distorted pion wave functions $\phi_{n\ell}$ for the different n involved in the captures are negligibly small. It would appear (Leo 75) that this approximation is quite good, since the variations in pion binding energy with n(10's of keV) are small compared to the real well depth of the pion potential (10's of MeV (KE 69)). The magnitudes of $\phi_{n\ell}$ through the nuclear volume do vary* with n, of course, but this scale factor drops out in the ratio. Thus each of the sums in Eq. (3.6) reduces to one term. For light nuclei, the quantity to be compared with experiment is

$$R_\gamma = \frac{\lambda_\gamma(1s)}{\lambda_\gamma(1s)}\,\omega_s + \frac{\lambda_\gamma(2p)}{\lambda_\gamma(2p)}\,\omega_p \tag{3.7}$$

where $\omega_s = \sum_n (ns)$ and $\omega_p = \sum_n (np) = 1 - \omega_s$. Having made these necessary and perhaps reasonably well justified approximations, interest focuses on the ratio

$$r = \frac{\omega_\ell + 1}{\omega_\ell} = \frac{1 - \omega_\ell}{\omega_\ell} \tag{3.8}$$

---

*If the variations of $\phi_{n\ell}$ with n follow hydrogenic wave functions, one has (LB 62) for s-orbits $|\phi_{ns}(0)|^2 = |\phi_{1s}(0)|^2/n^3$, giving $\lambda_a(ns) = \lambda_a(1s)/n^3$, and for p-orbits $|\vec{\nabla}\phi_{np}(0)|^2 = \frac{n^2-1}{n^5}\,|\vec{\nabla}\phi_{2p}(0)|^2$, giving $\lambda_a(np) = \frac{n^2-1}{n^5}\,\lambda_a(2p)$. The λ_a here can be any partial capture rate, or the total absorption rate.

to represent the capture schedule for any nucleus. Accurate determinations of r as a function of (Z,A) are important to all π-capture experiments where quantitative comparisons between experiment and theory are sought. (Equation (3.7) applies to any capture channel simply by replacing the $\lambda_\gamma(n\ell)$ with the corresponding partial capture rates). From Table IV, one gets for the p/s ratio $r(^1H) = 0$, $r(^4He) = 0.19$, $r(^6Li) = 1.5\pm0.4$, and $r(^{12}C) = 11.5 \pm 4.5$. The pionic x-ray data for light nuclei $4 \leqslant A \leqslant 16$ needed for use of Eq. (3.7) are given in Table V.

Also given in Table V are values for the distortion factors C_s and C_p which relate $\lambda_\gamma(1s)$ and $\lambda_\gamma(2p)$ calculated with hydrogenic wave functions to those calculated with strong interaction distortions included. Studies with optical potentials (e.g. KE 69) show that ϕ_{1s} and ϕ_{2p} deviate considerably from hydrogenic wave functions. For example (KE 69), in ^{16}O, $|\phi_{1s}(0)|^2$ is reduced to 0.3 of the hydrogenic value (due to the dominance of the repulsive πN s-wave interaction in s atomic orbits); for ^{40}Ca, $|\phi_{2p}|^2$ develops a small ripple at ~4 F, and its magnitude is larger than the hydrogenic wave function throughout the nucleus (due to the dominance of the attractive πN p-wave interaction in p atomic orbits). Although in principle the distorted wave finctions can be used directly in the radial integrals of λ_γ, the more frequently employed procedure is to take distortions into account by simple multiplicative factors defined relative to hydrogenic wave functions. Noting that for the latter $|r^{-\ell}\phi_{n\ell}|^2$ is slowly varying through the nuclear volume, and that in some cases the same is true of the distorted wave functions, the multiplicative factor

$$C(n\ell) = \frac{|\langle N'L'|\ r^{-\ell}\phi_{n\ell}\ \text{(optical pot.)}|NL\rangle|^2}{|\langle N'L'|\ r^{-\ell}\phi_{n\ell}\ \text{(hydrogenic)}\ |NL\rangle|^2} \tag{3.9}$$

is calculated (e.g., Del 70, SW 74) and used to scale the transition rates,

viz., λ_γ (optical pot.) = $C(n\ell)\lambda_\gamma$ (hydrogenic). In general, $C(n\ell)$ depend not only on the pion orbit $n\ell$, but on the initial (NL) and final (N'L') nucleon states. The approximations leading to Eq. (3.9) are best met when NL = N'L', and doubtful when broad regions of nuclear excitations (e.g., giant dipole resonance) are involved (Ver 75). For a limited range of excitation energy, and when N'L' = NL, the use of a single value of C(1s) and C(2p) for all transitions may be justified (SW 74, Ver 75). The values of Table V are for 1p shell nucleons in harmonic oscillator orbits and with $\phi_{n\ell}$ calculated with optical potentials similar to those of Krell and Ericson (KE 69). Values of C(5g) and C(4f) needed for ^{209}Bi may be found in Ref. (Bae+ 74).

4. THEORY OF PHOTOPRODUCTION OF PIONS NEAR THRESHOLD AND CALCULATION OF (π^-,γ) TRANSITION RATES

Two methods have been used in the theoretical treatment of nuclear radiative pion capture and its inverse, nuclear photoproduction of pions

$$\pi^- + A_i(Z,N) \rightleftharpoons A_f(Z-1,N) + \gamma \qquad (4.1)$$

The first method applies the impulse approximation (IA), using an effective Hamiltonian constructed from the on-shell nucleonic amplitude. The nuclear matrix elements for this Hamiltonian are obtained by a summation over all nucleons in the nucleus with a pion wave function distorted by the strong interaction. The second method, referred to in the literature as the elementary particle (EP) treatment, applies current algebra techniques to relate the nuclear matrix elements to the matrix elements of the nuclear weak axial current, appearing in processes like μ-capture and β-decay. For pion four-momenta equal to zero (soft pion limit) and with the hypothesis of partially conserved axial-vector current (PCAC), the radiative capture matrix elements are seen to be proportional to the weak interaction axial vector form factor.

In the use of the (π^-,γ) reaction as a general tool for nuclear structure studies, the IA must be employed to obtain a complete analysis of the experimental branching ratio. First, this is true since captures occur from p,d,f,...orbits for nuclei from ^{3}He to ^{209}Bi, the only pure s-state capture nuclei being the hydrogen isotopes. For orbits with $\ell > 0$, the soft pion results do not apply. Second, the initial and final nuclear state wave functions are most generally expressed in a shell model basis. The use of these together with the IA in calculations of the π-capture matrix elements ties this new process to the many other reactions, and the internal excitation spectrum of the nucleus, for which the shell model has provided the basic framework for analyses. In the EP treatment, the invariant form factors contain

both the nuclear structure and transition operator. Numerical values of the form factors can be obtained only if the necessary data on other reactions is available, and to date there are only a few cases where these are adequate.

4.1 IMPULSE APPROXIMATION HAMILTONIAN

The radiative capture rate for transitions from pionic orbits with quantum numbers n,ℓ and initial (final) nuclear states of angular momenta $J_iM_i(J_fM_f)$ may be written (e.g., MW 73) as

$$\Lambda_\gamma(n\ell\,;\ i\to f) = \frac{k}{m_\pi}\cdot\frac{1}{\left(1+\frac{k}{M_A}\right)}\cdot\frac{1}{(2J_i+1)(2\ell+1)}\cdot\int d\hat{k}\sum_{M_fM_im}|\langle J_fM_f|H_{eff}|J_iM_i\rangle|^2 \qquad (4.2)$$

$\vec{k}$ is the momentum of the emitted photon, m_π the pion mass, and M_A the target nucleus mass. The effective IA Hamiltonian is given by

$$H_{eff} = i\left(1+\frac{m_\pi}{m_n}\right)\sum_{j=1}^{A}\sum_{\lambda=\pm1} e^{-i\vec{k}\cdot\vec{r}_j}F_{j\lambda}\,\phi_{n\ell}^{m}(\vec{r}_j)\,\tau_j^+ \qquad (4.3)$$

where $\phi_{n\ell}^{m}$ is the pion wave function and τ^+ is the isospin ladder operator $\tau^+|p\rangle=|n\rangle$. The factor $\left(1+\frac{m_\pi}{m_n}\right)$, where m_n is the nucleon mass, results from the transformation of the pion-nucleon to the pion-nucleus center-of-mass system (c.m.). The elementary amplitude $F_{j\lambda}$ for the nucleonic process $\pi^-p\to n\gamma$ (Sec. 4.2) is

$$\begin{aligned}F_{j\lambda} = {} & A(\vec{\sigma}_j\cdot\hat{\varepsilon}_\lambda) + B(\vec{\sigma}_j\cdot\hat{\varepsilon}_\lambda)(\vec{q}\cdot\vec{k}) + C(\vec{\sigma}_j\cdot\vec{k})(\hat{\varepsilon}_\lambda\cdot\vec{q}) \\ & - iD\hat{\varepsilon}_\lambda\cdot(\vec{q}\times\vec{k}) + E(\vec{\sigma}_j\cdot\vec{q})(\vec{q}\cdot\hat{\varepsilon}_\lambda)\end{aligned} \qquad (4.4)$$

where $\vec{q}$ is the pion momentum in the πp c.m. system, $\vec{\sigma}_j$ the Pauli spin operator for the jth nucleon, and $\hat{\varepsilon}_\lambda = \frac{1}{\sqrt{2}}(-\lambda,-i,0)$ the photon helicity. In writing H_{eff} as in Eq. (4.3) it has been assumed that, (1) the kinematical complications due to the differences between nuclear and nucleon c.m. systems

can be neglected, (2) the modification of the nucleonic amplitude due to the presence of the other nucleon can be neglected, (3) the nucleonic amplitude $F_{j\lambda}$ contains only s- and p-wave terms (higher ℓ-waves contribute additional terms to Eq. (4.4)). Included in (1) is the neglect of Fermi motion of nucleons and the use of the operator $-i\vec{\nabla}\,\phi_{n\ell}$ for $\vec{q}\phi_{n\ell}$ (MW 73). Delorme et al. (DFK 75) have included terms in $F_{j\lambda}$ up to d-waves and contributions (DEF 75) from incoherent scatterings of the pions before the absorption, as well as meson exchange between neighboring nucleons. Both effects produce a renormalization of the nucleonic amplitude, which, however, is estimated to be negligibly small for light nuclei.

4.2 RADIATIVE CAPTURE ON PROTONS

4.2.1 GENERAL SCATTERING AMPLITUDE

The process $\pi^- p \to n\gamma$ is the inverse of the photoproduction of pions, $\gamma n \to \pi^- p$, for which a well established theory exists. Using the notation of Pilkuhn (Pil 67), the most general Lorentz-invariant matrix element for photoproduction may be written in the c.m. system in the form

$$T(\lambda_n,\lambda_\gamma,\lambda_p,\theta) = 8\pi\sqrt{s}\;\chi_p^+(\lambda_p)\;F\;\chi_n(\lambda_n) \tag{4.5a}$$

$$F \equiv F_1(\vec{\sigma}\cdot\hat{\varepsilon}) - iF_2(\vec{\sigma}\cdot\hat{q})(\vec{\sigma}\cdot(\hat{k}\times\hat{\varepsilon})) + F_3(\vec{\sigma}\cdot\hat{k})(\hat{q}\cdot\hat{\varepsilon}) + F_4(\vec{\sigma}\cdot\hat{q})(\hat{q}\cdot\hat{\varepsilon}) \tag{4.5b}$$

Here $q = (\omega,\vec{q})$, $k = (k,\vec{k})$, $p_1 = (E_1,-\vec{k})$, and $p_2 = (E_2,-\vec{q})$ denote the pion-, photon-, neutron-, and proton-four-momenta; $\sqrt{s}$ is the total energy in the c.m. systems, $\hat{\varepsilon}$ the polarization vector for a photon of helicity $\lambda_\gamma(\pm 1)$, and $\vec{\sigma}$ the nucleon spin matrices; λ_n,λ_p are the initial and final nucleon helicities; χ_p and χ_n are the two component Pauli-spinors, $\cos\theta = (\hat{q}\cdot\hat{k})$ is the c.m. scattering angle ($\hbar$=c=1). The decomposition of the

amplitudes F_i into multipole amplitudes may be found in the pioneering work of Chew, Goldberger, Low, and Nambu (Che+ 57). Keeping only s- and p-wave terms, one finds

$$\begin{aligned} F_1 &= E_{0+} + E_{2-} + 3(M_{1+} + E_{1+}) \cos\theta \\ F_2 &= 2M_{1+} + M_{1-} \\ F_3 &= 3(E_{1+} - M_{1+}) \\ F_4 &= -3E_{2-} \end{aligned} \tag{4.6}$$

where $E_{\ell\pm}$ ($M_{\ell\pm}$) stands for the electric (magnetic) multipole amplitude of multipole order $2^{\ell\pm1}$ (2^{ℓ}) leading to a final state with $j = \ell\pm\frac{1}{2}$ and parity $(-1)^{\ell}[-(-1)^{\ell}]$. Since the electromagnetic current has an isoscalar and isovector component, the multipole amplitudes are further characterized in isospin according to transitions $\frac{1}{2} \to \frac{1}{2}$ for the isoscalar amplitude, and $\frac{1}{2} \to \frac{1}{2}$, $\frac{1}{2} \to \frac{3}{2}$ for the isovector amplitudes. The particular isospin combination for π^- production is

$$M_j^{(\pi^-)} = M_j^{(0)} + \tfrac{1}{3}(M_j^{(1)} - M_j^{(3)})$$

where $M_j = E_{\ell\pm}$ or $M_{\ell\pm}$, and the indices $(\alpha) = (0),(1),(3)$ label amplitudes leading to states with total isospin $\frac{1}{2}$, $\frac{1}{2}$, and $\frac{3}{2}$, respectively. In the treatment of nuclear radiative π-capture it has become conventional (DE 66) to reorder the pion photoproduction matrix elements into a form similar to Eq. (4.4):

$$F = A(\vec{\sigma}\cdot\hat{\varepsilon}) + B(\vec{\sigma}\cdot\hat{\varepsilon})(\vec{q}\cdot\vec{k}) + C(\vec{\sigma}\cdot\vec{k})(\hat{\varepsilon}\cdot\vec{q}) + iD(\vec{q}\cdot\vec{k}\times\hat{\varepsilon}) + E(\vec{\sigma}\cdot\vec{q})(\vec{q}\cdot\hat{\varepsilon}) \tag{4.7}$$

with

$$\begin{aligned} A &= E_{0+} + E_{2-} \\ B &= (M_{1+} - M_{1-} + 3E_{1+})(qk)^{-1} \\ C &= (-M_{1+} + M_{1-} + 3E_{1+})(qk)^{-1} \\ D &= -(2M_{1+} + M_{1-})(qk)^{-1} \\ E &= -3E_{2-}(q)^{-2} \end{aligned} \tag{4.8}$$

Knowledge of the coefficients A through E is, of course, essential for the application of the results for the capture on nucleons to the nuclear case.

4.2.2 BORN APPROXIMATION FOR MULTIPOLES AT THRESHOLD

Near threshold the main contribution to the multipole amplitudes stems from the three gauge-invariant first order Born-diagrams (Fig. 5), the one-pion exchange in the t-channel, and the nucleon poles in the direct and the crossed channel. In general Watson's theorem (Wat 54) assures that as long as the inelasticity of the pion-nucleon system is small, the phases of the multipole amplitudes are identical to the pion-nucleon phase-shifts for channels with equal spin and isospin. Thus, near threshold where πN phase shifts approach zero, the γN multipoles become essentially real. The explicit formulae for $E_{\pm}^{BORN}$ ($M_{\pm}^{BORN}$) can be found, e.g., in the paper by Donnachie and Shaw (DS 66). The leading terms near threshold ($q/m_{\pi}\to 0$) are of order q^{ℓ}, so that the amplitudes A-E approach in this limit a constant value. In particular one finds for the Born approximation at q=0

$$E_{0+} = -\gamma\{1 + \tfrac{1}{2}\alpha \frac{\mu_p' + \mu_n'}{1 + \alpha}\} = -32.1 \times 10^{-3} m_{\pi}^{-1} \tag{4.9}$$

$$(qk)^{-1}E_{1+} = -\frac{\gamma}{6} \frac{1 + \alpha}{(1 + \frac{\alpha}{2})^2} \{1 - \frac{\alpha^2}{2}\} m_{\pi}^{-2} = -5.2 \times 10^{-3} m_{\pi}^{-3}$$

$$(qk)^{-1}M_{1+} = \frac{\gamma}{6} \frac{1 + \alpha}{1 + \frac{\alpha}{2}} \left\{(1 + 2\mu_p')\alpha + \frac{1 + \alpha}{1 + \frac{\alpha}{2}}\right\} m_{\pi}^{-2} = 10.1 \times 10^{-3} m_{\pi}^{-3}$$

$$(qk)^{-1}M_{1-} = -\frac{\gamma}{12} \{4 \frac{1 + \alpha}{1 + \frac{\alpha}{2}} - \alpha(2 + \mu_p' - 3\mu_n' - \frac{3(\mu_p' + \mu_n')}{1 + \alpha})\} \frac{1+\alpha}{1+\frac{\alpha}{2}} m_{\pi}^{-2} = -8.1 \times 10^{-3} m_{\pi}^{-3}$$

$$(q^2)^{-1}E_{2-} = -\frac{\gamma}{6}\{-\frac{3}{5} \frac{1}{1 + \frac{\alpha}{2}} + 2(1 + \alpha) - \frac{1}{10}\alpha^2(11\mu_p' + 1)\} m_{\pi}^{-2} = -9.3 \times 10^{-3} m_{\pi}^{-3}$$

with $\gamma = \sqrt{2} \frac{ef}{\sqrt{4\pi}} \frac{1}{(1 + \alpha)^{\frac{1}{2}}}$, $\alpha = \frac{m_{\pi}}{m_{\pi}}$, $\frac{e^2}{4\pi} = \frac{1}{137}$, $f^2 = .081$

$\mu_p' = 2.79$ and $\mu_n' = -1.91$.

Using the results of Eq. (4.9) we can form the appropriate linear combinations for the momentum dependent terms and obtain

$$\begin{aligned} A &= -32.1 \times 10^{-3} m_\pi^{-1} \\ B &= 2.6 \times 10^{-3} m_\pi^{-3} \\ C &= -33.8 \times 10^{-3} m_\pi^{-3} \qquad \text{(Born approximation)} \\ D &= -12.1 \times 10^{-2} m_\pi^{-3} \\ E &= 28.0 \times 10^{-3} m_\pi^{-3} \end{aligned} \tag{4.10}$$

While the C,E, and D terms are of order A/m_π^2 and $A/3m_\pi^2$, the Born result for the B-term is of the order m_π/m_n times smaller. Since the Born contributions dominate near threshold, we expect relatively large corrections only for the B-term when other contributions are considered, as discussed below.

Except for the factor $(1 + \frac{m_\pi}{m_n})^{-\frac{1}{2}}$, the leading electric dipole amplitude $A = E_{0+}$ in the Born-approximation is equal to the Kroll-Rudermann (KR 54) threshold value and agrees very well with experimental findings (Sec. 4.2.4). The soft-pion-PCAC value for A (Sec. 4.3), expressed in terms of the pion decay constant $f_\pi = .932\ m_\pi$ and the ratio of the axial-vector to vector weak coupling constant $g_A/g_V = 1.24$ is

$$A = \frac{e}{4\pi} \frac{g_A}{g_V} \frac{1}{f_\pi} = -31.3 \times 10^{-3} m_\pi^{-1} \tag{4.11}$$

4.2.3 INFLUENCE OF THE P_{33}-RESONANCE AND DISPERSION RELATION CALCULATIONS

For increasing values of q/m_π the P_{33}-resonance (E_{cm}= 1232 MeV, $q/m_\pi = 1.65$, $\Gamma = 110$ MeV), which dominates the magnetic dipole $M_{1+}^{(3)}$ and electric quadrupole $E_{1+}^{(3)}$ amplitudes, influences the coefficients B, C, and D. The impact of this resonance and higher πN resonances is generally taken into account in the theoretical description of photoproduction by writing a dispersion relation of the form

$$\mathrm{Re}M_j^{(\alpha)}(\omega) = M_j^{\mathrm{BORN}(\alpha)}(\omega) + \frac{1}{\pi} P \int_{\omega_0}^{\infty} \frac{\mathrm{Im}M_j^{(\alpha)}(\omega')}{\omega' - \omega} d\omega'$$

$$+ \sum_{\beta,k} \int_{\omega_0}^{\infty} K_{jk}^{(\alpha,\beta)}(\omega',\omega)\ \mathrm{Im}M_j^{(\beta)}\ d\omega' \qquad (4.12)$$

$$(\omega = \sqrt{s} - m_n)$$

The kernels $K_{jk}^{(\alpha\beta)}$ are known non-singular functions which couple a given multipole with all the others. The solution of this system of coupled integral equations can be traced from the original work of Chew, Goldberger, Low and Nambu (Che+ 57) and a series of subsequent papers (Jur 72) with increasing sophistication, to the most recent work of Berends, Donnachie and Weaver (BDW 67). We give their results for the coefficients A - D as a function of q together with the Born results in Fig. 6. As can be seen, significant deviations from the Born approximation appear as expected at q = 0 in the B-term, and with increasing q for all momentum dependent terms. The deviations reflect the influence of the P_{33}-resonance.

4.2.4 NUMERICAL EVALUATIONS OF THE A,B,C,D, AND E COEFFICIENTS

Almost all previous calculations for nuclear radiative pion capture use the BDW multipole tables as a starting point to determine the coefficients, however, with sometimes different results (KOS 68, MW 73,Table VI). To examine this procedure, and to determine a set of recommended values for these coefficients, we compare the BDW results with "model-independent" multipole analyses and with the experimental results.

Near threshold the $\gamma n \to \pi^- p$ data are usually obtained from the relative π^+ and π^- yields from a deuterium target irradiated with a photon beam, viz,

$$\sigma(\gamma n \to \pi^- p) = \frac{\sigma(\gamma d \to \pi^- pp)}{\sigma(\gamma d \to \pi^+ nn)} \times \sigma(\gamma p \to \pi^+ n) \qquad (4.13)$$

where $\sigma(\gamma p \to \pi^+ n)$ is independently determined with a proton target. The strong final state interactions are presumed to cancel in the ratio, whereas Coulomb-corrections and other, smaller deuterium corrections are taken into account with theoretical estimates. The only other source of data is the Panofsky ratio for pions at rest,

$$P_1 = \frac{\sigma(\pi^- p \to \pi^\circ n)}{\sigma(\pi^- p \to \gamma n)} = 1.533 \pm 0.021 \tag{4.14}$$

(Coc+61). Since the pions are captured from an s-state, we may relate P_1 to the s-wave singlet and triplet pion-nucleon scattering lengths, as determined in charge-exchange experiments (BCC 73) at somewhat higher energies,

$$P_1 = \frac{1}{9} \frac{q_{\pi^\circ}}{k} \frac{(a_1 - a_3)^2}{|E_{0+}^{(\pi^-)}|^2} \tag{4.15}$$

Using $a_1 - a_3 = (.262 \pm .004)\frac{1}{m_\pi}$ (BCC 73) we find $|E_{0+}^{\pi^-}| = (32.9 \pm 0.6)*10^{-3}\,\frac{1}{m_\pi}$, which is close to the Born value (RW 75).

Using their own $\pi^- p \to n\gamma$ data (Ada+68) and various combined data for the π^-/π^+-ratio (Ada+66, Ben+56, San+54), Adamovich et al. (Ada+69) deduce threshold values for $E_{0+}^{(\pi-)}$ given in Fig. 6 and Table VI. Through a fit of the π^-/π^+-ratio-data with a power-series in cos θ, angular distributions (Ada+69) as well as total cross-sections (Ada+69) for $\gamma n \to \pi^+ p$ are calculated ($q/m_\pi \leq .8$). Since the ratio of forward to backward cross-sections is given by

$$\frac{\frac{d\sigma}{d\Omega}(0^\circ)}{\frac{d\sigma}{d\Omega}(180^\circ)} = \frac{A + B(qk)^2}{A - B(qk)^2}, \tag{4.16}$$

the energy-dependence of A and B near threshold was also obtained. The results are shown in Fig. 6. The accuracy of the data doesn't allow extraction of the

C,D, and E coefficients.

Pfeil and Schwela (PS 73) have performed a multipole analysis for higher energies ($q/m_\pi > .58$) in which the real parts of E_{0+}, E_{1+}, M_{1+}, and M_{1-} were taken as free parameters. The imaginary parts were obtained by use of Watson's theorem and experimental pion-nucleon phase shifts (AL 72). Born approximation values were used for all multipoles with $\ell > 2$. At the lowest energies ($q/m_\pi = .59, .82$) the M_{1-} multipole is further restricted to its Born value. Their results are shown in Fig. 6.

We have determined threshold values for the coefficients B, C and D by fitting a curve of the form $(a + bqk)$ to the five values with $q < 1.19\ m_\pi$. For the B-term a similar fit was made to the Adamovich data. The results are summarised in Table VI and the curves given in Fig. 6. The two analyses can only be compared at one energy ($q/m_\pi = .59$), where a 10% descrepancy appears for the E_{0+} -value. The statistical errors are given as about 1%. Since the BDW-calculation as well as the pure Born-result agree with the Pfeil + Schwela result at this energy and reproduce the Adamovich-values at threshold, we disregarded this discrepancy in the evaluation of the errors given for our "recommended" values in Table VI. We can also fit a smooth curve given by $E_{0+} = a + b\ (q\ k)^2 m_\pi^{-4} + c\ (q\ k)^4 m_\pi^{-8}$ through the threshold and the Pfeil and Schwela values. For the B-term the Adamovich et al. and Pfeil and Schwela result overlap at $q = .59\ m_\pi$, but the threshold extrapolation yields different values outside their respective error bars. We feel that the Pfeil and Schwela result, which relies more heavily on the higher accuracy Bonn π^-/π^+-ratio measurements (Hol + 72) for $q > 1.06\ m_\pi$, should be preferred but the error bars should be increased to encompass the Adamovich result. In light of the preceding discussion it is clear that new data on $\pi^- p \to n\gamma$ at low energies are in urgent demand.

The radiative pion-capture Hamiltonian, Eqs. (4.3) and (4.4), is obtained by time-reversal of the pion photoproduction matrix elements. Maguire and Werntz have shown that this is the Hermitian conjugate of Eq. (4.7), apart from a sign change of the non-spin flip D-term. This sign change was overlooked in earlier work (DE66, RP73, KOS 68). The elementary cross sections, of course, contain no interference terms between D and the others, and remain unchanged.

4.3 CALCULATION OF 1s-RADIATIVE PION CAPTURE IN THE "ELEMENTARY PARTICLE SOFT-PION" ANSATZ

In the elementary particle treatment (KP 65) of nuclei one attempts to establish relations between weak and electromagnetic reactions involving the same nuclear states. The nuclear matrix elements are replaced by a set of nuclear model independent form factors analogous to the nucleon case. The link between radiative pion capture from a 1s-state and weak processes, such as μ-capture and β-decay, is based on the hypothesis of partial conservation of axial vector current (PCAC). It states that the divergence of the axial current (a_μ) is equal to the pion field (ϕ_π)

$$\partial^\mu a_\mu = f_\pi m_\pi^2 \phi_\pi \tag{4.17}$$

where f_π is the pion decay constant ($f_\pi = .932\ m_\pi$). Several theoretical articles (PFE 67, Ef 67) are concerned with its application to radiative pion capture and the subject has been recently reviewed by Ericson and Rho (ER 72). We give here only the general idea, omitting all the details of the derivation.

For the nucleon case, $\pi^- p \to n\gamma$, the transition amplitude is written, apart from normalization factors, as

$$< n(p_f)\ \gamma(k)|j_\pi|\ p(p_i) > \tag{4.18}$$

where $j_\pi = (\Box + m_\pi{}^2)\ \phi_\pi$ describes the pion source. The PCAC hypothesis (Eq. (4.17)) has to be modified for the presence of the electromagnetic field (A_μ) to read

$$(\partial^\mu - ieA^\mu)\ a_\mu = f_\pi\ m_\pi^2\ \phi_\pi \tag{4.19}$$

Inserted into the amplitude (Eq. (4.18)), this leads to

$$\frac{f_\pi\ m_\pi^2}{m_\pi^2 - q^2} < n\gamma|j_\pi|p > = iq^\mu < n\gamma|a_\mu|p > - ie < n\gamma|A^\mu a_\mu|p > \tag{4.20}$$

Since we deal with pion capture at rest ($\vec{q}$=0), the soft pion limit ($q\to 0$) is obtained by setting $m_\pi \to 0$. In this limit (the exact prescription is given in (ER 72)), the amplitude reduces to

$$q \to 0 : \quad < n\gamma|j_\pi|p > = -\frac{ie}{f_\pi} < n|\varepsilon^\mu a_\mu|p >$$

$$= -ie\ \frac{g_A}{g_V}\ \frac{1}{f_\pi}\ \bar{u}_n\ \varepsilon^\mu \gamma_\mu \gamma_5 \tau^+ u_p \tag{4.21}$$

where ε^μ is the photon polarization 4-vector. The connection to μ-capture is obvious now, recalling that the axial vector part of the $\mu^- p \to n\nu_\mu$ matrix element is obtained by replacing $\frac{e}{f_\pi}\ \varepsilon^\mu$ by the leptonic current $\frac{G}{\sqrt{2}}\ (\bar{u}_{\bar{\nu}} \gamma^\mu (1+\gamma_5) u_\mu)$. Replacing the spinors $\bar{u}_p$ and u_n (Eq. (4.21)) by two-component Pauli-spinors, the non-relativistic limit of the amplitude is obtained

$$-ie\ \frac{g_A}{g_V}\ \frac{1}{f_\pi}\ \chi_n^+\ \vec{\sigma}\cdot\hat{\varepsilon}\ \tau^+\ \chi_p \tag{4.22}$$

This is completely equivalent to the dominant term in the impulse approximation Hamiltonian.

The nuclear π-capture case is obtained by replacing the $|p>$ and $|n>$ by nuclear states. The physical amplitude differs slightly for nuclear

transitions from the soft-pion amplitude. It includes corrections due to nuclear intermediate states, incoherent rescattering (i.e., the pions rescatter before absorption, exciting the nucleus in the intermediate state) and vector meson intermediate states. The modified amplitude is (ER 72)

$$M = -\frac{ie}{f_\pi} \langle f|\varepsilon^\mu a_\mu|i\rangle - .22\,\frac{ieg_A}{f_\pi g_V} \langle f| \sum_j \vec{\sigma}_j\cdot\hat{\varepsilon}\ \tau^+\delta(\vec{r}_j)|i\rangle \tag{4.23}$$

If exchange effects are neglected in the axial current matrix element, the above two terms may be combined. Introducing the axial vector form factor $F_A(q^2)$ for the nuclear transition $|i\rangle \to |f\rangle$, Eq. (4.23) becomes

$$M = -\frac{ie}{f_\pi}\,1.22\ F_A(q^2) \tag{4.24}$$

Collecting all the normalization factors above, the 1s-radiative π-capture transition rate is given (Del70) by

$$\Lambda_\gamma(1s) = (1.22)^2\,\frac{e^2}{2\pi^2 f_\pi^2}\,C_s(Z\alpha m_\pi')^3\,\frac{k}{m_\pi}\left(1 - \frac{k}{m_\pi+M_A}\right) S(J_i,J_f)\ F_A^2(q^2) \tag{4.25}$$

Here C_s is the distortion factor of the pionic wave-function (Sec. 3) and $S(J_i,J_f)$ is a spin dependent factor.

Numerical examples for the evaluation of $\lambda_\gamma(1s)$ can be found for ^{3}He(GK 68, FE, PF 70), ^{6}Li(GK, FE, Del70), and ^{14}N (Bae+75). These were all obtained using β-decay to determine $F_A(q^2=0)$ and then extrapolating to the relevant q^2 by use of

$$\frac{F_A(q^2)}{F_A(0)} = \frac{F_M(q^2)}{F_M(0)} \tag{4.26}$$

where $F_M(q^2)$ is the electromagnetic form factor of the M1 transition

connecting the target nucleus ground state with the excited state analog of the (π^-,γ) final state. Taking the $^6Li(1^+,T=0)$-$^6He(0^+,T=1,g.s.)$ transition as an example, $F_A(q^2)$ is determined as follows (Del70):

(i) β-decay ft-value: $^6He \rightarrow {}^6Li + e^- + \bar{\nu}_e$

$$F_A^2(0) = \frac{2}{3}\frac{\pi^3 \ln 2}{G^2 m_e^5 \, ft_{\frac{1}{2}}} \tag{4.27}$$

(ii) inelastic electron scattering: $^6Li(e, e')^6 \overset{*}{Li}(0^+, T=1; E_x=3.56 \text{ MeV})$, beam energy E_e

$$\frac{d\sigma}{d\Omega} = \frac{\alpha^2}{12E_e^2}\left(1 + \frac{2E_e}{M_A}\sin^2\frac{\theta}{2}\right)^{-1} \frac{1+\sin^2 \frac{1}{2}\theta}{2\sin^2 \frac{1}{2}\theta}\left(\frac{q}{m_\pi}\right)^2 F_M^2\,(q^2) \tag{4.28}$$

(iii) γ-decay lifetime: $^6\overset{*}{Li}(0^+, T=1; E_x=3.56 \text{ MeV}) \rightarrow {}^6Li+\gamma$

$$\Gamma_\gamma(^6\overset{*}{Li} \rightarrow Li + \gamma) = 2\alpha\, m_\pi \left(\frac{E_x}{m_\pi}\right)^3 F_M^2\,(0) \tag{4.29}$$

Reactions (i) to (iii) may then be used in Eq. (4.26) to determine $F_A(q^2)$.

The use of Eq. (4.24) is generally justified by the good agreement of the calculated μ-capture rate with experiment, where $F_A(q^2)$ is determined in a similar way and the vector form-factors are obtained directly from the electromagnetic ones via CVC.

Table VII lists the results for ^3He, ^6Li and ^{14}N, which are compared to the impulse approximation results and the experiments in Secs. 4 and 5.

5. RESULTS ON LIGHT NUCLEI, ISOTOPES OF HYDROGEN AND HELIUM

Radiative capture on these nuclei has played an important role in the study of threshold π-N, γ-N, and π-N-N interactions, the search for resonances in the A = 3 and A = 4 nucleon systems, and the study of π-absorption mechanisms in nuclei. A synopsis is given in Table VIII.

5.1 HYDROGEN

Study of radiative capture on protons is a necessary prerogative both from the experimental and theoretical point of view for the application of the (π^-,γ) reaction to nuclear structure physics. It provides a convenient calibration of the detectors (Sec. 2) and the basis for the theoretical analysis (Sec. 4). Historically it was one of the prime reactions in determining properties of pions; e.g., one of the most accurate early mass determinations consisted of measuring the absolute energy of the $\pi^- p \rightarrow n\gamma$ photon (CP 54). The Panofsky ratio links s-wave π-nucleon scattering to pion photo-production at threshold. As such, it is an important experimental quantity in the chain of low-energy pion reactions used to test the symmetries of charge independence and time reversal invariance. Starting with π-N elastic and charge exchange scattering, the hypothesis of charge independence, together with extrapolation to zero energy, yield values of the isospin singlet (a_1) and triplet (a_3) scattering lengths which appear in the Panofsky ratio (Eq.4.15). Using the Panofsky ratio for hydrogen and the impulse approximation (IA) for the radiative capture rate for deuterium $\lambda_\gamma(\pi d \rightarrow nn\gamma)$, one obtains a direction relation between the measured deuterium branching ratio $\lambda_n(\pi^- d \rightarrow nn)/\lambda_\gamma(\pi^- \rightarrow nn\gamma)$ and the cross section $\sigma(\pi^- d \rightarrow nn)$. The latter is related by charge symmetry to $\sigma(\pi^+ d \rightarrow pp)$ which is measured directly,

or by the time reversed reaction $\sigma(pp \to d\pi^+)$. This consistency test is discussed in various text books (Käl 64, CT 74) and articles (Rya 63, Rog 67, SM 76) and will not be treated here. The experimental results for hydrogen and some keys to their interpretation are given in Table VIII. The spectrum is shown in Fig. 7a.

5.2 DEUTERIUM

As early as 1951 it was suggested (WS 51) that a_{nn}, the singlet neutron-neutron scattering length, could be determined from the final state interaction of the two neutrons in the radiative absorption in pionic deuterium. With the exception of the μ-capture process in deuterium, which is quite difficult to measure, radiative pion capture provides the only reaction where the two neutrons are not accompanied by another strongly interacting particle. Furthermore, the photon spectrum (Fig. 7b) peaks sharply towards higher energies, or low relative momenta for the neutrons, which is a favorable situation for studying n-n interactions. Theoretical treatments (Ban 64, McV 61, GGS 75a) are generally in the framework of the IA, which leads to transition amplitudes proportional to

$$M \sim \int d^3r \; \phi_\pi(r) \; \phi_d(2r) \; e^{i\vec{q}\cdot\vec{r}} \phi^s_{nn}(p,2r) \qquad (5.1)$$

where ϕ^s_{nn} is the singlet final state of two neutrons with relative momentum p and separation $2r$, $\phi_d(2r)$ is the initial deuteron state and ϕ_π is the initial pion wave function. In the simplest ansatz, only the ^1S_o neutron-neutron scattering state is retained, with

$$\phi_{nn} \sim \cos\delta_o j_o(pr) + \sin\delta_o \, n_o(pr) \qquad (5.2)$$

where j_o and n_o are spherical Bessel- and Neumann- functions, respectively. The scattering length enters via

$$p \cot \delta_o(p) = - \frac{1}{a_{nn}} + \frac{1}{2} r_{nn} p^2 \qquad (5.3)$$

where r_{nn} is the effective range (a_{nn} = 16.4 F, r_{nn} = 2.6 F, e.g. (Sal+ 72)). The transition matrix element for small p then reduces to approximately the form

$$M^2 \sim \left| \frac{\sin \delta_o(p)}{p} \right|^2 \cong \frac{1}{p^2 a_{nn} + 1} \quad . \qquad (5.4)$$

The kinematic relation between photon energy k and relative neutron momentum for small values of p ($\vec{p} = \vec{p}_1 - \vec{p}_2$) is

$$k = q_{max} - \frac{p^2}{m} \qquad (5.5)$$

(q_{max} = 131.5 MeV/c), indicating that only in the last 0.5 to 1 MeV is there a strong dependence of the spectrum shape on a_{nn}. The early determinations of a_{nn} from the measurement of the γ-spectrum (PC 54, Rya 63, Nic+ 68) consequently yield large errors. A more precise determination of a_{nn} can be obtained in a kinematically complete experiment where both the neutrons and the photon are detected and n-n(θ) and n-γ(θ) angular- and energy - correlations are measured. Such an experiment (Had+ 65, Sal+ 72) yielded a_{nn} = 16.4 ± 1.6 F. The error contains an uncertainty of ± 1 F from the theoretical analysis (Ban 64). The sign is given by the photon spectrum. A more recent theoretical analysis (GGS 75a) shows that this contribution can be reduced considerably, so that in a new experiment of similar type an accuracy of 0.3 F could be achieved.

The absolute rate for radiative capture is only weakly model dependent and can be calculated to an accuracy of ± 10% with the IA. Using the

theoretical value cited in (Bis+ 76) and the experimental branching ratio, a total width for the pionic 1s level of 1.02 ± 0.11 eV is calculated (Table IX). Such a small width cannot be measured directly. Its indirect termination through radiative pion capture is quite useful, since this number serves as a test for pion two-nucleon absorption models used in calculations for heavier nuclei (KR 66, PR 73).

5.3 TRITIUM

Study of radiative capture in tritium, $\pi^- t \rightarrow nnn\gamma$, affords an attractive possibility for study of the 3-neutron excitation spectrum - with the hope of revealing evidence for T = 3/2 resonances or even a bound ^3n system should these exist. The latter would give an unambiguous signature, producing a sharp line (E_γ > 127 MeV) separated in energy from the breakup continuum. The available data on the existence of T = 3/2 resonances and a possible ^3n state are scarce, inconclusive, and sometimes conflicting, and these have promoted equally conflicting theoretical interpretations (e.g., (Pai 72), (FH 75)). All reactions studied, except that of radiative pion capture, are plagued by the fact that although a (3p) or (3n) system is produced, there is at least one additional strongly interacting particle in the final state. The π^- capture reaction has only an extra photon in the final state. Furthermore, from study of the $\pi^- d \rightarrow nn\gamma$ and $\pi^- {}^3He \rightarrow dn\gamma$ and $pnn\gamma$ reactions it is known that radiative capture of stopped pions produces final states in which nucleons are preferentially found with low relative momenta, a favorable situation for the search of resonant states.

The photon spectrum was recently measured (Bis+ 76) using a 23 cm^3 liquid tritium target and the Berkeley pair spectrometer in the extended low-energy pion channel (LEP) at Los Alamos (LAMPF). The small target size and the short beam time limited the total number of tritium events to about 1000 (Fig. 7c). An additional 1000 events appeared in the raw spectrum (Bis+ 76) originating from the 1% ^1H and 2.8% ^2H contamination in the target, the stainless steel target cell and vacuum jacket, and the beam defining counter in front of the target. The shape of each of these components was quite well determined either by direct measurement in the experiment or from previous work. The absolute normalization was based on hydrogen runs which were interspersed with the tritium runs.

The measured branching ratio of 4.5 ± 0.8% is considerably less than for hydrogen and deuterium, and nearly the same as that for the radiative breakup of ^3He (Table IX). Examination of the spectrum (Fig. 7c) shows that there is no evidence for a bound ^3n state and an upper limit of 0.3% is measured for the branching ratio. Also, there is no evidence for a relatively narrow T = 3/2 resonance in the (3n) excitation spectrum. Thus the suggestion of such a state by Sperinde et al. (Spe+ 70) on the basis of the double-charge exchange reaction $^3He(\pi^-,\pi^+)3n$ is not supported by the radiative π^- capture results. The calculation of Phillips and Roig (PR 75), which puts in no resonances, describes the data rather well (Fig. 7c). These authors treat the interaction of the outgoing neutrons in the Amado model (Ama 63) and calculate the transition rate with the IA. The calculated radiative rate is $\lambda_\gamma(\pi^- t \rightarrow nnn\gamma) = 7\times10^{13}$ sec^{-1} and the non-radiative rate, calculated with a pair-absorption model (PR 73), is $\lambda_n(\pi^- t \rightarrow nnn) = (1.0 \pm 0.3)10^{15}$ sec^{-1}. These give a branching ratio of

6.5 ± 2.0% which is in reasonable agreement with the data. By using the experimental branching ratio and the theoretical λ_γ a total width of 1.02 ± 0.18 eV is obtained for the tritium 1s pionic level width. This is approximately equal to that of hydrogen and deuterium (Table IX), but much less than the 3.67 eV given by the phenomenological extrapolation (CE 74) of data on heavier nuclei.

5.4 HELIUM-3

A straightforward impulse approximation calculation allows one to relate the Panofsky ratio in ^{3}He to the equivalent quantity in hydrogen (Tru+ 74)

$$P_3 = 2P_1 \frac{q_{03}}{k_3} \frac{k_1}{q_{01}} \frac{m_3+m_\pi-\omega_{03}}{m_3+m_\pi-k_3} \frac{m_n+m_\pi-k_1}{m_n+m_\pi-\omega_{01}} \frac{|M_o|^2}{|M|^2} . \tag{5.6}$$

where m_3 = mass of ^{3}He; m_n = mass of ^{1}H; $(\omega_o,\vec{q})$ = π_o four momentum; and k is the photon momentum. The matrix element for radiative capture $|M|^2$ is related to the Gamow-Teller matrix element $M_{GT} = \langle {}^3H \,|\, \sum_{j=1}^{3} \tau_j^{(+)} \vec{\sigma}_j \,|\, {}^3He \rangle$ and the axial form factors of the mass-3 system and the nucleon by (e.g. Tru+ 74)

$$|M|^2 = \frac{2}{3}|M_{GT}|^2 \left(\frac{F_A(q^2)}{F_A(0)}\right)^2 \left(\frac{f_A(0)}{f_A(q^2)}\right)^2 \approx 2\left(\frac{F_M(q^2)}{F_M(0)}\right)^2 \times 0.95 \tag{5.7}$$

where the dependence on q^2 of the axial-form factor is assumed (Sec. 4.3) to follow the measured behavior of the electromagnetic form factor. The charge-exchange matrix element $|M_o|^2$ is related to the vector-form factors and Fermi matrix element by

$$|M_0|^2 = |M_F|^2 \left(\frac{F_V(q^2)}{F_V(0)}\right)^2 \left(\frac{f_V(0)}{f_V(q^2)}\right)^2 \approx 1 \times 0.97 . \tag{5.8}$$

Inserting into Eq. (5.6) the values $F_M(q^2)/F_M(0)$ = 0.776 ± 0.016 as determined by use of ^{3}He and ^{3}H electron scattering data (McC 70), and the

experimental value $P_1 = 1.533 \pm 0.021$ (Coc+ 61), one obtains P_3 ($= P_1 \times 2.73 \quad |M|^2/|M|^2$) = 2.49, in satisfactory agreement with the experimental value 2.68 ± 0.13. The radiative transition rate calculated by use of Eq. (5.7) is $\lambda_\gamma(\pi^- \, {}^3He \rightarrow {}^3H\gamma) = 3.6\times10^{-15}\text{sec}^{-1}$. Since P_1 appears in the determination of the experimental value of P_3 (Tru+ 74) as well as in the theoretical expression, the comparison is independent of the particular value of P_1 chosen and can therefore be considered a <u>direct</u> test of the IA in s-wave pion-nucleus interactions.

The agreement between the experimental P_3 and recent theoretical values obtained by the current-algebra methods (Sec. 4) is not quite as satisfactory. Ericson and Figurea (EF 67, EF 69) obtain values between 1.9 and 2.1, depending on whether the charge-exchange cross section is calculated in the IA on the soft-pion technique. In calculating the radiative transition rate the inclusion of corrections for ρ-meson exchange, incoherent rescattering, and nuclear intermediate states has the effect of increasing the radiative rates (4.43×10^{15} sec^{-1} (EF 69), 4.1×10^{15} sec^{-1} (EF 72), 3.86×10^{15} sec^{-1} (Sec. 4.3)) and thereby reducing P_3. It would appear therefore that some of the corrections are smaller than have been estimated.

Phillips and Roig (PR 74) calculated P_3 with the IA using more sophisticated three nucleon bound state wave functions, which are identical in form to ones obtained solving the Fadeev equation with separable N-N potentials. Wave functions with varying percentages of S' and D state contributions are tried. Best agreement with experiment is obtained with P(S') = 1.6% and P(D) = 5% which give $\lambda_\gamma = 3.33\ 10^{15}$ sec^{-1} and $P_3 = 2.79$. The small difference with the experimental value is of the same magnitude and direction as is expected from the meson exchange

corrections to the IA calculation of the tritium β-decay.

The experimental spectrum (Fig. 8a) contains in addition to the tγ final state (135.8 MeV) and the tπ° final state (53.1 - 85.7 MeV), the two radiative breakup channels dnγ (129.8 MeV endpoint) and pnnγ (127.7 MeV endpoint). In Fig. 9 this part of the spectrum is shown enlarged and with the tγ line subtracted out, and is compared to the calculations of Phillips and Roig (PR 74). The total calculated rate for 1s capture into these two channels is 3.06×10^{15} sec^{-1}, of which 74.8% goes into the dnγ state and 25.2% into the pnnγ state. The interaction among the final state nucleons is calculated in the Amado model (Ama 63). If it is neglected, the total rate increases by a factor of 1.6. This calculation requires no resonances in the A = 3 system, and as is apparent from Fig. 9 and Table X, it fits the data rather nicely in shape as well as in magnitude.

^{3}He is the only nucleus where all pionic absorption channels are measured and a calculation exists for each of them. We compare the results in Table X. If the theoretical radiative rates for 1s-capture are scaled by the experimental branching ratios, a total width Γ_a (1s) = 37 eV is obtained. This is in good agreement with the 36 eV (CE 74) obtained by extrapolation from heavier nuclei, and not too far from the measured 45 eV for ^{4}He (Bac+ 74). The individual non-radiative channels are not discussed here, but again, they provide a crucial test case for the two-nucleon absorption model and some calculations are referred to in the Table.

5.5 HELIUM-4

The ^{4}He spectrum (Fig. 8b) appears structureless. However, its shape is more sharply peaked than what is given by the pole-model for quasifree capture with a ^{3}H + n + γ final state (Bis+ 70a). One also observes a sharp drop in the radiative capture rate from ≈15% for ^{3}He to 1.5% for ^{4}He. The shape and magnitude of the spectrum could be well described by an R-matrix calculation assuming the excitation of three broad $T_z = -1$ resonances in ^{4}H: $J^\pi = 2^-$ at 3.4 MeV above the ^{3}H + n threshold; 1^- at 5.1 MeV; and 1^- at 7.4 MeV (Bis+ 70a). The location of these resonances was known from 4-nucleon phase-shift analyses. The curve shown in Fig. 8b is based on the simple configurations: $|2^-\rangle = |^3P_2\rangle$;

$$|1^-, \alpha\rangle = -0.782\,|^1P_1\rangle + 0.625\,|^3P_1\rangle\ ;\ |1^-, \beta\rangle = -0.625\,|^1P_1\rangle + 0.782\,|^3P_1\rangle\ .$$

The mixing between the two 1- states is not uniquely determined by the spectrum analyses. Whereas originally only 1s-capture was considered, a later calculation (RW 71) included 2p-capture, giving Λ_γ (1s) = 1.3×10^{15} sec^{-1} and Λ_γ (2p) = 1.8×10^{10} sec^{-1}. Using the latest x-ray data on ^{4}He (Table V) one gets a branching ratio of 1.85±0.16% of which 86% is from the s-state. An interesting further result of this work was to demonstrate that the n-$\gamma(\theta)$ correlation depends strongly on the angular momentum of the absorbed pion, which may prove useful in future work for separating contributions from different atomic orbits.

6. RESULTS ON 1p-SHELL NUCLEI

6.1 OVERVIEW OF GENERAL FEATURES

The sensitivity of the (π^-,γ) transitions to the structure of individual nuclear states is most clearly seen in the photon spectra of 1p shell nuclei (Fig. 10). Examination of these spectra reveals three general features.

Continuum. The largest fraction (70-90%) of the photons form a continuum spectrum with a maximum energy between 110 and 120 MeV, falling off sharply at the high-energy end, near 125 MeV, and extending down below 50 MeV. This continuum is associated with the 3-body final state of quasi-free (QF) capture on a proton in the nucleus i.e., $\pi^- + A \rightarrow (A-1) + n + \gamma$. The spectrum is much more sharply peaked than 3-body phase space (Fig. 10a) but broader than some Fermi-gas model calculations (DMW 65, Bis+ 70c). It is well fitted in most cases by the pole-model discussed below.

GDR excitations. Superimposed on the QF continuum one sees the suggestion of resonance-like enhancements. Peaks stand out clearly in the ^{12}C and ^{14}N data. From the precisely measured energies in these two cases, one can associate the peaks with transitions to analogs of known states in the GDR region of the target nuclei. In ^{12}C these are 1^- and 2^- components, in ^{14}N they appear to be 2^- and 3^- components. The observation of these peaks was a primary motivation for the first high-resolution experiments and their presence in the ^{12}C data (Bis+ 70b) gave nice confirmation to theoretical expectations (DE 66, AE 66, Mur+ 67). Unfortunately the excitation energies of the GDR ($\sim$ 20 MeV in the target nucleus) is such that the peaks occur near the maximum of

the QF continuum, making ambiguous the extraction of absolute branching ratios. As a practical procedure, the pole model plus one or more Briet-Wigner (BW) forms were fit to the data and the area under the BW has been associated with resonance capture.

Bound states. At the high energy end of the spectrum, corresponding to transitions to particle-stable and low-continuum states, one sees for each nucleus one strong dominating transition. The experimental branching ratios for these peaks are nearly free from uncertainties in background subtraction. In ^{6}Li, ^{10}B, ^{12}C, and ^{14}N the strong transitions can be associated with the $T_z = +1$ analogs of giant M1 states built on the ground state of the target nucleus. The corresponding states in the target ($T_z = 0$, $T = 1$), all of which have been identified in 180° electron scattering, have the largest M1 matrix elements with the ground state (Fag 75). More detailed analyses show that there is some fragmentation of the M1 strength in ^{10}B and ^{14}N (Sec. 6.4). Since ^{16}O is doubly magic, it has no giant M1 states. Nevertheless, there is a sharp peak in the spectrum (Fig. 10e) which spans the region of the four lowest energy states in ^{16}N. The 2^- ground state is a known collective M2 state of ^{16}O which dominates (DW 72) electron scattering at momentum transfers $q \sim 150$ MeV/c and has the largest transition rate in μ-capture (CDK). In π^- capture, $\sim$ 85% of the observed strength has been attributed (SW 74) to the 2^- state. Thus there appears to be a sensitivity in π^- capture to collective M2 states, so far observed only in ^{16}O.

In addition to the above strong transitions, the spectra show weaker population of states in the 0-10 MeV region of excitation of the final state nucleus. With present data, the specific nuclear states cannot be identified; however, since the transition strength is appreciable, it is clear that a

a whole spectroscopy of nuclear levels excited by (π^-,γ) transitions is there for future high-resolution, better statistics studies.

Table XI gives the currently measured radiative branching ratios for the 1p shell nuclei which can be associated with excitation of specific states. For states in the GDR region, the branching ratios are subject to the uncertainties of subtracting the QF continuum. The values given are obtained from the pole model + BW fits discussed in the original papers. To indicate the magnitude of the uncertainties, values are given for ^{12}C and ^{16}O which assume zero background under the peaks.

6.2 POLE MODEL FOR QUASI-FREE CAPTURE

A reasonably good description of the photon continuum for nuclei ranging from ^{3}He to ^{209}Bi is given by the pole-model of Dakhno and Prokoshkin (DP 68). This model and higher order rescattering diagrams are discussed by Shapiro (Sha 63) in the context of dispersion theory for direct nuclear interactions. The matrix element corresponding to the one-pole graph (Fig. 11) is

$$A(t) = \frac{Gg}{t-m^2} \tag{6.1}$$

where m is the proton mass, $t = (p_\gamma + p_n - p_\pi)^2$ is the 4-momentum transfer squared, and p_γ, p_n, and p_π are the four momenta of the photon, neutron, and π^-, respectively; the nucleonic amplitude g, and G the amplitude for the virtual proton decay of the target, are taken as constants. The Q-value at the nucleon vertex is treated as a free parameter since the excitation energy of the recoil nucleus is not known. This parameter is $\Delta = M_{A-1} + m_n + E^*_{A-1} - M_A$ where M_A and M_{A-1} are the initial and final state nuclear masses, E^*_{A-1} is the average excitation energy of the recoil

nucleus, and m_n is the neutron mass. The photon energy spectrum is given by

$$\frac{dN(E_\gamma)}{dE_\gamma} = \text{const.} \times (Gg)^2 \times E_\gamma^2 \int_{-1}^{+1} d(\cos\theta) \frac{E_n p_n^3}{(t-m^2)^2} \frac{E_{A-1}}{p_n^2(M_A+m_\pi-E_\gamma)+p_n E_\gamma E_n \cos\theta} \quad (6.2)$$

where E_n and E_{A-1} are the total energies of the neutron and recoil nucleus, respectively. The curves shown with the data (Fig. 10) were computed with Eq. (6.2). Since the normalization and excitation energy E^*_{A-1} are not specified by the model, best values were determined by fits to the data. For nuclei with $6 \leq A \leq 40$, E^*_{A-1} ranges between 0 and 5 MeV; for ^{209}Bi, E^*_{A-1} = 11 MeV gives a reasonable fit (Nix+ 72). In each case the pole model curve was fit to a portion of the γ-spectrum thought to be free of resonance excitations, viz., corresponding to nuclear excitation energies well above the GDR region. Neutron energy spectra and neutron-$\gamma(\theta)$ correlations calculated (DP 68) with this model show the neutron and γ-ray to be emitted preferentially at 180° and the neutron spectrum to peak at a kinetic energy near 10 MeV. These general trends have been verified by Lam _et al_. (Lam+ 74) in studies of ^{12}C, ^{16}O, and ^{40}Ca in which the n-γ correlation was measured for neutron energies between 1 and 28 MeV.

The pole model is clearly a first approximation. It ignores the motion of the proton in the nucleus and the final state interaction between the outgoing neutron and recoil nucleus which are known to modify considerably the photon spectra of ^{2}H and ^{4}He. Nevertheless, one obtains a remarkably good description of the γ-spectrum in nearly all other cases studied.

Effect of final state interactions in the $^{14}N(\pi^-,\gamma n)^{13}C$ reaction were investigated with neutron optical potentials (LV 74). The strong distortion of the neutron wave causes considerable reduction in the total capture rates and pushes the spectrum shape towards the high energy end. This peaking is more pronounced for d-wave than p-wave neutrons (the dominant two ℓ-values) which could lead to structure in the continuum. In general, however, one expects a distribution of states with different Q-values to contribute, which would smooth out such structure.

Both the pole-model and the above study do not clearly distinguish QF and resonance capture. Ultimately, one hopes for a unified theoretical treatment which treats explicitly the coupling of these channels.

6.3 $\pi^- + {}^6Li \rightarrow {}^6He(g.s) + \gamma$ AS TEST CASE OF THE THEORY

The data on this multiplet of states (Fig. 12) is unusually complete: β-decay, μ-capture, π-capture, and (γ,π^+) cross sections are measured for the $^6Li \rightleftarrows {}^6He$ (g.s.) transitions; the magnetic dipole moment and electric quadrupole moment of ^6Li(g.s.), and the ^6Li (3.56 MeV) lifetime are measured; inelastic electron scattering to the latter state has been studied by several groups, and the transition form factor is well measured at $40 < q < 400$ MeV/c. Theoretically, the states in question are expected to be well described as shell model states having two 1p-shell valence nucleons outside an inert α-particle-like core, since $1\hbar\omega \simeq 20$ MeV for $1s \rightarrow 1p$ and $1p \rightarrow (2s1d)$ excitations (Ver 74). Thus core excitation admixture to p^2 wave functions may be small. For these reasons the $^6Li(\pi^-,\gamma)^6He$(g.s.) transition is a good test case for determining the level of accuracy that can be achieved in the description (γ,π) and (γ,π) reactions on complex nuclei.

The photon spectrum for ^{6}Li is shown in Fig. 10a. Although the g.s. peak stands out clearly, the analysis (Bae+ 73) on the width of this peak indicated that there is some population of the 2^+ state at 1.8 MeV. The uncertainty that the presence of the 2^+ state introduces in the extraction of the ground state peak area is small since the instrumental line shape of the spectrometer is well determined and a single line can be normalized to the ^{6}Li spectrum at the high energy side of the g.s. peak where contributions from other channels are small. The resulting branching ratio (Table XII) is $R_\gamma = 0.306 \pm 0.035\%$. The earlier activation measurement (Deu+ 68) yielded $R_\gamma = 1.0 \pm 0.1\%$ (for a discussion of this discrepancy see Sec. 2).

Experiment and theory are compared in Table XII. The accuracies with which the radiative transition rates $\lambda_\gamma(1s)$ and $\lambda_\gamma(2p)$ can be calculated differ significantly since the contributions of the q-dependent terms of the full IA Hamiltonian (Eq. 4.4), with the larger uncertainties in the B and C coefficients, are much larger in $\lambda_\gamma(2p)$ (VB 72). The D-term does not contribute to a $1^+ \rightarrow 0^+$ transition, independent of the capture orbit. (Since the D-term does not contain $\vec{\sigma}$, only natural parity states are excited (Ver 75); e.g., for J_i $(J_f) = 0$, must have $\pi_i \pi_f = (-1)^L$, where $L = J_f(J_i)$.) The E-term contribution to $\lambda_\gamma(2p)$ is small since $\vec{q} = -i\vec{\nabla}$ operating twice on $\phi_{2p}(r) \sim r$ results in a negligibly small nuclear matrix element.

<u>$\Lambda_\gamma(1s)$</u>. Variations in this quantity among authors using the elementary particle approach arise from different values of the axial-vector form factor $F_A(q^2)$, treatment of the 1s π-orbit distortion, and other

small corrections, e.g. the ρ-exchange contribution. The most detailed study is Delorme's (Del 72) who obtained $(2.3\pm0.5)\times10^{15}$ sec^{-1}. This result makes use of $F_A^2(o) = 2.615$ taken from β-decay and $|F_M(q^2)/F_M(o)| = 0.54\pm0.1$ taken from the F_M^2 measurement of Hutcheon et al. (Hut+ 68). Delorme used the factor 1.35 for the corrections to the soft-pion amplitude (Eq. 4.24). Recent studies (ER 72) use 1.22, which would reduce the above value to $(1.88\pm0.41)\times10^{15}sec^{-1}$ (Table VIII).

Five groups calculated $\lambda_\gamma(1s)$ with the IA and p^2 shell model wave functions. An important point demonstrated by these studies is that for diffuse nuclei such as ^6Li and ^6He care must be taken in specifying the nuclear size parameter, appearing, e.g., in some treatments as the M1 transition radius for the $^6Li(e,e')^6Li(3.56\ MeV)$ transition. Perhaps the most complete study of $\lambda_\gamma(1s)$ in this regard is that of Bergstrom (Ber 75), discussed below, who obtains 1.23×10^{15} sec^{-1}. In the same study the discrepancy with recently measured (Deu+ 74) photoproduction cross sections is nearly resolved, and all other data are satisfactorily described.

$\underline{\lambda_\gamma(2p)}$. Variations in the calculated values $(4.1\text{-}5.9)\times10^{10}$ sec^{-1} are due to differences in the amplitudes of the p^2 nuclear wave function, the p-shell harmonic oscillator parameter b, values of the A,B,C, coefficients, and distortion factors. The results are sensitive to b with larger b's reducing $\lambda_\gamma(2p)$.

From the entries in Table XII, one sees that the photon contributions R_s and R_p are nearly equal. The theoretical values most consistent with all the data on these states are $R_s = 0.166\pm0.039\%$ (Ber 75) and

R_p = 0.138±0.053% (MW 73), giving R_γ = 0.304±0.058%, in good agreement with the measurement 0.306±0.035% (Bae+ 73).

The above calculation of $\lambda_\gamma(1s)$ makes use of the unified analysis of weak and electromagnetic processes in nuclei advocated by Walecka (Wal 75) and others (e.g., DW 72, DW 73), an approach that has been pushed the farthest for the ^{6}Li - ^{6}He states under discussion. Central to this approach is to use electron scattering data to determine the so-called one-body nuclear densities, including their spatial distribution, and then to evaluate the matrix elements of any one-body operator in terms of these densities. The one-body operators are constructed from the appropriate free nucleon amplitudes. It is further assumed that the states of ^{6}Li can be described in terms of two p-shell valence nucleons moving around an inert ^{4}He-like core. With these restrictions, the ^{6}Li (g.s.) configuration amplitudes are determined by the experimental quadrupole and magnetic dipole moments, and the ^{6}Li(3.56) amplitudes by the measured M1 transition form factor. The measured momentum dependence in this form factor determines the spatial extent of the transition matrix element $\int R_f(r)\, R_i(r)\, j_2(qr)\, r^2 dr$ where $R_f(r)$ and $R_i(r)$ are the $\ell = 1$ radial nucleon wave functions of the excited and ground states, respectively, and j_2 is a spherical Bessel function. With the wave functions thus determined from the electromagnetic data, predictions can be made for other processes. The results of two such analyses are compared with the data in Table XIII. One sees that the predictions for β-decay and μ-capture are in good agreement with the data but that for (π^-,γ) and (γ,π^+) reactions there are some significant differences. The DW wave functions give $\lambda_\gamma(1s) = 1.67\times10^{15}$ sec^{-1} (Ver 74) and $a_{Li}/a_p = 0.12$ (KD 74) for the ratio

of ^{6}Li to proton photoproduction cross sections, Bergstrom (Ber 75) obtains 1.23×10^{15} sec^{-1} and 0.09, respectively, both in better agreement with the data. Bergstrom finds that the M1 transition form factor in the region $40 < q < 400$ MeV/c is not described well with a harmonic oscillator basis. Using a generalized model for the $\ell = 1$ radial transition density, he finds an rms transition radius of 3.3 to 3.4 F which is larger than the 3.1 F used by DW. This larger spatial extent has the effect of reducing $\lambda_\gamma(1s)$ and $\sigma(\gamma,\pi^+)$.

The good quantitative agreement with the large class of data given in Table XIII, establishes a predictive power for this phenomenological approach which is relatively rare in nuclear physics. It shows that the IA for radiative pion capture from the 1s orbit, using the effective Hamiltonian $A(\vec{\sigma}\cdot\hat{\varepsilon})\ \tau^+ e^{-i\vec{k}\cdot\vec{r}}\phi_\pi(\vec{r})$ with A determined on the free nucleon process and ϕ_π consistent with the pionic atom data, can be relied upon in making a prediction of $\lambda_\gamma(1s)$ to an accuracy of 10% or better. To achieve this level of accuracy, the radial extent of the initial and final nuclear state must be adequately determined through other reactions at momentum transfers spanning $q = m_\pi$.

The above phenomenological approach has been criticized by Vergados (Ver 74) on the grounds that the structure of the nuclear states as determined by the strong interactions between the six nucleons comprising these states is never dealt with. For example, he found that the ^{6}Li (3.56) wave function as determined by use of Kuo-Lee two-body matrix elements differs significantly with the DW wave functions in the amount of the $^3P_0$ component. This discrepancy is in large part removed by Bergstrom, who uses the DW approach, but finds wave functions similar to those of Vergados. These results emphasize the importance of achieving consistency

not only on the matrix elements of one-body operators, but also on the strong interaction two-body operators which enter in calculations of both structure and the cross sections for scattering nucleon projectiles.

6.4 ANALOGS OF GIANT M1 STATES

In 1963 Kurath suggested that in self-conjugate light nuclei there exists a concentration of magnetic dipole transition strength between T = 0 ground states and excited T = 1 states similar to the well known concentration of E1 strength in the GDR. The most direct observation of such M1 states was expected to be in 180° electron scattering since (e,e') cross sections at backward angles are dominated by the transverse magnetic transitions. Indeed much concentration of isovector M1 strength has now been observed in light nuclei (Fig. 13). The tendency to concentrate the transition strength reflects, of course, the basic correlations in the nuclear wave functions. Further study of these spin and isospin correlations in the neighboring $T_z = T_z(\text{target}) + 1$ nuclei is afforded by π^- and μ-capture reactions.

In the limit of zero momentum transfer and 1s-state capture, both π^- and μ-capture are completely governed by the Gamow-Teller (GT) operator $\vec{\sigma}\tau^+$. For $q \sim m_\mu$, Mukhopadhyay (Muk 73) has shown for μ-capture that terms other than GT matrix elements are small in the strong allowed transitions of a $(1p)^n$ shell model vector space. Specifically, the 1s capture rates $\lambda(\mu^- A \to A\nu_\mu)$ calculated with Cohen-Kurath (CK 65) intermediate coupling wave functions, show a single state dominating μ-capture in ^{6}Li, ^{10}B, ^{12}C, and ^{14}N. Experimental verification of these predictions is limited and

must necessarily be indirect, e.g., through observation of secondary and tertiary β- and γ-rays since the neutrino emitted in the primary interaction cannot be detected.

Radiative pion capture provides an excellent new probe for study of the analogs of M1 states since a precise measurement of the γ-ray energy identifies the nuclear state. One might expect a complication in that π's are captured predominantly from $\ell > 0$ orbits. In this case $\vec{q}$-dependent terms make large contributions (VB 72) to the capture rate which could mitigate the dominance of $\vec{\sigma}\,\tau^+$ matrix elements. However, when the pion momentum operator $\vec{q} = -i\vec{\nabla}$ operates on $\phi_{2p}(r)$, which has a nearly linear dependence on r through the nucleus, the B- and C- term matrix elements are dominated by $\vec{\sigma}\,\tau^+$ much the same as the A-term (MW 72, Ver 75). The D-term does not contain $\vec{\sigma}$, so it can excite only natural parity states. The E-term matrix elements are negligibly small for s- and p- state capture. Thus in light nuclei the π- capture transition rates should reflect quite closely the M1 correlations of the target nucleus.

Experimental confirmation of these expectations is given by the spectra of ^{6}Li, ^{10}B, ^{12}C, and ^{14}N. The p-shell capture probabilities range from $\sim$ 60% to $\sim$ 90% in these nuclei. Nonetheless, in each case the strongest transitions in the excitation region from the ground state up to the GDR are to the analogs of the well known M1 states: in ^{12}C, the 1^+ state at 15.1 MeV; in ^{6}Li the 0^+ state at 3.56 MeV; in ^{10}B the 2^+ state at 7.48 MeV; in ^{14}N the 2^+ states at 9.17 and 10.43 MeV. For ^{6}Li and ^{12}C shell model calculations are in excellent agreement with both the measured M1 rates and form factors and the (π^-,γ) branching ratio; good qualitative agreement is obtained on ^{10}B and ^{14}N, discussed in more detail below. Comparisons are given in

Table XI and the systematic trends are displayed in Fig. 13.

Several transitions were isolated experimentally in the recent study (Bae+ 75) of ^{10}B and ^{14}N. ^{10}B has a 3^+ g.s., therefore, isovector M1 transitions connect to 2^+, 3^+, and 4^+ T = 1 states, of which there are 25 with p^6 configurations. The electron scattering results (Fag 75) show the M1 strength to be largely contained in a single state, the 2_2^+ state at 7.48 MeV in ^{10}B. The (π^-,γ) reaction preserves much of this concentration of transition strength (Fig. 14). Furthermore, the first two excited states of ^{10}Be, at 3.4 and 6.0 MeV, can be resolved in the data, and branching ratios extracted which are quite free of background subtraction uncertainties. The measured values are $(2.5\pm0.4)10^{-4}$, $(4.4\pm0.7)^{-4}$, and $(10.5\pm1.3)10^{-4}$ for the 0^+, 2_1^+, and 2_2^+ states, respectively. Shell model calculations by Vergados (Bae+ 75) in a p^6 vector space and using Kuo-Lee 2-body interactions yield branching ratios $(3.6\pm0.7)10^{-4}$, $(8.5\pm1.7)10^{-4}$, and $(16.9\pm2.7)10^{-4}$, respectively (the uncertainties are due to the x-ray data). Thus the relative strengths are quite well accounted for, although the absolute values are high by $\sim$ 1.7. The data show additional strength to higher lying states in ^{10}Be (7-12 MeV), but because of the high level density this cannot be associated uniquely with specific states.

The M1 strength in ^{14}N is concentrated (90%) nearly equally between two states, 2_1^+ at 9.2 MeV and 2_2^+ at 10.4 MeV. The $^{14}N(\pi^-,\gamma)^{14}C$ data (Fig.14) show that the greatest strength does indeed go to the analogs of these states, with measured branching ratios $(7.7\pm0.9)10^{-4}$ and $(4.0\pm0.6)10^{-4}$, respectively. Shell model calculations (Bae+ 75) with p^{-2} configurations give $(24.3\pm2.7)10^{-4}$ and $(1.2\pm0.2)10^{-4}$, respectively, in poor agreement with the data. This discrepancy can be explained in terms of the $(sd)^2$

admixtures of Lie (Lie 72), whose wave functions for ^{14}N give a good description of nearly all data on states below 13 MeV. A weak-coupling scheme is used involving the low-lying eigenstates of p^{-2} and p^{-4} $(sd)^2$ model spaces diagonalized separately in the SU(3) basis. Results are that ^{14}N (g.s.) contains only 4% $(sd)^2$, but that the 2_1^+ and 2_2^+ states contain 49% and 56% respectively of $(sd)^2$. These admixtures merely cause a redistribution of the (π^-,γ) transition strength lying in the p^{-2} part of the wave function (the one body operator of (π^-,γ) transitions cannot connect the nearly pure p^{-2} g.s. with the $(sd)^2$ components of the 2^+ states). The total strength of the 2_1^+ state, $R_\gamma = 0.96\ (24.3)10^{-4}$ is distributed mainly into two fragments. Taking Lie's admixtures, this means 51% goes to the 2_1^+ state giving $R_\gamma = 11.9\times10^{-4}$, and 44% goes to the 2_2^+ state giving $R_\gamma = 10.3\times10^{-4}$, much closer to the measured values. This spreading of the M1 strength to two states is also consistent with the $^{14}N(\mu^-,\nu_\mu)^{14}C$ results as discussed by Mukhopadhyay (Muk 73).

Additional transition strength to higher states in ^{14}C has tentatively been identified with a 1^+ state at 11.3 MeV (Fig. 14) which appears (Fag 75) to have the largest M1 matrix element in ^{14}C. In view of the relatively large measured (π^-,γ) branching ratio of $(5.1\pm0.7)10^{-4}$ for this state, one might expect it to be a strong M1 state in ^{14}N. However, if this state is indeed nearly pure p^{-2} (Lie 72), the M1 matrix element to ^{14}N(g.s.) is quite small (Bae+ 75). Also, preliminary results (Ens+ 75) on $^{14}N(e,e')$ show no concentration of M1 strength in the E_x = 14 MeV region of ^{14}N. Clearly, higher resolution (π^-,γ) data would be of interest.

In Fig. 14 one sees that the transition $^{14}N(\pi^-,\gamma)^{14}C(g.s.)$ is very weak, as was anticipated by the $\sim 10^6$ hindrance of the β-decay between the same two states and by the small M1 transition density to the 2.313 MeV 0^+ state in ^{14}N (Ens+ 74). Shell model calculations overestimate both the (π^-,γ) and β-rates although small values are predicted (Bae+ 75, Table XI). The PCAC and soft-pion calculation for the 1s radiative capture yields the negligible small branching ratio of $R_s = 1.9\times10^{-9}$ (Table VII). Thus the observed branching ratio of $(3\pm2)10^{-5}$, if not equal to zero, is likely to be due to p-state capture.

6.5 ANALOGS OF THE GIANT-DIPOLE RESONANCE

Early interest in nuclear structure physics with the (π^-,γ) reaction was not with M1 state, but centered on the expected dominant role of the spin-isospin (si) components of the GDR (DMW 66, DE 66, AE 66). In the SU(4) classification (e.g.Wal 66) these states have L = 1, S = 1, $J^\pi = 0^-$, 1^-, 2^-, T = 1, and $T_z = 0, \pm 1$ relative to a $J^\pi = 0^+$ target nucleus. In this representation the si modes are distinct from the isospin i modes (L = 1, S = 0, T = 1) which give rise to the large E1 photoabsorbtion cross sections. Approximate validity of SU(4) symmetry for the GDR (based on an assumed weak spin dependence in the residual 2-body interaction) was proposed by Foldy and Walecka (FW 64) to account for total μ-capture rates. Both the S = 0 and S = 1 states are excited in μ-capture through the Fermi and GT operators, respectively. In inelastic electron scattering both modes are also seen and considerable effort has gone into interpreting cross sections on 1p- and sd-shell nuclei within, in this framework (e.g. DW 70). Perhaps the clearest example of si modes of the GDR is ^{12}C where the (e,e')

data show strong excitation of 1^- and 2^- states at 19.1 and ~23 MeV (Don+ 68). The 0^- component has not been found definitely. The identification of the 1^- and 2^- states as $\underset{\sim}{s}i$ vibrations, however, is not without ambiguity in ^{12}C (or other nuclei) since the energies of the 1^- states coincide closely with 1^- states populated in photoexcitation. Since the latter proceeds through the E1 operator $\vec{r}$, it cannot induce $(S = 0) \rightarrow (S = 1)$ transitions. If the states seen in (e, e') and photoabsorption are the same, considerable mixing of S = 0 and S = 1 states is indicated.

Since radiative μ-capture is dominated by the $\vec{\sigma}\tau^+$ operator, and has experimental advantages over μ-capture, it held promise for selectively investigating the analog $\underset{\sim}{s}i$ components of the GDR. This expectation was supported with the first high resolution (π^-,γ) spectrum on ^{12}C. The 2^- and 1^- states stand out clearly (Fig. 1) above the QF continuum and are identified with states in ^{12}C at 19.9 MeV and 23.7 MeV, respectively. The 1^- peak is probably a doublet, as discussed below, corresponding to the 1^- states in ^{12}C at 22.6 and 25.4 MeV. The dashed curve of Fig. 1c shows the spectrum calculated by Kelly and Überall (KU 68) using ^{12}C wave functions (KIA 67) tailored to describe the observed splitting of the E1 GDR into two 1^- components. When used to compute (π^-,γ) rates, they give a qualitative description of the data.

In the above calculation and in most subsequent ones, the distinction between $\underset{\sim}{s}i$ and $\underset{\sim}{i}$ modes is not explicitly maintained. Large shell model wave functions are used and here the distinctions occur in the elementary nucleon matrix elements. The (π^-,γ) operator has large spin-flip matrix elements (e.g. p 3/2 → 1d 3/2), and the E1 operator has large non spin-flip matrix elements (e.g. p 3/2 → d 5/2) (Ver 75b). However, the

characterization of the total nuclear wave function in terms of si and i components is not made. An exception is the calculation for ^{16}O discussed below.

The ^{12}C data first showed up the problem of separating the QF continuum from the resonance. In fact ^{12}C has turned out to be a favorable case, with the peaks standing out more clearly than in other 1p shell nuclei (Fig. 10). The data defines the resonance peak position quite precisely and the areas are only subject to ~ 30% uncertainty from the continuum subtraction. However, for ^{6}Li, ^{10}B and ^{16}O, the data do not define the resonances very well, with both positions and areas being quite uncertain. In ^{14}N a peak stands out corresponding to ^{14}C (20 MeV), but its area is not well defined. Notwithstanding this basic ambiguity in defining "resonance" capture, some semi-quantitative features on GDR excitations of 1p shell nuclei have been learned. The results for ^{14}N illustrate perhaps most completely the general features. A brief discussion of each case follows.

^{12}C. The shell model analysis of (π^-,γ), (μ^-, ν_μ), and E1 matrix elements by Skupsky (Sku 71) shows that three states dominate these processes: two 1^- levels calculated to be at 22.4 and 25.9 MeV in ^{12}C and one 2^- level at 20.6 MeV. The two 1^- states are largely responsible for the observed splitting of the dipole strength in photoexcitation. The 2^- level, not seen in photoabsorption, dominates μ-capture where its strength results entirely from the axial vector interaction. In π-capture all three transitions are strong. The calculated radiative branching ratio (Table XI) are $R_\gamma(1^-) = 0.19\%$ and $R_\gamma(2^-) = 0.28\%$; measured values are 0.159±0.016% and

0.185±0.019%, respectively. If no pole model subtraction is made for the 2^- state, one obtains 0.30% (Table XI) - much closer to the theoretical value. Generally speaking, Skupsky's calculation accounts quite well for the main features of the $^{12}C(\pi^-,\gamma)$ data, as well as that of μ-capture, electron scattering and photoexcitation.

^{16}O. The (π^-,γ) spectrum shows no single peak in the GDR region, although enhancement can be seen (Fig. 10) above the pole-model continuum. A fit to the data with the pole mode + 1 BW yields a peak position corresponding to $E_x(^{16}O)$ = 20.7 MeV and R_γ = 0.22% (Table XI). In ^{16}O (e, e'), a peak is seen (Sic+ 69) at E_x = 20.4 MeV with much of the strength attributed to a $J^\pi = 2^-$ state. This state was identified (Bis+ 72) as the analog of the above (π^-,γ) state. The ^{16}O photoabsorption data (Ber 73, BF 75) show no peak at this energy.

One of the motivations for performing the ^{16}O (π^-,γ) experiment was the suggestion by Murphy et al. (Mur+ 67) that spin-isospin quadrupole states (L = 2, S = 1, T = 1) should dominate the capture rates from 2p orbit. Since ~ 90% of the captures are from p orbits, it was hoped that evidence for these not-too-well-established collective modes could be found. Murphy et al. calculated 1.65% for the total strength of dipole and quadrupole states, which exceeds considerably the 0.22% attributed (Bis+ 72) to resonance capture. Although there are ambiguities in subtracting the QF continuum, the $^{16}O(\pi^-,\gamma)$ data lend little support to the proposed selective excitation of si quadrupole resonances.

Vergados extended the study of $^{16}O(\pi^-,\gamma)$ using large $1\hbar\omega$ and $2\hbar\omega$ shell model vector spaces and residual Kuo-Lee interactions. He finds that

for this doubly closed shell nucleus the distinction between i and si dipole modes can be maintained, since the matrix elements of the E1 operator $\vec{r}$ are large for different 1^- states than those of the $[rY^1 \otimes \sigma]_{J=1}$ operator characterizing si dipole modes. Furthermore, the capture rates $\lambda_\gamma(1s)$ and $\lambda_\gamma(2p)$ are large when the si matrix elements are large for 0^-, 1^-, and 2^- states. The strongest (π^-,γ) state is 2^- at $\simeq$ 21 MeV in ^{16}O, supporting the identification given by Bistirlich et al. (Table XI). The second strongest (π^-,γ) state is predicted to be the 2^- at 13.0 MeV in ^{16}O. This too is in agreement with the data, although the calculated branching ratio 0.38% is much larger than the measured value of 0.15±0.03%. The giant quadrupole states are predicted to be strongly excited (R_γ = 0.88% for the six strongest 1^+, 2^+, 3^+ states) and widely distributed in excitation energy (30-50 MeV). The latter result is certainly consistent with the data.

Szydlik and Werntz (SW 74) calculated the branching ratios for $^{16}O(\pi^-,\gamma)^{14}N$ using semi-phenomenological matrix elements calculated with $(1p)^{-1}(sd)^1$ wave functions (DW 72) and scaled to give agreement with (e, e') cross sections and μ^- capture rates; they obtain good agreement with the data (Table XI).

^{10}B The (π^-,γ) data exhibits little resolved structure in the GDR region and no clear separation between QF and resonance capture can be ascertained. The ^{10}B photo-absorption cross sections (HS 73) show two peaks at 20.1 and 23.1 MeV. The analogs in ^{10}Be are expected at ~ 18.7 and ~ 21.7 MeV. Since ^{10}B has a 3^+ ground state, these states must have $J^\pi = 2^-, 3^-, 4^-$. Spin-isospin dipole states can have $J^\pi = 1^-$ to 5^-. With this large span on J_f it is perhaps not surprising to observe

considerable fragmentation of the (π^-,γ) transition strength.

^{6}Li The GDR in the mass-6 system is not well concentrated, showing up as a very broad enhancement in the photo-absorption data (BS 75). The ^{6}Li (π^-,γ) ^{6}He spectrum is also broad. It is one of the few cases where the pole model does not fit well; 3-body phase space (Fig. 10) describes that data poorly. There is the suggestion of resonances at higher excitation energy, so the data was analyzed with three BW forms superimposed on the pole model, yielding (Bae+ 73): R_γ(15.6 MeV) = 0.14%, R_γ(23.7 MeV) = 0.28%, and R_γ(29.7 MeV) = 0.34% (E_x in ^{6}He). Supporting evidence for a resonance at ~ 23 MeV can be found in the mirror nucleus ^{6}Be (Ver+ 74) and in ^{6}Li at ~ 26 MeV (VCM 71). These studies identified this state with the ^{33}F (L = 3, T = 1, S = 1) predicted by Thomson and Tang (TT 69) at ~ 27 MeV in ^{6}Li. The ^{6}Li (π^-,γ) data gives the first evidence for this state in ^{6}He. The calculations of Vergados (Ver 74) show sizeable strength to 2^- and 3^- states in this excitation region, with R_γ (2^-, 24 MeV) = 0.2%, R_γ (3^-, 20 MeV) = 0.2%, and R_γ (3^-, 36 MeV) = 0.35%.

Vergados (Ver 75b) suggested that the strong excitation of states with $J_f = J_i + 2$ may be a general feature of the (π^-,γ) reaction. He finds that major contributions to the transition strength arise from the spherical tensor operator characterized (VB 72, Ver 75b) by J = 2, L = 1, S = 1, precisely what is needed to excite si dipole states with the highest allowed J (2^- in ^{12}C and ^{16}O, 3^- in ^{14}N and ^{6}Li). The statistical factor $(2J_f+1)/(2J_i+1)$ also favors the highest J_f. If the preferred excitation of states with $J_f = J_i + 2$ is indeed characteristic of the (π^-,γ) reaction, this property will be very useful in mapping out the spin-isospin

structure of the GDR since $J_f = J_i + 2$ states cannot be excited in E1 photoexcitation. The latter reaction has been the main source of data on the GDR.

^{14}N The data show a peak standing out above the continuum at $E_\gamma = 118$ MeV corresponding to $E_x(^{14}N) = 22.2$ MeV. The fit assuming the pole model + one BW gives a branching ratio of 0.205 + 0.020% for the resonance (Table XI). The $^{13}C(p,\gamma)^{14}N$ excitation function (ROP 71) shows a broad structure between 18 and 24 MeV, with prominent peaks at 22.1 and 22.6 MeV. Much of the observed (p,γ_0) strength is associated (ROP 71) with 2^- states.

Vergados (Ver 75a) calculated shell model wave functions for ^{14}N in a model space of the $1\hbar\omega$ excitations ($1p \rightarrow sd$, $1s \rightarrow 1p$). Within this space there are 20, 50, 56, 43, and 24 shell model components in the 0^-, 1^-, 2^-, 3^-, and 4^- $T = 1$ subspaces, respectively. The 0^-, 1^-, and 2^- wave functions could be tested in the comparison (Ver 75a) with the $^{13}C(p,\gamma)^{14}N$ data. The experimental E1 spectrum is fairly well described, although small shifts (1-2 MeV) in excitation energies are required.

The calculated (π^-,γ) branching ratios for ^{14}N are presented graphically in Fig. 15. As in photoexcitation, the calculated energies are lower by several MeV than the peaks in the spectra (Fig. 15a). The total radiative branching ratio to all negative parity states is 1.95%, with 0.06% to 0^- states, 0.42% to 1^- states, 0.66% to 2^- states, 0.73% to 3^- states, and 0.07% to 4^- states. A more complete comparison is given in Fig. 15b. The curves in this figure were obtained by: (a) assignment to each theoretical level a BW shape with FWHM = 1 MeV, (b) shifting all E_x up by 2.5 MeV (approximately the amount suggested by the photoexcitation

study), (c) folding the theoretical spectrum ($R_s + R_p$ vs E_γ)with the instrumental line shape and detection efficiency, and (d) normalizing the theoretical spectrum to the number of stopped pions. The resulting spectrum was multiplied by 0.4 to approximately fit the data in the GDR region. Thus the figure corresponds to R = 0.4(1.95) = 0.78% for the calculated negative parity states. The choice of the factor 0.4 is arbitrary. Clearly a factor < 1 is needed since the calculated branching ratio of 1.95% to $1\hbar\omega$ excitations is almost equal to the measured 2.13±0.21% for the total branching ratio. If the $1\hbar\omega$ states are associated with the BW contribution obtained in the fit to the data with the pole-model + BW, a reduction factor of 0.1 is needed.

Although the normalization cannot be settled until the central question of how to separate QF and resonance capture is settled, the qualitative features of Fig. 15b are quite interesting. (1) the 3^- states appear to be responsible for the observed peak at ^{14}C(20 MeV). These states cannot be reached by E1 transitions with ^{14}N(g.s.) and thus are difficult to observe in other reactions. The 0^- states are weak in both (p,γ) and (π^-,γ) reactions. The 4^- states, also not observed in E1 photoexcitation, are weak in (π^-,γ) capture. (2) The localization of $1\hbar\omega$ transition strength to E_x = 20±8 MeV is nicely emphasized in the figure. At lower E_x the $0\hbar\omega$ positive parity states account for most of the observed transition strength. At higher E_x, $2\hbar\omega$ positive parity excitations and QF capture account for much of the observed transition strength. With these features qualitatively understood, one hopes that the theoretical calculations will soon progress to where each of these components are separately described and a composite curve produced which will fit the entire experimental spectrum.

7. RESULTS ON MEDIUM MASS AND HEAVY NUCLEI

At present there exist few investigations of radiative π-capture in the broad reign of the periodic table from A = 17 to A = 238. Nonetheless, a few basic facts are established. (1) The total radiative branching ratios, 1-3% (Table III), are nearly the same as for light nuclei. Thus large reductions in counting rates will not be encountered in the future. This verifies the early theoretical estimate of Brueckner, Serber, and Watson (BSW 51) and more recent estimates (GE 70, Guy 72) for nuclei from ^{40}Ca to ^{208}Pb. (2) QF capture still constitutes a major fraction (70-95%) of the total capture rate as can be seen in the spectra of ^{24}Mg, ^{40}Ca and ^{209}Bi (Figs. 16, 17). The pole-model with the Q-value at the nucleus vertex treated as a free parameter describes this component quite well. This together with the good description of the data from ^{3}He to ^{16}O shows the pole model to be a rather useful parametrization of QF capture. (3) For the s-d shell nuclei ^{24}Mg and ^{40}Ca, there is appreciable transition strength ($R_\gamma \sim 0.3\%$) to the particle stable and low continuum states. For ^{209}Bi, this strength has nearly disappeared, with $R_\gamma < 5\times10^{-4}$.

Point (3) above provides a basis for anticipating that the (π^-,γ) capture reaction can be used to study structure of low-lying states (e.g., M1 and M2 states) in medium-mass nuclei. Since the transition strength is appreciable and the levels are narrow, the observed strength must be due to sharp lines, poorly resolved. The data of Fig. 16 (Bis+ 72) were recorded with targets of natural abundances, which in the case of Mg [^{24}Mg(79%), ^{25}Mg(10%), ^{26}Mg(11%)] might have obscured structure in the spectrum. ^{24}Mg is the only example thus far measured of a permanently deformed nucleus with a well-developed g.s. rotational band (EV 73), but this has not yet been related to the (π^-,γ) rates.

Study of the doubly closed shell nucleus ^{40}Ca would seem to be basic to establishing the usefulness of the (π^-,γ) reaction as a general tool of nuclear structure. Unfortunately, there is much fragmentation of the transition strength. The suggestion of a peak can be seen at $E_x(^{40}K) = 7.4$ MeV; the analog in ^{40}Ca is at $E_x \sim 15$ MeV. The photoabsorption data (ACK 66, BS 64) on ^{40}Ca have a peak 19.5 MeV (GDR) and negligibly small cross sections at 15 MeV, thereby demonstrating little relation of the GDR to the 7.4 MeV state. The $^{40}Ca(e,e')$ studies of the 15 MeV region are inconclusive (see e.g., survey given in Ref. (Übe 71)), although this would appear to be the most promising reaction for observing this state in ^{40}Ca and relating it to the (π^-,γ) state. In regard to the distribution of (π^-,γ) strength, Guy and Eisenberg (GE 70) show that simple 1p-1h wave functions predict considerable fragmentation, although 44% of the 1^- strength goes to two states at 14.9 MeV and 12.8 MeV in ^{40}Ca, which perhaps is related to the peak in the spectrum. More detailed discussions of ^{40}Ca and ^{24}Mg are not possible at present. In view of the tentative structure observed in the $^{40}Ca(\pi^-,\gamma)$ spectrum, and since ^{40}Ca is particular important to shell model studies, taking additional, higher resolution, data would seem to be worthwhile.

7.1 $^{209}Bi\,(\pi^-,\gamma)^{209}Pb$ AND OBSERVATION OF A NEW COLLECTIVE STATE

Examination of the photon spectrum for ^{209}Bi (Fig. 17) shows that there is little transition strength to the pure single-particle states of ^{209}Pb at $E_x = 0$-4 MeV. Considerable strength is observed at 120-130 MeV (6-16 MeV excitation in ^{209}Pb) and there is a peak at $E_\gamma \sim 129$ MeV. The curves shown in Fig. 17b and the R_γ given in Table XIV correspond to the fit using the pole-model with $\Delta = 16$ MeV, a fixed line width (Γ_1) of zero for the peak at ~ 129 MeV, and a BW form of variable width (Γ_2) and position

to describe the data between the endpoint of the pole-model continuum and the line at E_x = 7.9±0.4 MeV. The latter serves primarily to extract a branching ratio for the total strength to this region and to define a background under the line, and cannot be regarded as evidence for a single "resonance" excitation in this region. By making reasonable variations on Δ, it is found that the range of BW parameters E_x = 11-15 MeV and Γ_2 = 1-4 MeV are consistent with the data.

To relate the extracted branching ratios to calculated transition rates, the x-ray data must be examined directly since capture schedules have not been published for heavy nuclei. The measured broadening of 1.7±0.5 keV (Sch+ 68) for the 5g → 4f x-ray line and the yield Y(5g → 4f) = 0.42±0.05 (Kun 69) establish that a sizeable fraction of the captures occur from the 4f orbit. The additional information

$$\lambda^{e.m.}\ (5g \rightarrow 4f)/\lambda_a(5g) = 5.76\times10^{16}\ \mathrm{sec}^{-1}/5.93\times10^{15}\ \mathrm{sec}^{-1} = 9.7$$

and

$$\lambda^{e.m.}\ (4f \rightarrow 3d)/\lambda_a(4f) = 1.77\times10^{17}/(2.6\pm0.8)10^{18} = 0.07\pm0.02$$

(Bae+ 74) shows that 4f captures dominate over 5g and 3d captures. If the above ratios hold for orbits of higher n with same ℓ (Sec. 3) most of the captures must occur from nf orbits. It is expected that some capture takes place from $\ell = 0$, 1, and 2 orbits following the assumption (EK 61) of a statistical $(2\ell + 1)$ population as the initial condition in the pionic cascade; however, this fraction is small under the usual assumptions for an initial n(n = 14 (EK 61)). Thus the radiative branching ratios should be given quite accurately by summing over f orbits. By taking $\lambda_\gamma(nf)/\lambda_a(nf)$ to be independent of n, the comparison of experiment and theory for

^{209}Bi can be made by using $R_\gamma = \lambda_\gamma(4f)/\lambda_a(4f)$ with the experimental $\lambda_a(4f) = (2.6\pm0.8)\ 10^{18}\ sec^{-1}$ (Sch+ 68).

The calculated values of λ_γ given in Table XIV for the single particle transitions were computed with hydrogenic wave functions. Comparing such wave functions with optical-model wave functions, Lucas and Werntz (LW 74) deduced the distortion correction factors C(5g) = 1.38±0.20 and C(4f) = 1.14±0.15. The latter was applied to compute the values of R_γ in the table. The theoretical branching ratio $(0.30\pm0.09)10^{-4}$ for the summed strength to seven single-particle transitions is in good agreement with the measured value $(0.36\pm0.18)10^{-4}$.

State at 7.9 MeV. The two classes of shell-model configurations excited in ^{209}Bi(π^-,γ) are illustrated in Fig. 18: (i) those obtained by promoting the $1h_{9/2}$ proton to an unoccupied neutron orbital. These are the single-particle transitions going up to 4.25 MeV in ^{209}Pb for which transition rates are given in Table XIV (ii) transitions in which the $1h_{9/2}$ proton remains intact but one of the protons in the closed shells $j_2(N\leq4)$ is promoted into a neutron shell $j_1(N\geq6)$ resulting in configurations

$$|[j_1(n)j_2^{-1}(p)]\ J_1;\ 1h_{9/2}(p);\ J\rangle,$$

where J_1 in the angular momentum of the created p-h pair and J the total angular momentum of the state (doorway state). Such states are strongly mixed in the residual nucleus, possibly giving collective modes. It is not yet clear which type of collectivity is favored in (π^-,γ) on a heavy nucleus. In an effort to explain the peak at E_x = 7.9±0.4 MeV, one might consider: (a) collective states built on the ^{209}Pb ground state such as

the GDR, isoscaler quadrupole states GQR (LB+ 72), and M1 states; and (b), isovector collective modes built on the ^{209}Bi ground state, such as isovector quadrupole states, whose $T_>$ components would then be observed in ^{209}Pb. The evidence for these various collective modes was recently reviewed by Satchler (Sat 75) and theoretical treatments are given by Bohr and Mottelson (BM 75). Isovector and isoscaler quadrupole states are specifically treated by Bes, Broglia, and Nilsson (BBN 75). A level diagram illustrating the relevant states in ^{209}Bi-^{209}Pb is shown in Fig. 19.

The M1 states built on ^{209}Pb(g.s.) have the form

$$|2g_{9/2}(n) \otimes 1_2^+; J^\pi\rangle , \; J^\pi = 7/2^+, 9/2^+, 11/2^+,$$

where 1_2^+ is the M1 state in ^{208}Pb (illustrated in Fig. 18) given approximately by (Ver 71)

$$|1_2^+\rangle \simeq -0.62\,|h_{9/2}(p)\; h^{-1}{}_{11/2}(p)\rangle + 0.78\,|i_{11/2}(n)\; i^{-1}{}_{13/2}(n)\rangle .$$

The proton component of this state contains configurations of type (ii). The transition rates to all three states were calculated, giving $\lambda_\gamma(4f) = 2.6\times10^{12}$ sec^{-1} and $\lambda_\gamma(5g) = 1.1\times10^{10}$ sec^{-1}(Bae+ 74). Since these are less than the single-particle transitions in Table XIV, the (π^-,γ) peak does not seem to be related to M1 states, and in particular not to the 7.9 MeV state observed (Fag 75) in ^{208}Pb(e,e').

The GDR and GQR excitations built on the ^{209}Pb (g.s.) (states $g_{9/2}\otimes|L\rangle$ where $|L\rangle$ represents a collective p-h excitation of angular momentum L) have $T \geq 45/2$ and $\pi = (-1)^L$. By examining the possible p-h configurations in such wave functions, one sees that the number of components of type (ii) is greatly restricted by the condition that j_1 must be $2g_{9/2}$. In view of the established weakness of the single particle transitions, it is difficult to see how these

collective states, built on ^{209}Pb(g.s.), could produce strong transitions.

To find ^{209}Pb states that could lead to considerable coherence in the transition amplitudes due to close parentage to configurations (ii), one must look at the $T_>$ collective states built on ^{209}Bi(g.s.). The analog of a state at 7.9 MeV in ^{209}Pb is at ~ 26.5 MeV in ^{209}Bi (Coulomb displacement energy = 18.8 MeV (SZB 72)) – a relatively unexplored region of the continuum. The $T_>$ component of the GDR can be eliminated immediately, since this is virtually non-existent in nuclei with large neutron excess. An interesting possibility is the $T_>$ component of an isovector quadrupole excitation, which can exist since it is formed by $2\hbar\omega$ excitations, available to both neutrons and protons. Theoretical estimates (BBN 75, BM 75) for the energies of isovector quadrupole states vary by several MeV, with $135A^{-1/3}$ = 23 MeV being a typical value (BM 75). Thus, on the basis of excitation energy it would appear that the identification of the 7.9 MeV state as the analog of a $T_>$ component of the GQR of ^{209}Bi is not unreasonable. To estimate the possible (π^-,γ) strength to such a state, the λ_γ (4f) rates to all type (ii) doorway states (Fig. 18) with neutron-particle, proton-hole states coupled to $J_1 = 1^+$, 2^+, and 3^+ and $J^\pi = J_1^\pi \otimes 1h_{9/2} = 3/2^-, \cdots, 15/2^-$ were calculated. The summed rate $\Sigma\, \lambda_\gamma$ (4f) = 84×10^{13} sec^{-1}, gives $R_\gamma = (3.7\pm1.1)\times10^{-4}$ (Bae+ 74), where the indicated uncertainty is from the x-ray data and distortion factor. The experimental value is $(4.7\pm0.7)\times10^{-4}$ assuming the background shown in Fig. 17b. Notwithstanding the uncertainties in both the experimental and theoretical numbers, the calculation does demonstrate that the strength necessary to excite an isovector GQR can be obtained from the possible

doorway states,

Supporting evidence for the existence of the above collective and relatively narrow state is given by the recent (n,p) reaction studies of Kind et al. (Kin+ 75). These studies have shown the close correlation existing in (n,p) and (π^-,γ) reactions in the types of nuclear states excited. The levels that stand out in the (n,p) reactions at momentum transfers q = 50 to 400 MeV/c on ^{6}Li, ^{12}C, and ^{14}N are the ones that stand out in the (π^-,γ) reaction. The first comparison for heavy nuclei is made here on ^{209}Bi. It is indeed remarkable that the ^{209}Bi(n,p) ^{209}Pb spectrum (Fig. 20) shows a peak at E_x (^{209}Pb) = 8.1±0.5 MeV in close agreement with the 7.9±0.4 MeV of the (π^-,γ) data. The peak in Fig. 20b, which remains after subtraction of the QF component as given by 3-body phase space (^{208}Pb(g.s.) + n + p), has a width of 2.5 MeV(FWHM). This is approximately the resolution in the experiment; therefore, the level width is $\lesssim$ 2 MeV. This too is consistent with the 0-3 MeV of the (π^-,γ) data. Data (Kin+ 75) at other angles show correct kinematic tracking for this peak, thereby ruling out the possibility that it comes from a low-mass target impurity. The measured laboratory differential cross-section at T_n = 56 MeV and θ_{lab} = 15.5° is 1.4±0.2 mb/sr, using the peak area shown in Fig. 20b. The momentum transfer q = 89 MeV/c at this angle is not too different from the q = 129 MeV/c of the (π^-,γ) reaction. Measurement of the complete angular distribution and comparison with DWBA calculations may give an indication of the multipolarity - a most welcome piece of additional information. The data of Fig. 20 also demonstrate that the (n,p) transitions to the single-particle states of ^{209}Pb are weak. Thus, as with (π^-,γ), it

appears that the observed peak must be due to a collective state, most probably the $T_>$ component of a state built on ^{209}Bi and having an excitation energy of ~ 26.5 MeV.

This region of ^{209}Bi was investigated by Snover et al. (Sno+ 74) with the ^{208}Pb(p,γ) capture reaction in which deexcitation γ-rays for E_p = 17.5 - 25.0 MeV were measured. The coefficients of the Legendre-polynomial-fits to the γ-ray angular distributions show resonances through the GDR region as well as an additional resonance at E_x ~ 23.7 MeV having a width Γ ~ 3.5 MeV. The authors identify the latter with a possible isovector quadrupole resonance. Electron scattering data systematics (^{208}Pb,(NT 73)) were used to eliminate the M1 multipolarity. Although it is premature to identify the (p,γ) "resonances" as the parent analog of the (p,n) and (π^-,γ) state, the excitation energy difference of ~ 2.8 MeV is probably not sufficient to rule out the correspondence since it depends to some extent on assumed backgrounds in the data analyses and on the use of a Coulomb energy measured for lower energy states. The isospin was not determined in the (p,γ) study, but if it is $T_<$, the correspondence is of course ruled out.

If indeed some $(GQR)_{T_>}$ strength in ^{209}Bi is concentrated into a relatively narrow excitation region near 26.5 MeV, it would not be surprising to see it in charge exchange (π^-,γ) and (n,p) reactions based on what is known about these reactions. Clearly there is a significant advantage in studying such states in ΔT_z = + 1 reactions, since only the $T_>$ components are populated. Also, one observes them in regions of lower level densities and decay widths. In ^{209}Pb, the 7.9 MeV state is only 4 MeV above the neutron emission threshold (Fig. 19); furthermore, its

neutron-particle, proton-hole configuration, prohibits direct decay to $^{208}Pb(g.s.) + n$. The fact that perhaps some $T_>$ components of isovector collective states may be quite narrow, as demonstrated here for ^{209}Bi - ^{209}Pb, is of course a surprising, interesting, and unexplained result.

8. CONCLUSIONS AND OUTLOOK

If one views the early work on hydrogen and deuterium by Panofsky and collaborators at the 184" cyclotron in Berkeley from the perspective of this article-the (π^-,γ) reaction as a tool for quantiative nuclear structure studies - then the major accomplishments of this first period were in the great clarification on the nature of the probe: its spin-isospin-parity selection rules and the s-wave π-N coupling strength. The nature of the $\gamma N \rightleftarrows \pi N$ transition operator, particulary that $A(\vec{\sigma}\cdot\hat{\varepsilon})$ dominates near threshold, also emerged in this period from the interpretation of the π-capture experiments and the concurrent photoproduction studies.

The second period, delayed by nearly 15 years as many physicists shifted interests to higher energy reactions, began with the measurements of Petrukhin and Prokoshkin at Dubna and Davies et al. at Liverpool which showed that the radiative branching ratio is 1-3% throughout the periodic table. The publication in 1970 by Bistirlich et al. of the ^{12}C data showing fine structure in the photon spectrum near 120 MeV gave clear evidence that the (π^-,γ) reaction is selective to nuclear structure. An electron-positron pair spectrometer with optical spark chambers was employed to achieve a resolution of 2 MeV (FWHM) at 130 MeV. The continuing work in the six years since then has considerably elaborated on the possibilities for nuclear structure studies. Selective excitation of M1,M2, and GDR spin-isospin states was demonstrated. The possibility of uncovering new facets of nuclear structure, as e.g., in the new collective state in ^{209}Bi, was realized. The theoretical analysis of (π^-,γ) reactions on complex nuclei was initiated in this period and brought to its present level where modern shell model wave functions are employed together with the full IA Hamiltonian as

determined on the nucleonic process. The rather precise agreement between experiment and theory achieved for transitions in ^{3}He, ^{6}Li, ^{10}B, ^{12}C, ^{14}N, and ^{16}O has established a quantitative basis for this new probe comparable to that of weak- and electromagnetic-interaction probes.

The third phase, generated by the construction of meson factories and new high intensity electron linacs, is just getting underway. A welcome new feature will be the availability of data on the inverse reaction (γ,π), which offers the possibility of momentum-transfer-variation starting near $q = 0$, as well as selecting π's in all three charge states. The fixed-q studies of π-capture - which were necessary to first demonstrate that in fact this reaction is useful for nuclear structure investigations - will be greatly expanded with the anticipated x $(10^2 - 10^3)$ increase in π^- stopping densities and the use of multiwire proportional chambers in pair spectrometers (permitting event rates close in 100/sec.) Thus spectra with 10^4-10^5 events should be obtainable in running times of several hours, and resolutions approaching 0.5 MeV are anticipated. The combined improvement in counting statistics and resolution should sharpen considerably the spectroscopy of nuclear states in the low-excitation region and help in distinguishing resonance from quasi-free capture in the 10 to 40 MeV region. Clearly, some of the data taken in phase two, e.g., on ^{40}Ca and ^{209}Bi, should be repeated, and more data should be taken on all regions of the periodic table. The region above $A = 40$ is virtually unexplored.

In addition to the improved spectra, new types of data should be forthcoming. Among these are K_α - γ coincidence spectra. Such direct measurements of 1s radiative branching ratios and photon spectra will reduce the uncertainties in comparisons with theory. Also possible will be in the measurements of particle-γ correlations where the photons are detected

with high resolution. Differences in the neutron-γ correlation for quasi-free and resonance capture may give a means to distinguish these components, and thereby help solve this basic problem left from phase two. Accompanying the improvement in the quality and types of data, one would expect progress in the theoretical interpretation-perhaps culminating in a quantitative treatment of the complete radiative absorption channel based on a microscopic description of the nuclear structure.

ACKNOWLEDGMENTS

The authors wish to thank Drs. John Vergados and Carl Werntz for critically reading various sections of this article and for many enlightening discussions. We thank Dr. Nick King for communicating the unpublished ^{209}Bi(n,p) data and for permission to display them here. We are grateful to Mr. James Bistirlich for rendering invaluable assistance in all phases of the LBL studies, and for his help in the preparation of this manuscript.

REFERENCES

ACK 66 D. W. Anderson, B. C. Cook, and J. A. Kadlecek, Nucl. Phys. 83:584 (1966).

Ada+ 66 M. I. Adamovich, V. G. Larionova, A. I. Lebedev, S. P. Kharlamov, and F. R. Yagudina, Sov. Jour. Nucl. Phys. 2:95 (1966).

M. I. Adamovich, E. G. Gorzhevskaya, V. G. Larionova, V. M. Popova, S. P. Kharlamov, and F. R. Yagudina, Zh. Eksp. Teor. Fiz. 38:1078 (1960), [Sov. Phys. JETP 11:779 (1960)].

E. L. Goldwasser, G. Ascoli, U. E. Kruse, J. C. H. Park, J. D. Simpson, W. P. Swanson, and T. S. Yoon, Proc. 12th Int. Conf. on High Energy Physics, ed. Ya. A. Smorodinskii (Vol. I) Dubna (1964), 858.

W. P. Swanson, D. C. Gates, T. L. Jenkins, and R. W. Kenney, Phys. Rev. 137:B1188 (1965).

Ada+ 68 M. I. Adamovich, V. G. Larionova, S. P. Kharlamov, and F. R. Yagudina, Sov. Jour. Nucl. Phys. 7:360 (1968), ibid. 7:643 (1968).

Ada+ 69 M. I. Adamovich, V. G. Larionova, S. P. Kharlamov, and F. R. Yagudina, Sov. Jour. Nucl. Phys. 8:685 (1969); ibid. 9:496 (1969).

AE 66 D. K. Anderson and J. M. Eisenberg, Phys. Letters 22: 164 (1966).

AJ 74 D. K. Anderson and D. A. Jenkins, in Nuclear Spectroscopy and Reactions, Part B (J. Cerny, ed.), Academic Press, New York and London, (1974), p. 457.

AL 72 S. Almehed and C. Lovelace, Nucl. Phys. B40:157 (1972).

Ama 63 R. D. Amado, Phys. Rev. 132:485 (1963).

ASL 74 F. Ajzenberg-Selove and T. Lauritsen, Nucl. Phys. A227: 1 (1974).

Bac 70 G. Backenstoss, Annual Review of Nuclear Science, 20:467 (1970).

Bac+ 73 G. Backenstoss, I. Bergstrom, J. Egger, R. Hagelberg, C. J. Herrlander, H. Koch, H. P. Dovel, R. H. Price, A. Schwitter, and L. Tauscher, Nucl. Phys. B66:125 (1973).

Bac+ 74 G. Backenstoss, J. Egger, T. von Egidy, R. Hagelberg, C. J. Herrlander, H. Koch, H. P. Povel, A. Schwitter, and L. Tauscher, Nucl. Phys. A232:519 (1974).

Bae+ 73 H. W. Baer, J. A. Bistirlich, K. M. Crowe, N. de Botton, J. A. Helland, and P. Truöl, Phys. Rev. C8:2029 (1973).

Bae+ 74 H. W. Baer, J. A. Bistirlich, N. de Botton, S. Cooper, K. M. Crowe, P. Truöl, and J. D. Vergados, Phys. Rev. C10:1140 (1974).

Bae+ 75 H. W. Baer, J. A. Bistirlich, N. de Botton, S. Cooper, K. M. Crowe, P. Truöl, and J. D. Vergados, Phys. Rev. C12:921 (1975).

Ban 64 M. Bander, Phys. Rev. 134:B1052 (1964).

Bay+ 75 W. Bayer et al., Submitted to Nucl. Phys. B.

BBN 75 D. R. Bes, R. A. Broglia, and B. S. Nilsson, Physics Reports 16:1 (1975).

BC 73 H. W. Baer and K. M. Crowe, in Int. Conf. on Photonuclear Reactions and Application, Asilomar 1973 (B. L. Berman, ed.) Lawrence Livermore Laboratory CONF-730301, 1973, p. 599.

BCC 73 D. V. Bugg, A. A. Carter, and J. R. Carter, Phys. Letters B44:278 (1973).

BDW 67 F. A. Berends, A. Donnachie, and D. L. Weaver, Nucl. Phys. B4:1 (1967).

Ben+ 56 M. Beneventano, G. Bernardini, D. Carlson-Lee, G. Stoppini, and L. Tau, Nuo. Cim. 4:323 (1956).

R. S. White, M. J. Jacobson, and A. G. Schulz, Phys. Rev. 88:836 (1952).

W. R. Hogg, E. H. Bellamy Proc. Phys. Soc. (London) 72:895

D. Carlson-Lee, Bull. Am. Phys. Soc. 3:334 (1958)

J. G. Ruthergeen, J. K. Walker Proc. Phys. Soc. (London) 76:430 (1960).

Ber 73 B. L. Berman, Atlas of Photoneutron Cross Sections Obtained with Monoenergetic Photons, Lawrence Livermore Laboratory Report, UCRL-74622 (1973).

Ber 75 J. C. Bergstrom, Nucl. Phys. 000:000 (1976), and private communication.

BF 75 B. L. Berman and S. C. Fultz, Rev. Mod. Phys. 47:713 (1975).

Bis+ 70a J. A. Bistirlich, K. M. Crowe, A. S. L. Parsons, P. Skarek, P. Truöl, and C. Werntz, Phys. Rev. Lett. 25:950 (1970); see also (Bis+ 72).

Bis+ 70b J. A. Bistirlich, K. M. Crowe, A. S. L. Parsons, P. Skarek, and P. Truöl, Phys. Rev. Lett. 25:689 (1970); see also (Bis+ 72).

Bis+ 70c J. A. Bistirlich, K. M. Crowe, A. L. Parsons, P. Skarek, and P. Truöl, in: High Energy Physics and Nuclear Structure (S. Devons, ed.) Plenum, New York, 1970, p. 877.

Bis+ 72 J. A. Bistirlich, K. M. Crowe, A. S. L. Parsons, P. Skarek and P. Truöl, Phys. Rev. C5:1867 (1972).

Bis+ 75 J. A. Bistirlich, S. Cooper, K. M. Crowe, E. R. Grilly, J. P. Perroud, R. H. Sherman, F. T. Shively, H. W. Baer, and P. Truöl, contribution to VI International Conf. on High Energy Physics and Nuclear Structure, Santa Fe (1975). Los Alamos Report, LA-6030-6, p. 180, and to be published.

Bis+ 76 J. A. Bistirlich, S. Cooper, K. M. Crowe, E. R. Grilley, R.H. Sherman, F. T. Shively, H. W. Baer and P. Truöl, Lawrence Berkeley Laboratory Report, LBL-4268; and to be published.

BKS 65 M. M. Block, J. B. Kopelman, and C. R. Sun, Phys. Rev. 140: B143 (1965).

Blo+ 63 M. M. Block, T. Kikuchi, D. Koetke, J. Kopelman, C. R. Sun, R. Walker, G. Culligan, V. L. Telegdi and R. Winston, Phys. Rev. Lett. 11:301 (1963).

BM 69 A. Bohr and B. R. Mottelson, Nuclear Structure, Vol. 1, (Benjamin, New York, 1969), p. 324.

BM 75 A. Bohr and B. R. Mottelson, Nuclear Structure, Vol. 2, (Benjamin, New York, 1975), p. 513.

BS 64 J. E. E. Baglin and B. M. Spicer, Nucl. Phys. 54:549 (1964).

BSW 51 K. Brueckner, R. Serber, and K. Watson, Phys. Rev. 81:575 (1951).

Can+ 74 F. Cannata, B. A. Lamers, C. W. Lucas, A. Nagl, H. Überall, C. Werntz, and F. J. Kelley, Can. J. Phys. 52:1405 (1974).

CDK 64 R. C. Cohen, S. Devons, and A. D. Kanaris, Nucl. Phys. 57:255 (1964).

CE 74 Il-Tong Cheon and T. von Egidy, Nucl. Phys. A234:401 (1974).

Che+ 57 G. F. Chew, M. L. Goldberger, F. E. Low, and Y. Nambu, Phys. Rev. 106:1345 (1957).

CK 65 S. Cohen and D. Kurath, Nucl. Phys. 73:1 (1965).

CLW 74 F. Cannata, C. W. Lucas, C. Werntz, Phys. Rev. Lett. 33:1316 (1974).

Coc+ 61 V. T. Cocconi, T. Fazzini, G. Fidecaro, M. Legros, N. H. Lipman, and A. W. Merrison, Nuovo Cimento 22:494 (1961).

CP 54 K. M. Crowe and R. H. Phillips, Phys. Rev. 96:470 (1954).

CS 55 W. Chinowsky and J. Steinberger, Phys. Rev. 100:1476 (1955).

CT 74 K. M. Crowe and P. Truöl, in Nuclear Spectroscopy and Reactions, Part B (ed. J. Cerny), Academic Press, New York and London, p. 493.

DD 69 S. Devons and I. Duerdoth, in Advances in Nuclear Physics, Vol. 2 (M. Baranger and E. Vogt, eds.), Plenum Press, New York (1969), p. 295.

DE 66 J. Delorme and T. E. O. Ericson, Phys. Letters 21:98 (1966).

DEF 75 J. Delorme, M. Ericson, and G. Fält, Nucl. Phys. A240:493 (1975).

Del 70 J. Delorme, Nucl. Phys. B19:573 (1970).

Deu+ 68 J. P. Deutsch, L. Grenacs, P. Igo-Kemenes, P. Lipnik and, P. C. Macq, Phys. Lett. 26B:315 (1968).

Deu+ 74 J. Deutsch, D. Favart, R. Prieels, B. Van Ostaeyen, G. Audit, N. de Botton, J.-L. Faure, Cl. Schule, G. Tamas, C. Tzara, Phys. Rev. Lett. 33:316 (1974).

DFK 75 J. Delorme, A. Figureau and M. Krell, to be published; (private communication).

DMW 66 H. Davies, H. Muirhead and J. N. Woulds, Nucl. Phys. 78:673 (1966).

Don+ 68 T. W. Donnelly, J. D. Walecka, I. Sick, and E. B. Hughes, Phys. Rev. Lett. 21:1196 (1968).

DP 68 L. G. Dakhno and Yu. D. Prokoshkin, Yadern. Fiz. 7:565 (1968) [transl.: Soviet J. Nucl. Phys. 7:351 (1968)].

DS 66 A. Donnachie and G. Shaw, Annals of Phhysics 37:333 (1966).

DW 70 T. W. Donnelly and G. E. Walker, Annals of Physics 60:209 (1970).

DW 72 T. W. Donnelly and J. D. Walecka, Phys. Letters 41B:275 (1972).

DW 73 T. W. Donnelly and J. D. Walecka, Phys. Letters 44B:330 (1973).

EF 67 M. Ericson and A. Figureau, Nucl. Phys. B3:609 (1967).

EF 69 M. Ericson and A. Figureau, Nucl. Phys. B11:621 (1969).

EK 61 Y. Eisenberg and D. Kessler, Nuovo Cimento 19:1195 (1961).

Ens+ 74 N. Ensslin, W. Bertozzi, S. Kowalski, C. P. Sargent, W. Turchinetz, C. F. Williamson, S. P. Fivozinsky, J. W. Lightbody and S. Penner, Phys. Rev. 9C:1705 (1974).

Ens+ 75 N. Ensslin, private communication on experimental runs subsequent to publication of Ref. (Ens+ 74).

ER 72 M. Ericson and M. Rho, Phys. Reports 5C:57 (1972).

EV 73 P. M. Endt and C. Van der Leun, Nucl. Phys. A214:1 (1973).

Fag 75 L. W. Fagg, Rev. Mod. Physics 47:683 (1975).

FE 70 L. P. Fulcher and J. M. Eisenberg, Nucl. Phys. B18:271 (1970).

FH 75 S. Fiarman and S. S. Hanna, Nucl. Phys. A251:1 (1975).

FW 64 L. L. Foldy and J. D. Walecka, Nuovo Cimento 34:1026 (1964).

GE 70 R. Guy and J. M. Eisenberg, Phys. Lett. 33B:137 (1970).

GGS 75a W. R. Gibbs, B. F. Gibson, G. J. Stephenson, Phys. Rev. C11:90 (1975).

0 0 0 0 4 4 0 8 5 9 3

GGS 75b W. R. Gibbs, B. F. Gibson and G. J. Stephenson, VI. Int. Conf. on High Energy Physics and Nuclear Structure, Santa Fe (1975), Los Alamos Report, LA-6030-6, p. 63.

GK 68 D. Griffiths and C. W. Kim, Phys. Rev. 173:1584 (1968).

GP 75 S. S. Gershtein and L. I. Ponomarev, in Muon Physics, Vol. III (eds., V. H. Hughes and C. S. Wu) Academic Press, New York, p. 141.

Guy 72 R. Guy, Nuovo Cimento 11A:1006 (1972).

Had+ 65 R. P. Haddock, R. M. Salter, M. Zeller, J. B. Czirr and D. R. Nygren, Phys. Rev. Lett. 14:318 (1965).

Hil+ 70 H. Hilscher, W.-D. Krebs, G. Sepp, and V. Soergel, Nucl. Phys. A158:584 (1970).

Hol+ 72 G. von Holtey, G. Knop, H. Stein, J. Stumpfig, and H. Wahlen, Phys. Letters B40:589 (1972).

HS 73 R. J. Hughes and B. M. Spicer, in: Int. Conf. on Photonuclear Reactions and Applications, Asilomar California, 1973, (B. L. Berman, ed.) Lawrence Livermore Laboratory CONF-730301, 1973, p. 153.

Hut+ 68 R. M. Hutcheon, T. E. Drake, V. W. Stobie, G. A. Beer, and H. S. Caplan, Nucl. Phys. A107:266 (1968).

Jur 72 For a complete review see e.g., A. Jurewicz, Photoproduction of Pions on Nucleons in the $\Delta(1236)$ Resonance Region, Frascati Report LNF-72155 (1972).

Käl 64 G. Källen, Elementary Particle Physics, Addison-Wesley, 1964.

KD 73 J. H. Koch and T. W. Donnelly, Nucl. Phys. B64:478 (1973) and Phys. Rev. C10:2618 (1974).

KE 69 M. Krell and T. E. O. Ericson, Nucl. Phys. B11:521 (1969).

KIA 67 M. Kamimura, K. Ikeda, and A. Arima, Nucl. Phys. A95:219 (1967).

Kim 71 Y. S. Kim, Mesic Atoms and Nuclear Structure (North-Holland, Amsterdam, 1971).

Kin+ 75 N. S. P. King, F. P. Brady, M. McNaughton, and J. Morales, Crocker Nuclear Lab. Annual Report, UCD-CNL 186, 1975, University of California, Davis; and N. S. P. King, private communication (1975).

Klo 64 P. K. Kloeppel, Nuovo Cimento 34:11 (1964).

KOS 68 M. Kawaguchi, H. Ohtsubo and Y. Sumi, Prog. Theor. Physics Suppl. (Kyoto), Extra No. 28, (1968).

KP 65 C. W. Kim and H. Primakoff, Phys. Rev. 140:566 (1965) and ibid. 139:B1447 (1965).

KR 54 N. M. Kroll and M. A. Ruderman, Phys. Rev. 93:233 (1954).

KR 66 D. S. Koltun and A. Reitan, Phys. Rev. 141:1413 (1966).

KU 68 F.J. Kelly and H. Überall, Nucl. Phys. A118:302 (1968).

Kun 69 A. R. Kunselman, Lawrence Radiation Laboratory Report No. UCRL-18654, 1969.

Kur 63 D. Kurath, Phys. Rev. 130:1525 (1963).

Lam+ 74 W-C. Lam, K. Gotow, B. MacDonald, and W. P. Trower, Phys. Rev. C10:72 (1974).

LB 62 M. Leon and H. A. Bethe, Phys. Rev. 127:636 (1962).

LB 72 M. B. Lewis and F. E. Bertrand, Nucl. Phys. A196:337 (1972).

LB+ 72 The isoscaler GQR identification has been suggested for a group of states in ^{208}Pb between 8.9 and 11.2 MeV excited in electron scattering (Fag 75), at 11 MeV in ^{3}He and ^{4}He scattering (MBC 73), and 11.2 MeV in proton scattering (LB 72). In ^{209}Bi a GQR was proposed at 11.5±1.0 MeV on the basis of proton scattering (BL 72). The GDR resonance in ^{209}Bi is at 13.6 MeV and has a width of 3.7 MeV (BF 75).

0 0 0 0 4 4 0 8 5 9 4

Leo 71 M. Leon, Physics Letters 37B:87 (1971).

Leo 75 M. Leon, private communication.

Lie 72 S. Lie, Nucl. Phys. A181:517 (1972).

LS 74 M. Leon and R. Seki, Phys. Rev. Lett. 32:132 (1974).

LS 75 M. Leon and R. Seki, Los Alamos Scientific Laboratory Report, LA-UR-75-1267, to be published.

LV 74 T.-S. H. Lee and J. D. Vergados, Phys. Letts. 53B:125 (1974).

LW 74 C. Lucas and C. Werntz, quoted in (Bae+ 74).

MBC 73 A. Moalem, W. Benenson, and G. H. Crawley, Phys. Rev. Lett. 31:482 (1973); M. B. Lewis, Phys. Rev. C7:2041 (1973).

McC+ 70 J. S. McCarthy, I. Sick, R. R. Whitney, and M. R. Yearian, Phys. Rev. Lett. 25:884 (1970).

McV 61 K. W. McVoy, Phys. Rev. 121:1401 (1961).

MPU 75 M. Moreno, J. Pestieau, and J. Urias, Phys. Rev. C12:514 (1975).

Muk 73 N. C. Mukhopadhyay, Phys. Letters 45B:309 (1973); ibid. 44B:33 (1973).

Mur+ 67 J. D. Murphy, R. Raphael, H. Überall, R. F. Wagner, D. K. Anderson, and C. Werntz, Phys. Rev. Lett. 19:714 (1967).

MW 73 W. Maguire and C. Werntz, Nucl. Phys. A205:211 (1973).

Nic+ 68 J. P. Nicholson, P. G. Butler, N. Cohen, and A. N. James, Phys. Letters 27B:452 (1968).

Nix+ 73 G. D. Nixon, N. de Botton, S.C. Cooper, K. M. Crowe and H. W. Baer, Bull. Am. Phys. Soc. 18:675 (1973).

NT 73 M. Nagao and Y. Torizuka, Phys. Rev. Lett. 30:1068 (1973).

PAH 51 W. K. H. Panofsky, R. L. Aamodt, and J. Hadley, Phys. Rev. 81:565 (1951).

Pai 72 G. Paić in: Few Particle Problems in the Nuclear Interaction (eds. I. Slaus, S. A. Moszkowski, R. P. Haddock, W. T. H. van Oers) North-Holland, Amsterdam, 1972, p. 539.

PC 54 R. H. Phillips and K. M. Crowe, Phys. Rev. 96:484 (1954).

PF 70 P. Pascual and A. Fujii, Nuovo Cimento, 65A:411 (1970) and 67A:135 (1970).

PFE 67 H. Pietschmann, L. P. Fulcher, and J. M. Eisenberg, Phys. Rev. Lett. 19:1259 (1967).

Pil 67 H. Pilkuhn, The Interaction of Hadrons, North Holland, Amsterdam, 1967, Ch. 10.

PP 64 V. I. Petrukhin and Yu. D. Prokoshkin, Nucl. Phys. 54:414 (1964).

PP 65 V. I. Petrukhin and Yu. D. Prokoshkin, Nucl. Phys. 66:669 (1965).

PR 73 A. C. Phillips and F. Roig, Nucl. Phys. B60:93 (1973).

PR 74 A. C. Phillips and F. Roig, Nucl. Phys. A234:378 (1974).

PR 75 A. C. Phillips and F. Roig, contribution to VI. Int. Conf. on High Energy Physics and Nuclear Structure, Santa Fe (1975) Los Alamos Report, LA-6030-6, p. 170, and private communication.

PS 73 W. Pfeil and D. Schwela Nucl. Phys. B45:379 (1973).

RE 73 A. K. Rej and T. Engeland, Phys. Letters, 45B:77 (1973).

ROP 71 F. Riess, W. J. O'Connell, and P. Paul, Nucl. Phys. A175:462 (1971).

Ros 67 C. M. Rose, Phys. Rev. 154:1305 (1967).

RP 73 F. Roig and P. Pascual, Nucl. Phys. B66:173 (1973).

RW 71 A. Raiche and C. Werntz, Phys. Rev. C4:2003 (1971).

RW 75 If Coulomb corrections are applied to the Panofsky ratio, the right hand side of Eq. (4.15) should be multiplied by 0.96. This would mean that E_{0+} reduces to $32.3\times10^{-2}\,\frac{1}{m_\pi}$.
G. Rasche and W. S. Woolcock, private communication.

Rya 63 J. W. Ryan, Phys. Rev. 130:1554 (1963).

Sal+ 72 R. M. Salter, M. Zeller, R. P. Haddock, D. Nygren, and J. B. Czirr, in Few Particle Problems in the Nuclear Interaction (eds. I. Slaus, S. A. Moszkowski, R. P. Haddock, W. T. H. van Oers) North-Holland, Amsterdam, 1972, p. 112.

San+ 54 M. Sands, J. G. Teasdale, and R. L. Walker, Phys. Rev. 95:592 (1954)
J. P. Burg and J. K. Walker, Phys. Rev. 132:447 (1963).
M. Beneventano, G. Bernardini, G. Stoppini, and L. Tau, Nuovo Cimento 10:1109 (1958).
J. Pine and M. Bazin, Phys. Rev. 132:2735 (1963).

Sap+ 72 W. W. Sapp, M. Eckhause, G. H. Miller, and R. E. Welsh, Phys. Rev. C5:690 (1972).

Sat 75 R. Satchler, Physics Reports C14:97 (1975).

Sch+ 68 H. Schmitt, L. Tauscher, G. Backenstoss, S. Charalambus, H. Daniel, H. Koch, and G. Poelz, Phys. Letters 27B:530 (1968).

SDU 74 J. B. Seaborn, V. Devanathan, and H. Überall, Nucl. Phys. A219:461 (1974).

Sha 63 I. S. Shapiro, in: Selected Topics in Nuclear Theory (F. Janouch, ed.) IAEA, Vienna, 1963, p. 85.

Sic+ 69 I. Sick, E. B. Hughes, T. W. Donnelly, J. D. Walecka, and G. E. Walker, Phys. Rev. Lett. 23:1117 (1969).

Sku 71 S. Skupsky, Phys. Letters 36B:271 (1971); Nucl. Phys. A178:289 (1971).

SM 76 J. Spuller and D. F. Measday, Phys. Rev. D (in press).

Sno+ 74 K. A. Snover, K. Ebisawa, D. R. Brown and P. Paul, Phys. Rev. Lett. 32:317 (1974).

Spe+ 70 J. Sperinde, D. Fredrickson, R. Hinkins, V. Perez-Mendez, and B. Smith, Phys. Letters 32B:185 (1970).

SW 74 P. Szydlik and C. Werntz, Phys. Letters 51B:209 (1974).

SZB 72 H. Seitz, S. A. A. Zaidi, and R. Bigler, Phys. Rev. Lett. 28:1465 (1972).

Tru 71 P. Truöl, in Proceedings of the Int. Conf. on π-Meson Nucleus Interactions, Strasburg 1971 (Universite Louis Pasteur, Strasbourg, France).

Tru+ 74 P. Truöl, H. W. Baer, J. A. Bistirlich, K. M. Crowe, N. de Botton and J. A. Helland, Phys. Rev. Lett. 32:1268 (1974).

TT 68 D. R. Thomson and Y. C. Tang, Nucl. Phys. A106:591 (1968).

Übe 71 H. Überall, Electron Scattering from Complex Nuclei, Part B (Academic Press, New York and London, 1971), p. 698.

VB 72 J. D. Vergados and H. W. Baer, Phys. Lett. 41B:560 (1972).

VCM 71 E. Ventura, C. C. Chang, and W. E. Meyerhof, Nucl. Phys. A173:1 (1971).

Ven+ 74 E. Ventura, J. Calarco, C. C. Chang, E. M. Diener, E. Kuhlmann, and W. E. Meyerhof, Nucl. Phys. A219:157 (1974).

Ver 71 J. D. Vergados, Phys. Lett. 36B:12 (1971).

Ver 73 J. D. Vergados, Nucl. Phys. A220:259 (1973).

Ver 75a J. D. Vergados, Nucl. Phys. A239:271 (1975).

Ver 75b J. D. Vergados, Phys. Rev. C12:1278 (1975).

Wal 66 J. D. Walecka, in: Preludes in Theoretical Physics (A. de Shalit, H. Feshbach, and L. Van Hove, eds.), Interscience, New York, 1966.

Wal 75 J. D. Walecka, in Muon Physics, Vol. II, (V. W. Hughes and C. S. Wu, eds.) Academic Press, New York, 1975, p. 113.

Wat 54 K. M. Watson, Phys. Rev. 95:228 (1954).

WS 51 K. M. Watson and R. N. Stuart, Phys. Rev. 82:738 (1951).

Zaĭ+ 65 O. A. Zaĭmidoroga, M. M. Kulyukin, R. M. Sulyaev, I. V. Falomkin, A. I. Filippov, V. M. Tsupko-Sitnikov, and Yu. A. Shcherbakov, Zh. Eksp. Teor. Fiz. 48:1267 (1965), and 51:1646 (1966). [Sov. Phys. JETP 21:848 (1965), and 24:1111 (1967)].

TABLE I. Parameters of pair spectrometers used in radiative pion capture studies of nuclear structure.

	Berkeley Optical Chambers	Berkeley Wire Chambers	SIN MWPC	
Magnet				
gap	33	33	50	cm
length	208	208	250	cm
width	41	41	60	cm
max B	10	10	12	kG
working B	8	8	8	kG
Acceptance (n_γ)[a]	2×10^{-5}	4.5×10^{-5}	1.1×10^{-4}	
Converter	0.011 Au	0.011 Au	0.011 Au	cm
target-conv. dist.	120	77.5	120	cm
Measured pts. on trajectory	3	5	5	
Wire angles with respect to mid-plane		±12°, 0°	90°, ±60°	
Spatial resolution of chambers	±0.3	±0.3	±0.1	cm
Resolution (FWHM at 130 MeV)	2[b]	1.8[b]	0.8[c]	MeV
Contributions to the resolution				
energy straggling				
200 mg/cm^2, converter	0.4	0.4	0.4	MeV
160 " , opt. chb.	0.4			MeV
80 " , wire chb.		0.2		MeV
40 " , MWPC			0.1	MeV
Angular + spatial resolution (multiple scatt. included)	0.6	1.6	0.6	MeV
Field map relative	0.4	0.4	0.1	MeV

[a] $n_\gamma = \frac{\Delta\Omega}{4\pi}$ x (conversion probability)

[b] measured

[c] calculated

TABLE II. Expected counting rates at meson factories for selected experiments in radiative pion capture studies.[a]

Reaction	Target Thickness (g/cm^2)	Other Particles Detected (energy) (MeV)	Branching Ratio (%)	Detector (Acceptance[b])	Rate (sec^{-1})
$\pi^- p \rightarrow n\gamma$	0.7		39.5		37
	0.7	neutron (8.9)	39.5	scintillator (0.12)	4.4
$^6Li(\pi^-,\gamma)$all	3.5		4.4		5.5
$^6He(0^+)$	3.5		0.3		0.5
$^6He(0^+,1s)$		x-ray(2p→1s,.26)	0.13	SiLi($5*10^{-4}$)	10^{-4}
$^6He(0^+,1s)$		x-ray(2p→1s,.26)	0.13	NaI($2*10^{-2}$)	$4*10^{-3}$
$^{12}C(\pi^-,\gamma)^{12}B$ (giant reso.)	4.0	neutron (4-6)	0.2	scintillator (10^{-3})	$3*10^{-4}$

[a] Calculations assume $1.8*10^6$/sec π^- entering the target after the degrader, which is the measured rate for the 200 MeV/c beam of the SIN E1 channel with an internal proton-current of 20 μA . The spot size of the degraded beam is 36 cm^2, the FWHM of the stopping distribution is 2.5 g/cm^2 CH_2. The acceptance of the SIN-pair-spectrometer of 1.1×10^{-4} (Table I) was used.

[b] This is the acceptance (solid angle × efficiency) for the second particle detected in coincidence with the photon.

TABLE III. Radiactive and charge exchange branching ratios for stopped π-absorption on nuclei.

Target Nucleus	Radiative (R_γ)[a] (%)	Charge Exchange ($R_{\pi o}$) (%)	Atomic Capture Orbitals[b]
^{1}H	39.5 ± 0.3[c,d]	60.5 ± 0.3[c,d]	3s, 4s
^{2}H	24.7 ± 0.7[d]	.08 ± 0.10[e]	3s, 4s
^{3}H	4.5 ± 0.8[f]	Q-forbidden	3s, 4s
^{3}He	14.3 ± 1.3[g]	17.8 2.3[g]	1s, 2p
^{4}He	1.50± 0.29[h]	Q-forbidden	1s, 2p
^{6}Li	3.4 ± 0.2[i,j]	<.4[i]	1s, 2p
^{7}Li	1.9 ± 0.2[j]	<.003[k]	1s, 2p
^{10}B	2.27± 0.22[l]	<.4[l]	1s, 2p
^{12}C	1.67± 0.08[m,j]	Q-forbidden	1s, 2p
^{14}N	2.13± 0.21[l]	<.4[l]	1s, 2p
^{16}O	2.24± 0.48[n]	Q-forbidden	1s, 2p
$^{26,24}Mg$	2.15± 0.43[n]	Q-forbidden	(1s), 2p (3d)
^{32}S	1.8 ± 0.1[j]		2p, 3d
^{40}Ca	1.94± 0.35[n]	<.5[n]	2p, 3d
Ti(nat)	1.5 ± 0.1[o]	<.004[k]	2p, 3d
$^{63,65}Cu$	1.5 ± 0.1[j]	<.004[k]	2p, 3d
Pb(nat)	2.1 ± 0.5[o]	<.002[k]	4f, 5g
^{209}Bi	0.98± 0.10[p]	<.5[p]	4f, 5g

[a] If several measurements exist, a weighted average is given.

[b](Bac 70); hydrogen isotopes given in Ref. (LB 62). [c](Coc 61); [d](Rya 63); [e](CS 55); [f](Bis+ 75); [g](Tru+ 74); [h](Bis+ 70a); [i](Bae+ 73); [j](DMW 66); [k](PP 64); [l](Bae+ 75); [m](Bis+ 70b); [n](Bis+ 72); [o](PP 65); [p](Bae+ 74).

TABLE IV. Pionic atom capture schedules for hydrogen, ^{4}He, ^{6}Li, and ^{12}C. The probabilities $\omega(n\ell)$ for π-absorption into the nucleus from orbital $n\ell$ as deduced from cascade calculations are given.

	^{1}H[a]	^{4}He[b]		^{6}Li[c]		^{12}C[c]	
	$\ell = 0$	$\ell = 0$	$\ell = 1$	$\ell = 0$	$\ell = 1$	$\ell = 0$	$\ell = 1$
n=7	0.003						
6	0.013						
5	0.09	0.70		0.006±0.004	0.005±0.005	0.0035±0.0015	0.038±0.007
4	0.44			0.016±0.006	0.035±0.001	0.0025±0.0015	0.082±0.008
3	0.39			0.022±0.007	0.130±0.006	0.0015±0.0008	0.145±0.002
2	0.04			0.019±0.005	0.430±0.075	0.003 ±0.001	0.63 ±0.05
1		0.14		0.335±0.065		0.06 ±0.02	
ω_s[d]	.979	0.84		0.40 ±0.09		0.08 ±0.03	
ω_p			0.16		0.60 ±0.09		0.92 ±0.03
ω_d				$\sim 1\times10^{-5}$		$\sim 7\times10^{-4}$	

[a] (LB 62); entries are for liquid hydrogen; values for liquid deuterium and tritium may be slightly different (Leo 75) since strong absorption rates $\lambda_a(ns)$ are different; values for gaseous targets are different (Leo 71).

[b] (Bac 74); values are for liquid ^{4}He; 1.21±0.8% (BKS 65) of π's decay in in the cascade.

[c] (Sap + 72)

[d] $\omega_\ell = \sum_n \omega(n\ell)$

TABLE V. Pionic X-ray data on light nuclei needed to relate theoretical radiative transition rates to the experimental branching ratios.

Nucleus	Absorption Widths ($\hbar\lambda_a$)		Capture Probabilities		Distortion Factors	
	$\Gamma_a(1s)$ (keV)	$\Gamma_a(2p)$ (eV)	ω_s	ω_p	C_s	C_p
^{4}He	0.045±0.003[a]	(7.2±3.3)10^{-4}[a]	0.84[a]	0.16[a]	0.77[b]	
^{6}Li	0.195±0.012[c]	0.015±0.004[d]	0.40±0.09[d]	0.60±0.09[d]	0.70[e]	1.2[e]
^{10}B	1.68±0.12[f]	0.032±0.06[f]	0.20[g]	0.80[g]	0.5[h]	1.4[h]
^{12}C	3.12±0.12[f]	2.6±0.9[d] (1.95[i])	.80±0.03[d]	0.92±0.03[d]	0.51[e]	1.41[e]
^{14}N	4.48±0.30[f]	2.1±0.3[f]	0.10[g]	0.90[g]	0.5[h]	1.4[h]
^{16}O	7.56±0.50[f]	4.68[j]	.086 .015[j]	0.914±0.015[j]	0.69[k]	1.18[k]

[a](Bac 74); [b](RW 71); [c](Bac + 73); [d](Sap + 72); [e](MW 73);

[f](Bac 70); references to original work and comparisons of various measurements and optical potential calculations are given.

[g]From extrapolation of ^{6}Li and ^{12}C capture schedules (Sap + 72).

[h]Assumed to be the same as for ^{12}C (MW 73).

[i]Optical potential value used by (MW 73).

[j]Average value given by (Bis + 72).

[k](SW 74).

TABLE VI. Theoretical and experimental values for the coefficients of the radiative π-capture matrix element.

		A ($10^{-3}/m_\pi$)	B ($10^{-3}/m_\pi^3$)	C ($10^{-3}/m_\pi^3$)	D ($10^{-3}/m_\pi^3$)	E ($10^{-3}/m_\pi^3$	
Kawaguchi et al. (KOS 68)	a)	-32	7.5	-37	-14		Previously
Ericson, Delorme (DE 66)	a),h)	-34±3	19	-17	-10		Used
Maguire, Werntz (MW 73)	a)	-33.2	4.8	-32.9	-11.7	30.4	Values
Roig, Pascual (RP 73)	a)	-31.9	4.2	-29.5	-10.9	20.7	
Schwela	b)	-31.7±.9	6.5±.2	-33±.9	-8.9±.6		
Phillips, Roig (PR 74)	a)	-31.8	5.9	-33.1	-13.1		
Born (text)		-32.1	2.6	-33.8	-12.1	28.0	Theoretical
Berends et al. (BDW 67)	c)	-33.1	5.2	-31.4	-12.5		Values
Adamovich et al. (Ada+69)	d)	-31.5±1.0					Experimental
Adamovich et al. (Ada+69)	e)	-32.5±.5	4.8±.3				Values
Adamovich et al. (Ada+69)	f)	-32.7±.7					
Adamovich et al. (Ada+69)	g)	-33.4±.4	7.4±.2				
Pfeil, Schwela (PS 73)	g)	-29.0±1.4	6.9±.3	-27.0±1.0	-13.7±1.7		
Panofsky ratio		-32.9±.6					
"recommended"	i)	-32.6±.4	7±3	-27±4	-14±2	28±2	

a) These authors use the multipole tables of ref. (BDW 67).
b) Private communication, using ref. (PS 73).
c) Our evaluation, see g)
d) Using data of ref. (Ada + 66)
e) Using angular distributions, data of ref. (Ben + 56) and (San + 54)
f) Using total cross-sections, data of ref. (Ben + 56) and (San + 54).
g) Our evaluation: polynomial fit in $(qk)^{2m}$ as described in the text
h) Electric quadrupole neglected
i) A: weighted average of entries d,f and Panofsky ratio; B,C,D: Pfeil, Schwela with errors increased to include uncertainties of extrapolation

0 0 0 4 0 8 3 9 9

TABLE VII. Radiative transition rates calculated with the "elementary-particle-soft-pion" ansatz.

Transition	^3He - ^3H [a]	^6Li - ^6He [b]	^{14}N - ^{14}C [c]
Z	2	3	7
$J_i^\pi, J_f^\pi, S(J_i, J_f)$	$1/2^+$, $1/2^+$, 2	$1^+, 0^+, 1/3$	$1^+, 0^+, 1/3$
k (MeV)	135.8	134.0	138.6
q^2/m_π^2	.947	.922	.977
$ft_{1/2}$ (sec)	1137	796.7	1.052×10^5
$F_A^2(0)$	1.488	2.615	1.978×10^{-6}
$\lvert F_M(q^2)/F_M(0)\rvert$	0.78±0.01	0.65±.03	1.38±.12
C_s	.97	.654	.50
$\Lambda_\gamma(1s)(sec^{-1})$	3.86×10^{15}	1.88×10^{15} (1.23×10^{15}) [d]	1.31×10^{11}
$\Lambda_a(1s)(sec^{-1})$	5.62×10^{16}	2.97×10^{17}	6.82×10^{18}
Λ_γ/Λ_a	6.86×10^{-2}	6.32×10^{-3}	1.9×10^{-8}
R_s		2.53×10^{-3} (1.66×10^{-3}) [d]	1.9×10^{-9}

[a] (ER 72); (Tru + 74) and references cited therein.

[b] (Del 70); (ER 72)

[c] (Bae + 75) and references cited therein.

[d] (Ber 75)

TABLE VIII. Summary of experimental values and some resulting interpretations for radiative capture of stopped π^- on hydrogen and helium nuclei.

	^1H	^2H	^3H	^3He		^4He
Panofsky ratio P [a]	1.533±0.021[b]	(3±4) 10^{-3}[c]	0[d]	2.28±0.18[e]	2.68±0.13[f]	
Radiative branching ratio, R (%)	39.5± 0.03[b]	24.7±0.7[g]	4.5±0.8[h]	t : 6.9±0.5 dn :3.6±1.2 pnn : tot:	6.6±0.8 [7.4±1.0] 14.0±1.0	1.50±0.20[i]
Nucleon ejection only, R_n (%)		75.3±9.7	95.5±0.8	73.7±5.9	68.3±2.6	98.5±0.3 ^{3}Hn:19.4±1.8[j]
Results	π, π^0 mass link π-N scattering ($\lvert a_1-a_3\rvert$) to pion photo-production at threshold $\left(E_{0^+}^{(\pi^-)}\right)$	odd parity of π^- determine a_{nn}	tri-neutron search (3n) excitation spectrum studied	impulse approx. tested for $P(^3He)/P(^1H)$ T=3/2,1/2 structure of A=3 system studied. soft-pion relations $R_\gamma \sim \lvert F_A(q^2)\rvert^2$; link to μ-capture and β-decay		T=1 (T_z=+1) structure of A=4 system; studied; observation of unbound states

[a] $P_i = \dfrac{\lambda(\pi^- + A_i \to \pi^0 + A_f)}{\lambda\ \pi^- + A_i \to \gamma + A_f}$;

[b] Ref. (Coc+ 61); [c] Ref. (CS 55); [d] Change-exchange Q-forbidden; [e] Ref. (Zai+ 67)

[f] Ref. (Tru+ 74); [g] Ref. (Rya 63); [h] Ref. (Bis+ 76); [i] Ref.)Bis+ 72); [j] Ref. (Blo 63)

0 0 0 0 4 0 8 8 0 0

TABLE IX. Radiative pion capture branching ratios and 1s-level widths for the isotopes of hydrogen and helium

Isotope	Reaction	Radiative Capture Branching Ratio (%)	Radiative Capture 1s Width (Theory) (eV)	Total 1s Level Width[a]
^1H	$\pi^- p \to n\gamma$	39.5 ± 0.3[b]	0.324 ± 0.008[c]	0.82 ± 0.02
^2H	$\pi^- d \to nn\gamma$	24.7 ± 0.7[d]	0.251 ± 0.025[e]	1.02 ± 0.11
^3H	$\pi^- t \to nnn\gamma$	4.5 ± 0.8[f]	0.046[g]	1.02 ± 0.18
^3He	$\pi^{-3}He \to t\gamma$	6.6 ± 0.8[h]	2.44[i]	37.0 ± 4.5
^4He	$\pi^{-4}He \to pnnn\gamma$	1.5 ± 0.3[j]	0.86[k]	57 ± 11 (45 ± 3)[ℓ]

[a]Obtained from $\lambda_a(1s) = \lambda_\gamma(1s)/R_\gamma$ (experiment); [b]Ref. (Coc+61)

[c]Using $|E^{\pi^-}_{0+}| = (3.26 \pm 0.04) \times 10^{-2}/m_\pi$ and

$$\Gamma_\gamma(1s) = \hbar 8\, |E^{\pi^-}_{0+}|^2\, (k/m_\pi)\, \left(1 + \frac{m_\pi}{m_p}\right)^{-2} (\alpha m_\pi)^3$$

[d]Ref. (Rya 63)

[e]Obtained from $\lambda(\pi^- d \to nn\gamma)/\lambda_\gamma(\pi^- p \to n\gamma) = 0.775 \pm 0.078$ (GGS 75b) and hydrogen rate given above.

[f]Ref. (Bis+ 76); [g]Ref. (PR 75); [h]Ref. (Tru+ 74); [i]Ref. (PR 74); [j]Ref. (Bis+ 72)

[k]Ref. (RW 71); [ℓ]measured, Ref. (Bac+ 74).

TABLE X. Branching ratios and radiative transition rates for absorption of stopped π^- in ^{3}He

Reaction	Experimental (Tru+ 74) (%)	Branching ratios (Zai+ 65) (%)	Theory $\lambda_\gamma(1s)$ (10^{15} sec^{-1})	R_s [a] (%)
$\pi^-{}^3$He$\to$tγ	6.6 ±0.8	6.9 ±0.5	3.3[b], 3.6[c]	5.8, 6.3
$\to$dnγ	[7.4 ±1.0]	3.6 ±1.2	2.3[b]	4.0
$\to$pnnγ			0.8[b]	1.4
$\to$tπ^0	17.8 ±2.3	15.8 ±0.8	9.6[b], 9.0[c]	16.8, 15.8
$\to$dn		15.9 ±2.3	9±4[d]	15.8
$\to$pnn		57.8 ±5.4	32±8[d]	56.1
$\to$dn+pnn	68.2 ±2.6	73.7 ±5.9	41±9	71.9
P(^{3}He)	2.68±0.13	2.28±0.18	2.9,[b] 2.8[e], 2.5[c]	
All channels			57±9, 56 [f]	

[a]Using $\Gamma_a(1s) = 5.7\times10^{16}$ sec^{-1} $\times\hbar$ = 37.5 eV and ω_s = 1.

[b]Ref. (PR 74); [c]Ref. (Tru+ 74); [d]Ref. (PR 73).

[e]Panofsky ratio corrected for pions capturing from 2p-state.

[f](Ref. CE 74), based on extrapolation of higher Z data.

TABLE XI. Radiative π-capture branching ratios for 1p-shell nuclei with excitation of individual nuclear states.

Nuclei	J_i^π	J_f^π	Experiment $E_x(T_z=1)$ (MeV)	Experiment $E_x(T_z=0)$ (MeV)	Experiment R_γ (%)	Shell Model R_γ (%)
$^6Li \to {}^6He$[a]	1^+	0^+	0.0	3.56	0.306±0.035	0.30[b], 0.44[c], 0.41[d]
		2^+	1.8	5.36	0.148±0.025	0.15[c]
$^{10}B \to {}^{10}Be$[e]	3^+	0^+	0.0	1.74	0.025±0.004	0.036[e]
		2^+	3.37	5.11	0.044±0.007	0.085[e]
		2^+	5.96	7.48	0.105±0.013	0.169[e]
$^{12}C \to {}^{12}B$[f]	$0^+(1^+,2^+,2^-)$		0.35	15.45	0.091±0.009	0.088[d]
		2^-	4.75	19.85	0.185±0.019(0.30)[g]	0.29[h]
		1^-	8.10	23.20	0.159±0.016(0.42)[g]	0.19[i]
$^{14}N \to {}^{14}C$[e]	1^+	0^+	0.0	2.31	0.003±0.002	0.01[e]
		2^+	7.01	9.17	0.077±0.009	0.12[j]
		2^+	8.32	10.43	0.040±0.006	0.10[j]
		1^+	11.3	13.75	0.051±0.007	0.049[e]
	giant reso.		20.0	22.2	0.205±0.020	
$^{16}O \to {}^{16}M$[f]	$0^+(2^-,0^-,3^-,1^-)$		0.0	13.0	0.15 ±0.03	0.18[k], 0.38[ℓ]
		2^-	7.70	20.7	0.22 ±0.05(0.58)[g]	0.61[ℓ]

[a]Ref. (Bae+ 73); [b]Ref. (Ber 75); [c]Ref. (Ver 74) [d]Ref. (MW 73); [e](Bae+ 75); [f]Ref. (Bis+ 72); [g]Assume pole-model contribution to peak area = 0; [h]Ref. (Sku 71); includes only 2^- state at E_x = 5.1 MeV. [i]Ref. (Sku 71), includes 1^- states at E_x = 7.0, 7.5, and 10.5 MeV. [j]Ref. (Bae+ 75), corrected for $(sd)^2$ admixtures of Lie(Lie 72); [k]Ref. (SW 74); [ℓ]Ref. (Ver 75b).

TABLE XII. Radiative transition rates and branching ratios for the $^6Li(\pi^-,\gamma)^6He(g.s.)$ reaction with stopped pions.

Method	Transition Rates[a]		Branching Ratios[b]			Reference
	$\lambda_\gamma(1s)$ (10^{15} sec^{-1})	$\lambda_\gamma(2p)$ (10^{10} sec^{-1})	R_s (%)	R_p (%)	R_γ (%)	
"elementary particle + soft pion" ansatz	1.65		0.22±0.05			(GK 68)
	1.86±0.18		0.25±0.06			(PF 70)
	$2.3^{+0.4}_{-0.2}$		0.31±0.09			(FE 70)
	2.3±0.5		0.31±0.10	0.31±0.05	0.62±0.11	(Del 70)
IA+Shell Model	1.51±0.15	5.26±0.60	0.20±0.05	0.14±0.05	0.34±0.07	(MW 73), b=2.05F
	1.64	5.86	0.22±0.05	0.15±0.06	0.38±0.08	(Ver 74), b=1.95
	1.67	5.46	0.22±0.05	0.14±0.05	0.37±0.07	(Ver 74),[c] b=2.0
	1.47±0.22	4.12±0.62	0.20±0.05	0.11±0.04	0.31±0.07	(RP 73), b=1.98
	1.23		0.17±0.04		0.30±0.06[d]	(Ber 75)
Experiment					0.306±0.035	(Bae+ 73)
					1.0 ±0.1	(Deu+ 68)

[a]The strong interaction distortion factors are included in the values given. Typical values are $C_s = 0.70$, $C_p = 1.2$ (MW 73).

[b]Obtained from $R_\gamma = R_s + R_p = \omega_s[\lambda_\gamma(1s)/\lambda_a(1s)] + \omega_p[\lambda_\gamma(2p)/\lambda_a(2p)]$ with $\omega_p = 0.60\pm0.09$, $\omega_s = 1 - \omega_p$ (Sap+ 72)

$\lambda_a(1s) = (195.2\pm12.5\text{eV})/\hbar = 2.97(1+0.064)10^{17}$ sec^{-1} (Bac+ 73) and

$\lambda_a(2p) = (0.015\pm0.004\text{ eV})/\hbar = 2.28(1\pm0.27)10^{13}$ (Sap+ 72)

(continued)

TABLE XII (cont.)

---

[c] $\lambda_\gamma(1s)$ and $\lambda_\gamma(2p)$ calculated using wave functions of Ref. (DW 73) and $C_s^\gamma = 0.65$, $C_p^\gamma = 1.1$.

[d] Obtained from $\lambda_\gamma(1s) = 1.23\times10^{15}$ sec^{-1} (Ber 75) and $\lambda_\gamma(2p) = (5.26\pm0.60)$ 10^{10} sec^{-1} (MW 72).

TABLE XIII. Shell model analysis of weak, electromagnetic, and pion photoproduction interactions with nuclear states $^6Li(1^+)$, $^6He(0^+)$, and $^6Li(0^+, 3.56\ MeV)$

Observable	Experiment[a]	Theory		
		Donnelly *et al.*[b]	Bergstrom[c]	
Quadrupole moment $^6Li(1^+)$	-0.80±0.08 mb	-0.80	-0.80	(fit)
Magnetic dipole moment $^6Li(1^+)$	+0.82201 n.m.	+0.82	0.822	
γ-lifetime: $^6Li(0^+) \rightarrow {}^6Li(1^+)$	8.16±0.19 eV[c]		8.16	
$^6Li(e,e)$ and (e,e') transverse magnetic dipole form factor $F_{M1}(q)$	$F^2_{M1}(q)$	$q < 200$ MeV/c	$q < 400$ MeV/c	
p-shall h.o. parameter		b = 2.03	parametrize transition density[d]	
β-decay (λ_γ): $^6He \rightarrow {}^6Li(1^+)$	0.858±0.002 sec^{-1}	0.877±0.023	0.855±0.024	(theory)
μ^--capture (λ_μ): $^6Li \rightarrow {}^6He$	$1.6 + 0.33)\times10^3 sec^{-1}$ $- 0.13$	$(1.39\pm0.04)\times10^3$	$(1.33\pm0.04)\times10^3$	
(π^-,γ) branching ratio (R_γ)	0.306±0.035 % [e]	0.37±0.07[f]	0.304±0.058[g]	
(γ,π^+) photoproduction, a_{Li}/a_{proton}	0.073±0.002[h]	0.12	0.090	

[a]Ref. (ASL 74)

[b]Ref. (DW 73, KD 74); based on shell model wave functions $\psi(^6Li, 1^+, T=0) = 0.810\ (p_{3/2})^2 - 0.581\ (p_{3/2}\ p_{1/2}) + 0.084\ (p_{1/2})^2$ and $\psi(^6He, 0^+\ T=1) = 0.80\ (p_{3/2})^2 + 0.60\ (p_{1/2})^2$.

[c]Ref. (Ber 75); based on $\psi(^6Li, 1^+) = 0.924\ ^3S_1 + 0.369\ ^1P_1 + 0.102\ ^3D_1$ and $\psi(^6He, 0^+) = 0.843\ ^3S_0 - 0.537\ ^3P_0$

(continued)

0 0 0 0 4 0 8 6 0 3

TABLE XIII (cont.)

[d]Best fit to $(1p)^2$ form factor gives b = 2.16 F with χ_ν = 3.4. This indicates that M1 form factor is not adequately described in $(1p)^2$ harmonic oscillator basis.

[e]Ref. (Bae+ 73)

[f]Ref. (Ver 74); calculated using wave functions of Ref. (DW 73), C_s = 0.65, C = 1.1, and π-atom data of Table XII.

[g]Obtained from $\lambda_\gamma = 1.23\times10^{15}$ sec^{-1} (Ber 75), $\lambda_\gamma(2p) = (5.26\pm0.60)\times10^{10}$ sec^{-1} (MW 72) and π-atom data of Table XII.

[h]Ref. (Deu+ 74)

TABLE XIV. Transition rates and branching ratios for radiative capture of stopped π^- on ^{209}Bi. The single-particle transitions $\pi^- + 1h_{9/2}$ (proton) $\rightarrow \gamma + j$ (neutron) with π^- in 4f or 5g orbits are compared with the experimental value for the sum of all transitions up to 4 MeV excitation in ^{209}Pb. (Bae+ 74).

Single-particle State in ^{209}Pb	$E_x(^{209}Pb)$[a] (MeV)	E_γ [b] (MeV)	$\lambda_\gamma(4f)$ $10^{13}sec^{-1}$	$\lambda_\gamma(5g)$ $10^{10}sec^{-1}$	$R_\gamma(4f)$[c] 10^{-4}
2g 9/2	0	136.8	0.93	4.17	0.041±0.012
1i 11/2	0.78	136.0	1.17	3.11	0.052±0.015
1j 15/2	1.43	135.5	3.69	10.70	0.163±0.048
3d 5/2	1.57	135.2	0.31	1.51	0.014±0.004
4s 1/2	2.04	134.8	0.08	0.35	0.004±0.001
2g 7/2	2.50	134.3	0.32	0.14	0.014±0.004
3d 3/2	2.54	134.3	0.15	0.58	0.007±0.002
			Theory	Sum:	0.30 ±0.09
			Expt. R_γ(0-4MeV) =		0.36 ±0.18
Experiment	7.9±0.4[d]	128.9±0.4	(Γ_1=0-3 MeV)		$R_\gamma=(4.7\pm0.7)10^{-4}$[e]
	13 ±2	124 ±2	(Γ_2=1-4 MeV)		$R_\gamma=(9.6\pm1.6)10^{-4}$[e]
				R_γ(total)	$=(98\pm10.0)10^{-4}$

[a]Ref. (BM 69)

[b]Assuming 4f capture; photons from 5g capture will appear at 0.59 MeV higher energies due to smaller π binding energy.

[c]Assuming 4f capture only; $R_\gamma = C_f\lambda_\gamma(4f)/\lambda_a(4f)$ with distortion factor $C(4f) = 1.14\pm0.15$ (LW 74) and $\lambda_a(4f) = (1.7\pm0.5\ keV)/\hbar = (2.6\pm0.8)10^{18}sec^{-1}$ (Sch+ 68).

[d]Assuming 4f capture; $E_x = 8.5\pm0.4$ MeV if assume 5g capture.

[e]Fit with $\Delta \equiv 16$, $\Gamma_1 \equiv 0$, $\Gamma_2 = 2.7\pm0.8$ MeV, $E_x = 7.9\pm0.4$ MeV, and $E_x = 11.7\pm0.2$ MeV.

Figure Captions

Fig. 1. Photon energy spectrum from π^- capture in ^{12}C (Bis + 70b, Bis + 72). (a) Spectrum with fitted function, using three Breit-Wigner forms plus the pole model for the continuum. (b) Photon spectrum for pions with a mean energy of 40 MeV used for in-flight background subtraction. (c) Spectrum with the pole model subtracted. The solid curve is the best fit. The dashed curve is the prediction of Kelly and Überall (KU 68) using the Arima model for the giant resonant states.

Fig. 2. Line shapes for measuring the 129.4 MeV photon of the $\pi^- p \to n\gamma$ reaction with a NaI crystal (Bay + 75)(b), and the pair spectrometers of Panofsky et al. (PAH 51)(a), Phillips and Crowe (PC 54)(a), and Nicholson et al. (Nic+ 68) (c). The latter achieved a resolution of 0.6 MeV (FWHM).

Fig. 3. Plan view of the experimental set up at the 184" cyclotron of the Lawrence Berkeley Laboratory used for investigations of radiative pion capture on nuclei. The inset shows the pair spectrometer and range-telescope geometry (Bis + 72, Bae + 73).

Fig. 4. (a) Acceptance of the LBL pair spectrometer as a function of photon energy (Bae + 73); $\eta_\gamma = (\Delta\Omega/4\pi)$ x (conversion probability) x (spark chamber detection efficiency). (b) Photon spectrum from π-capture on hydrogen.

Fig. 5. First order Born diagrams contributing to the pion photoproduction reaction $\gamma n \to \pi^- p$.

Figure Captions (Cont.)

Fig. 6. Real parts of coefficients of the radiative capture matrix element. (a) $A = E_{0+}$ vs. (qk/m_π^2); (b) $B \cdot qk = M_{1+} - M_{1-} + 3E_{1+}$; (c) $C \cdot qk = -M_{1+} + M_{1-} + 3E_{1+}$; (d) $D \cdot qk = -2M_{1+} - M_{1-}$. □ Adamovich et al. (Ada 69); × Adamovich et al. (Ben + 56), (San + 54), and (Ada + 69); △ Panofsky ratio; ● Adamovich et al. (Ada 69); ■ Pfeil and Schwela (PS 73). — Polynomial fit to results of (PS 73); ---- From (BDW 67); ....Born approximation (text); -·-·-·-· Polynomial fit to the results of (Ada + 69).

Fig. 7. Photon spectra for the hydrogen isotopes. The curve shown with the data for deuterium (Rya 63) is calculated for a n-n scattering length $a_{nn} = -16.4$ F. The curve shown with the data on tritium (Bis+ 76) is from the calculation of Phillips and Roig (PR 75). The interaction of the three outgoing neutrons are treated in the Amado model (Ama 63), with no resonances put in.

Fig. 8. Photon spectra for ^{3}He (Tru+ 74) and ^{4}He (Bis+ 70a). The curve in (a) is from a pole-model calculation with $\Delta = 6.8$ MeV (Sec.6). The curve in (b) is the result of an R-matrix calculation (Bis+ 70a) assuming excitation of the three states indicated.

Fig. 9. Comparison of the data on the radiative breakup reactions from π capture on ^{3}He with theoretical spectra (PR 74) calculated using the Amado model. The spectrum shows no sign of a resonance.

Fig. 10. Photon spectra for 1p shell nuclei. Solid curves are pole-model calculations. Three body phase space (curve in (a)) does not describe the continuum well.

Fig. 11. Pole graph for quasi-free radiative π-capture (DP 68).

Fig.12. Isobar level diagram for the levels of A = 6 nuclei (ASL 74) relevant to study of the $^{6}Li(\pi-,\gamma)^{6}He(g.s.)$ transition.

Fig.13. Measured M1 transition strengths in 1p shell nuclei (in Weisskopf units vs. excitation energy, $g=(2J_f+1)/(2J_i+1)$ (Fag 75)). Strong $(\pi-,\gamma)$ transitions to the analog states in the $T_z = T_z(\text{target})+1$ nuclei have been observed in the nuclei identified by an X.

Fig.14. Photon spectra and level diagrams for $(\pi-,\gamma)$ transitions to the particle - stable and low - continuum state of ^{10}Be and ^{14}C (Bae+ 75). The spectra are after subtraction of the pole model and BW contributions (Fig. 10). In ^{10}Be the M1 transition to the 7.5 MeV state dominates 180° electron scattering and is seen to dominate the $(\pi-,\gamma)$ spectrum. In ^{14}C, the analogs of the two strong M1 states at 9.2 and 10.4 MeV in ^{14}N dominate the $(\pi-,\gamma)$ spectrum. The $^{14}N(g.s.)$ state is seen to be extremely weak as expected from the 10^6 hindered Gamow-Teller β-decay rate.

Fig.15. Results of the shell model calculation (Ver 75a) for $1\hbar\omega$ excitations in the reaction $^{14}N(\pi-,\gamma)^{14}C$ are compared to the data (Bae+ 75). (a) Branching ratios to the strongest states. The data are on arbitrary scale. (b) Theoretical branching ratios (x0.4) folded with the instrumental resolution and acceptance. The solid curve is the summed strength and corresponds to a branching ratio of 0.78%.

Fig.16. Photon spectra for ^{nat}Mg and ^{40}Ca (Bis+ 72). The curves are pole-model calculations with Δ = 16 MeV and 13 MeV, respectively. The data show appreciable transition strength to the particle-stable and low-continuum states of the residual nuclei of Na and ^{40}K, respectively.

Fig.17. Photon spectrum for ^{209}Bi (Bae+ 74). The curve in (a) is a pole-model calculation (Δ = 16 MeV) normalized to the data between 70-110 MeV; in (b) the curve is a fit to the full spectrum (pole-model + BW + line). The data show weak excitation of the single-particle states in ^{209}Pb (0-4 MeV) and strong excitation of a state at 7.9 MeV in ^{209}Pb which was tentatively identified (Bae+ 74) with the $T_>$ component of an isovector quadrupole excitation at ~26.5 MeV in ^{209}Bi (Fig. 19).

Fig.18. Shell-model levels in the ^{208}Pb region. The single-article transitions (i) of the ^{209}Bi(π^-,γ)^{209}Pb reaction and the (ii) neutron-particle proton-hole excitations discussed in the text are illustrated. The relationship of the M1 excitations to the ^{209}Bi(π^-,γ) reaction is also discussed in the text.

Fig.19. Level diagram for giant resonance states of ^{209}Bi and ^{209}Pb. The peak in the γ-spectrum of the ^{209}Bi(π^-,γ)^{209}Pb reaction at E_x = 7.9±0.4 MeV is tentatively identified as the excitation of the analog of the $T_>$ component of an isovector quadrupole state of ^{209}Bi at 26.5 MeV. The well-known GDR and possible isoscaler quadrupole resonances (LB+ 72) are also shown.

Fig.20. Proton energy spectrum from the ^{209}Bi(n,p)^{209}Pb reaction obtained by King et al. (Kin+ 75). The data in (b) are what remain after subtraction of the QF continuum as given by 3-body phase space. The peak at E_x(^{209}Pb) = 8.1±0.5 MeV is identified with the peak at 7.9±0.4 MeV observed in the (π^-,γ) reaction (Fig. 17).

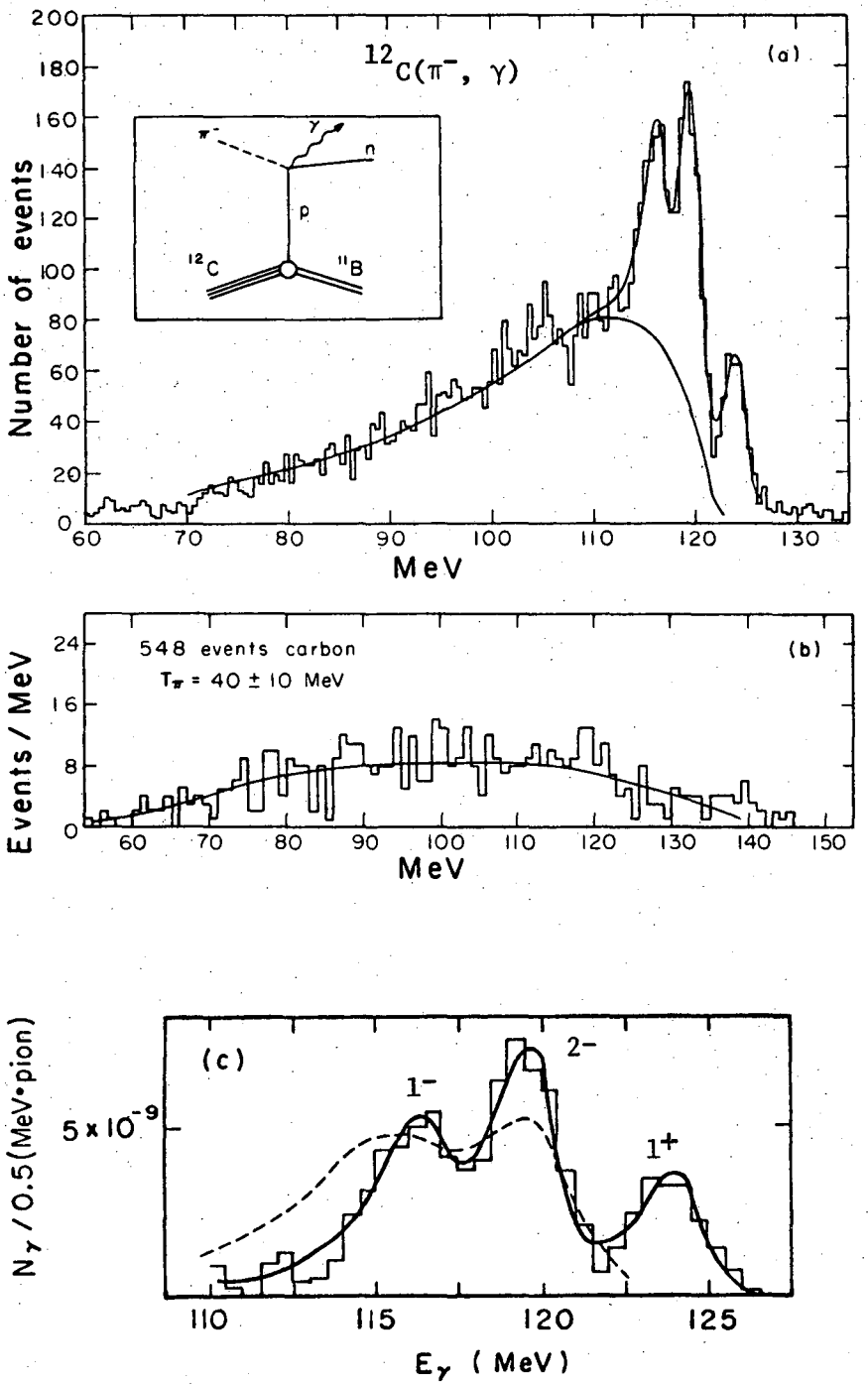

Fig. 1

XBL 733-307

0 0 0 0 4 4 0 8 6 0 7

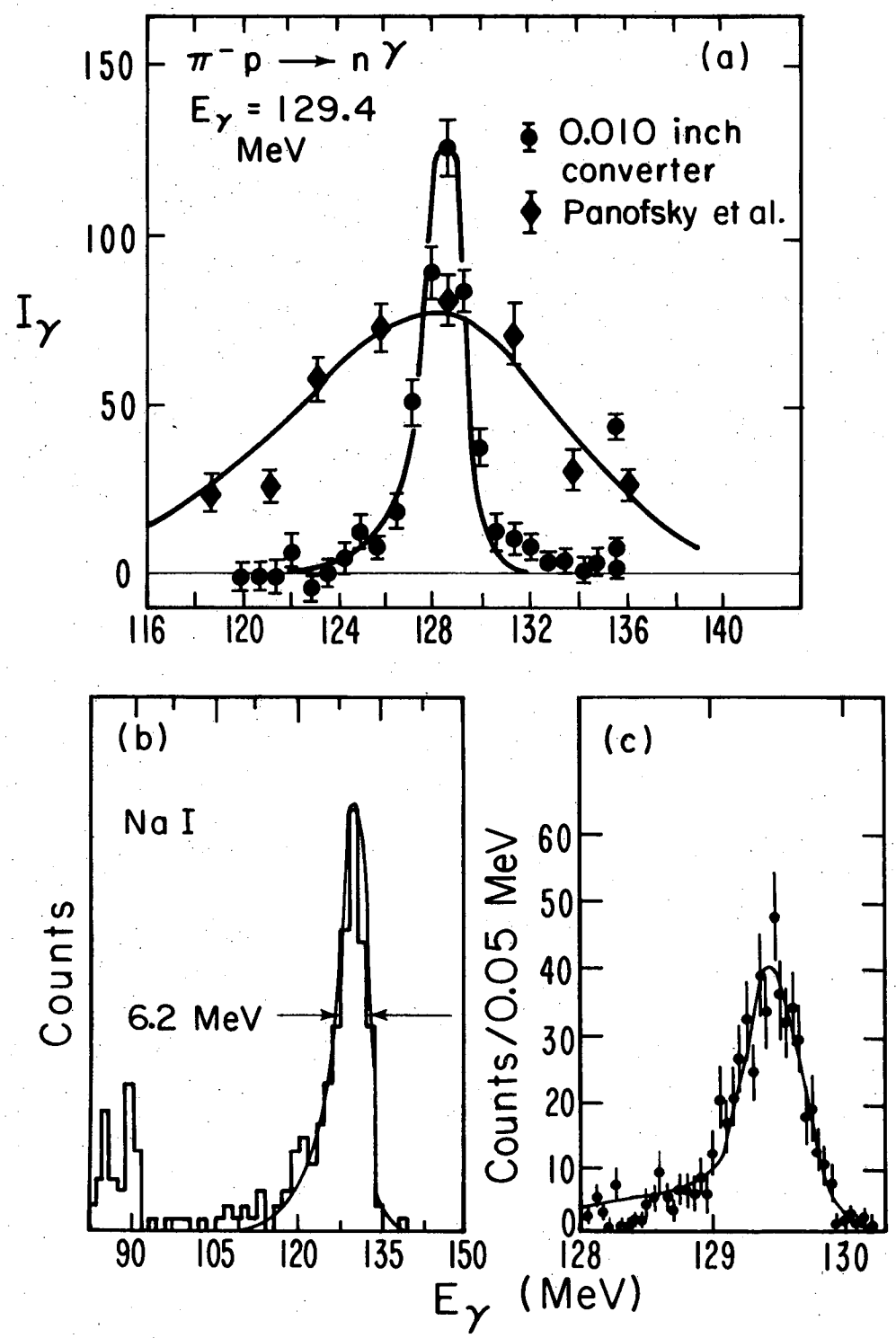

Fig. 2

XBL757-3435

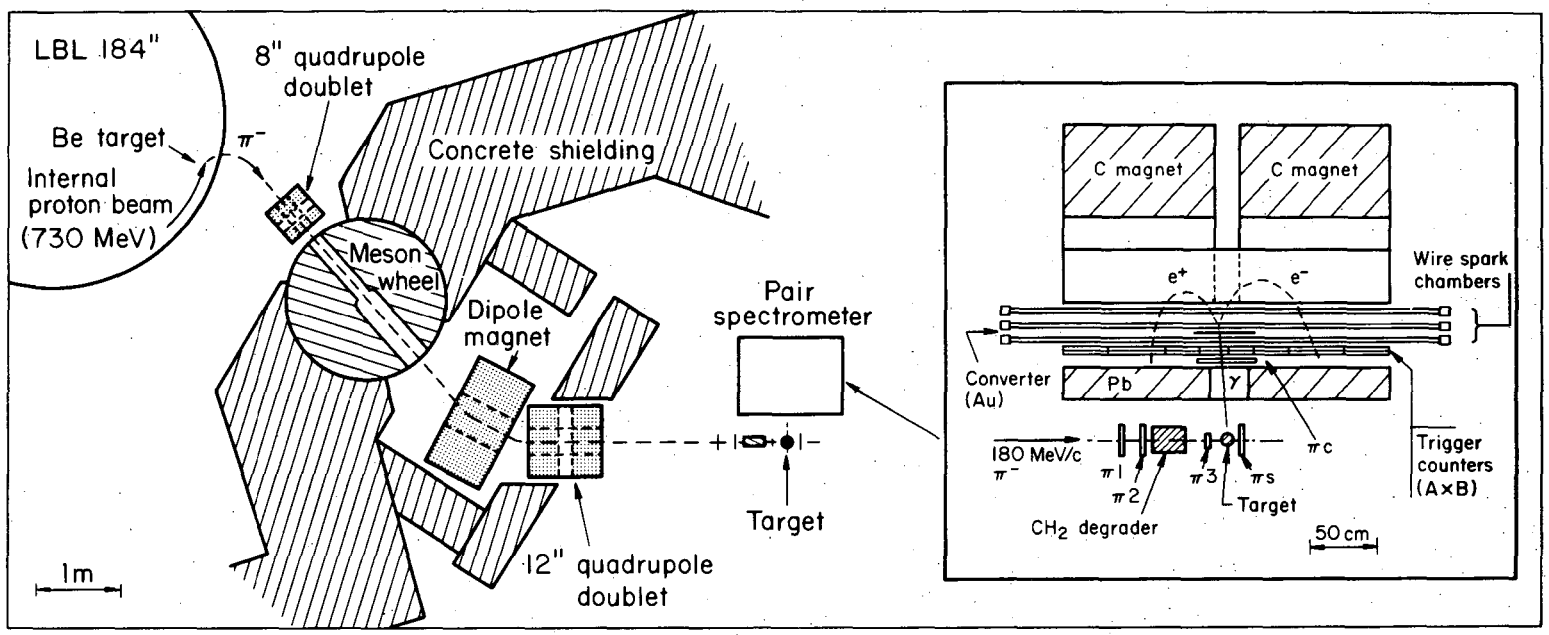

XBL 747-3689

Fig. 3

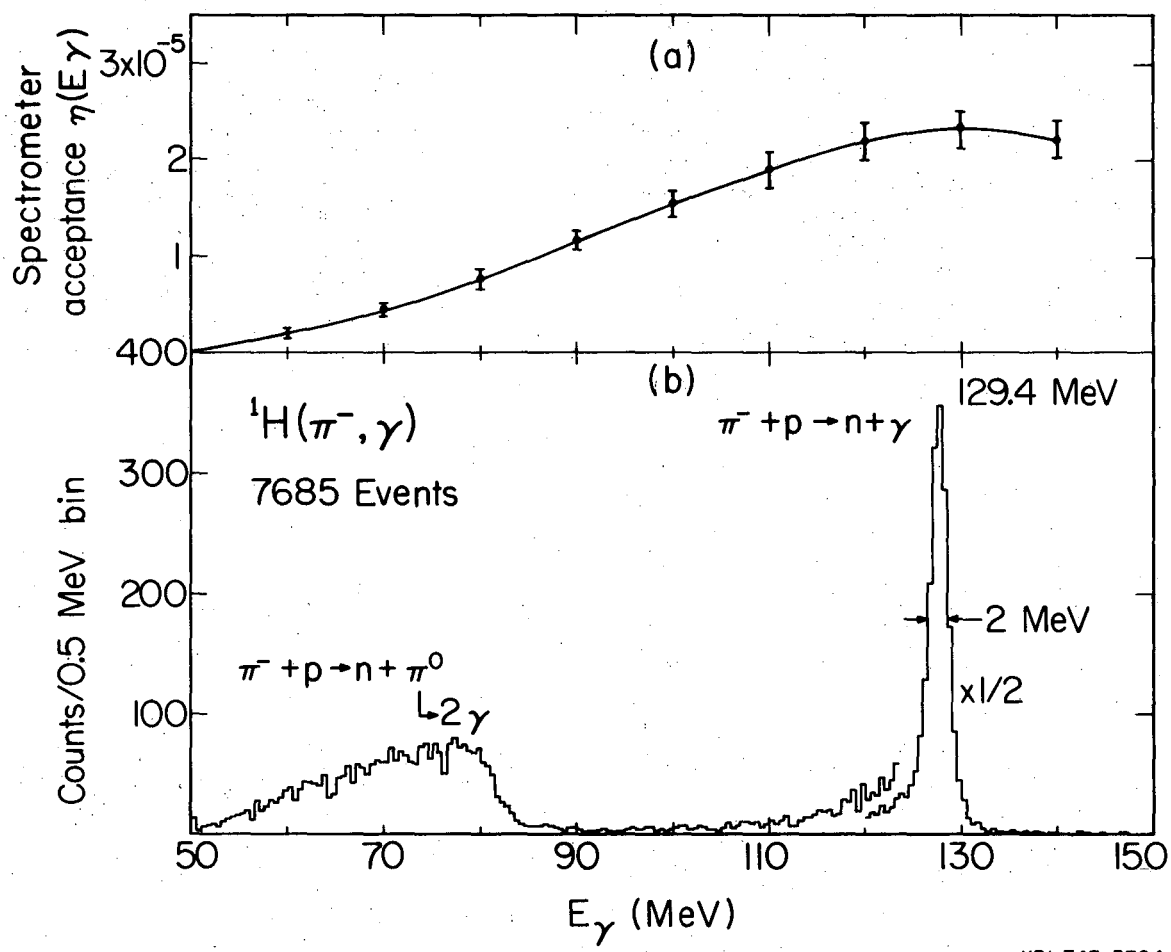

XBL 747-3704

Fig. 4

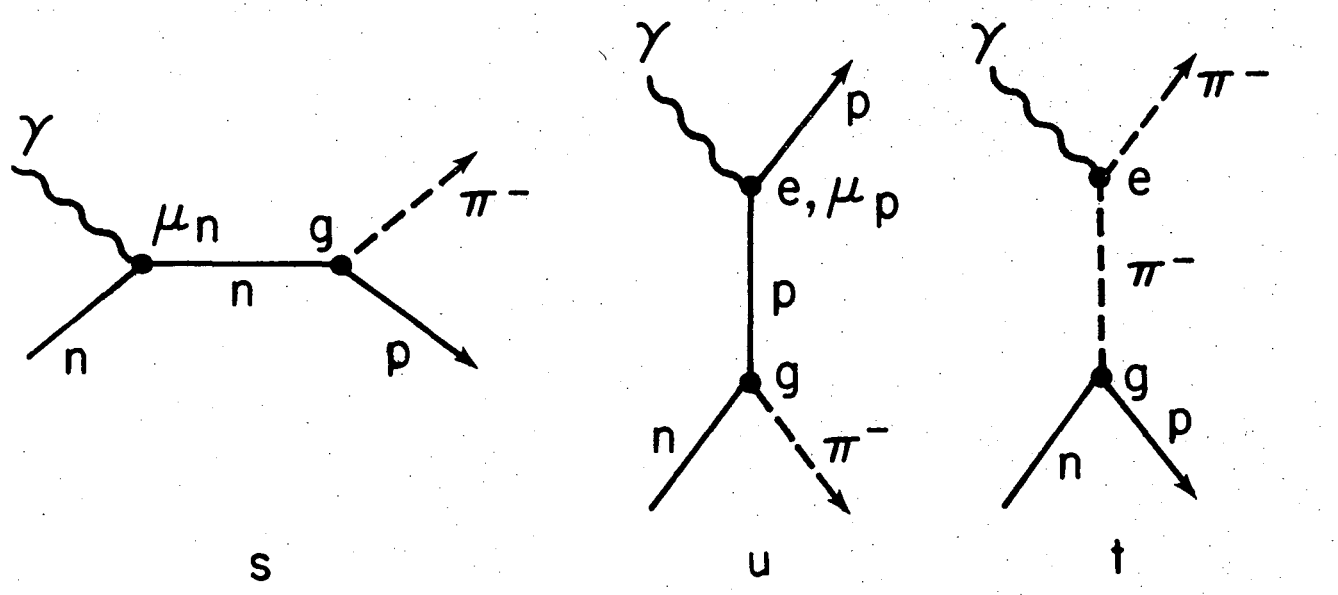

Fig. 5

XBL757-3593

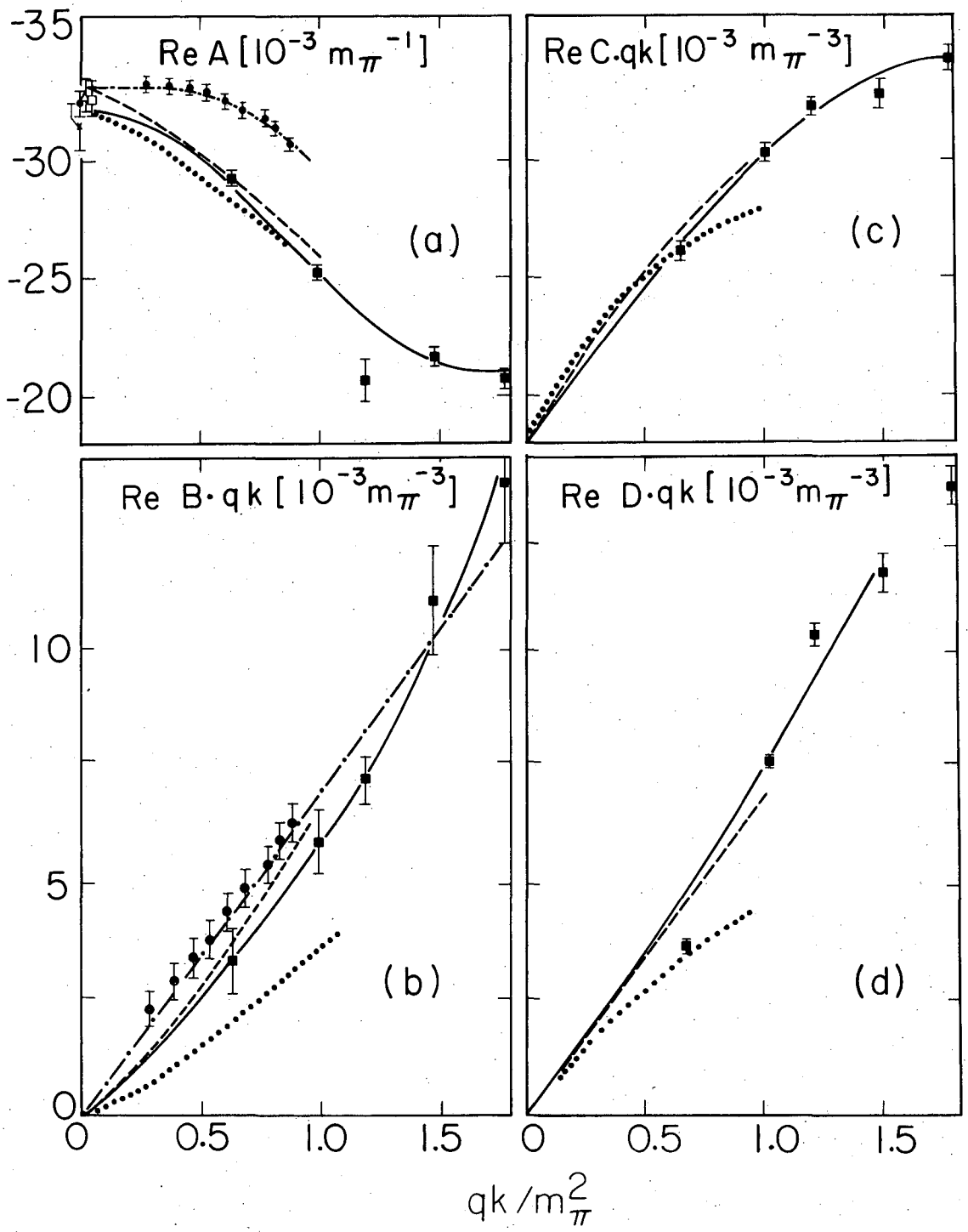

Fig. 6

XBL7512-9942

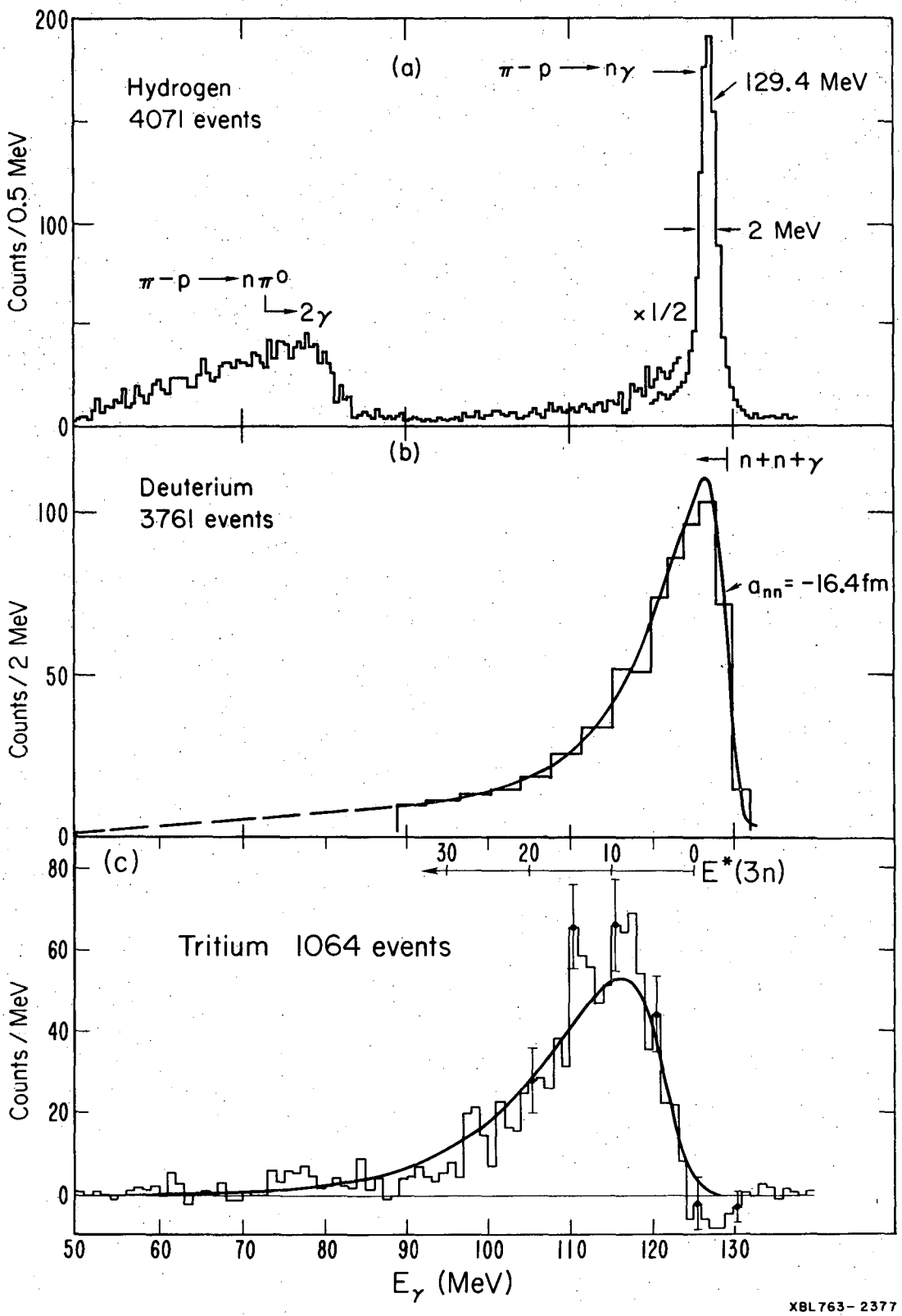
(a)
Hydrogen
4071 events
π − p → nγ
129.4 MeV
2 MeV
π − p → nπ°
→ 2γ
×1/2
Counts / 0.5 MeV
(b)
Deuterium
3761 events
n+n+γ
a_nn = −16.4fm
Counts / 2 MeV
(c)
30
20
10
0
E*(3n)
Tritium 1064 events
Counts / MeV
E_γ (MeV)
XBL763-2377

Fig. 7

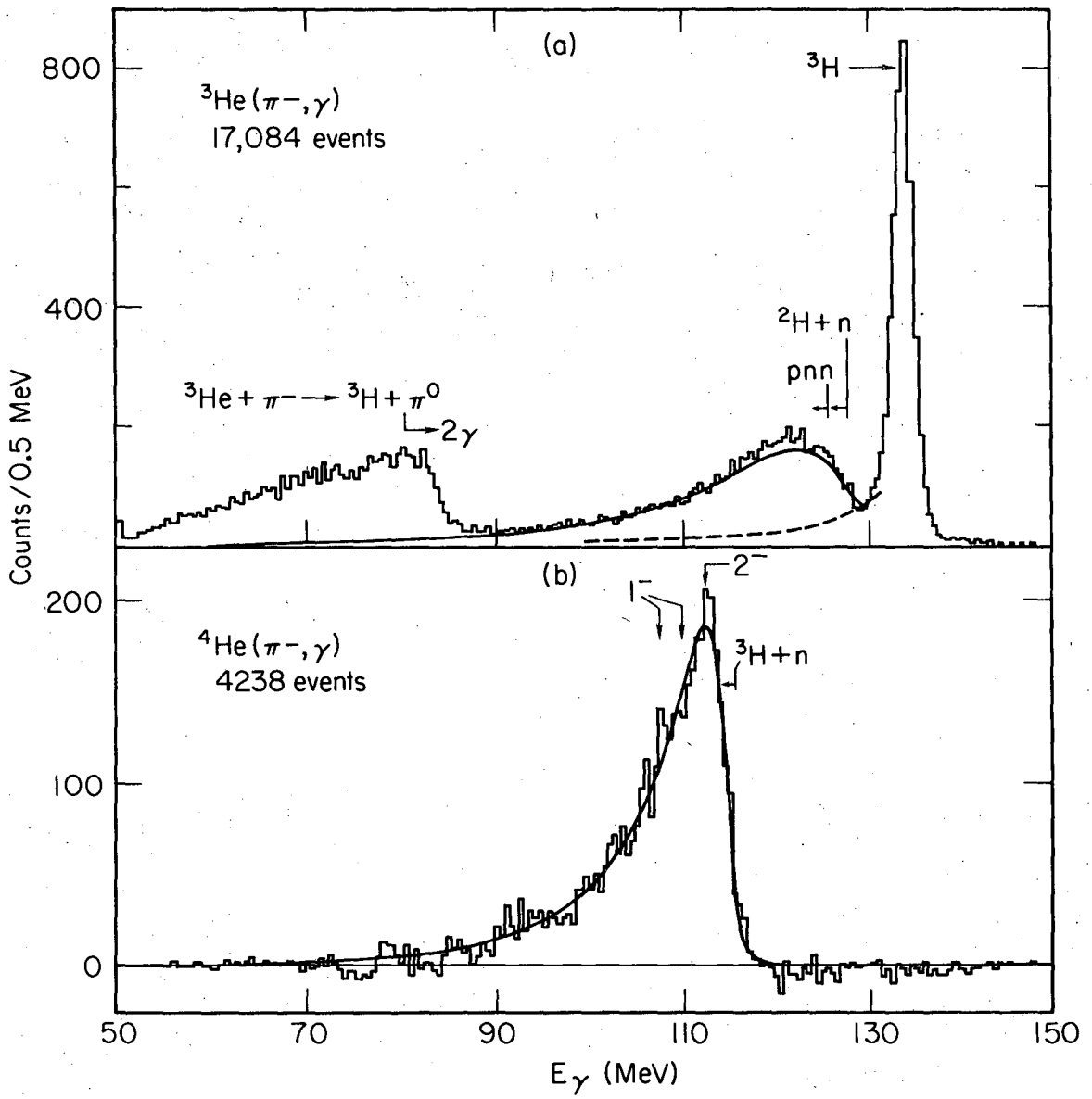

XBL763-2376

Fig. 8

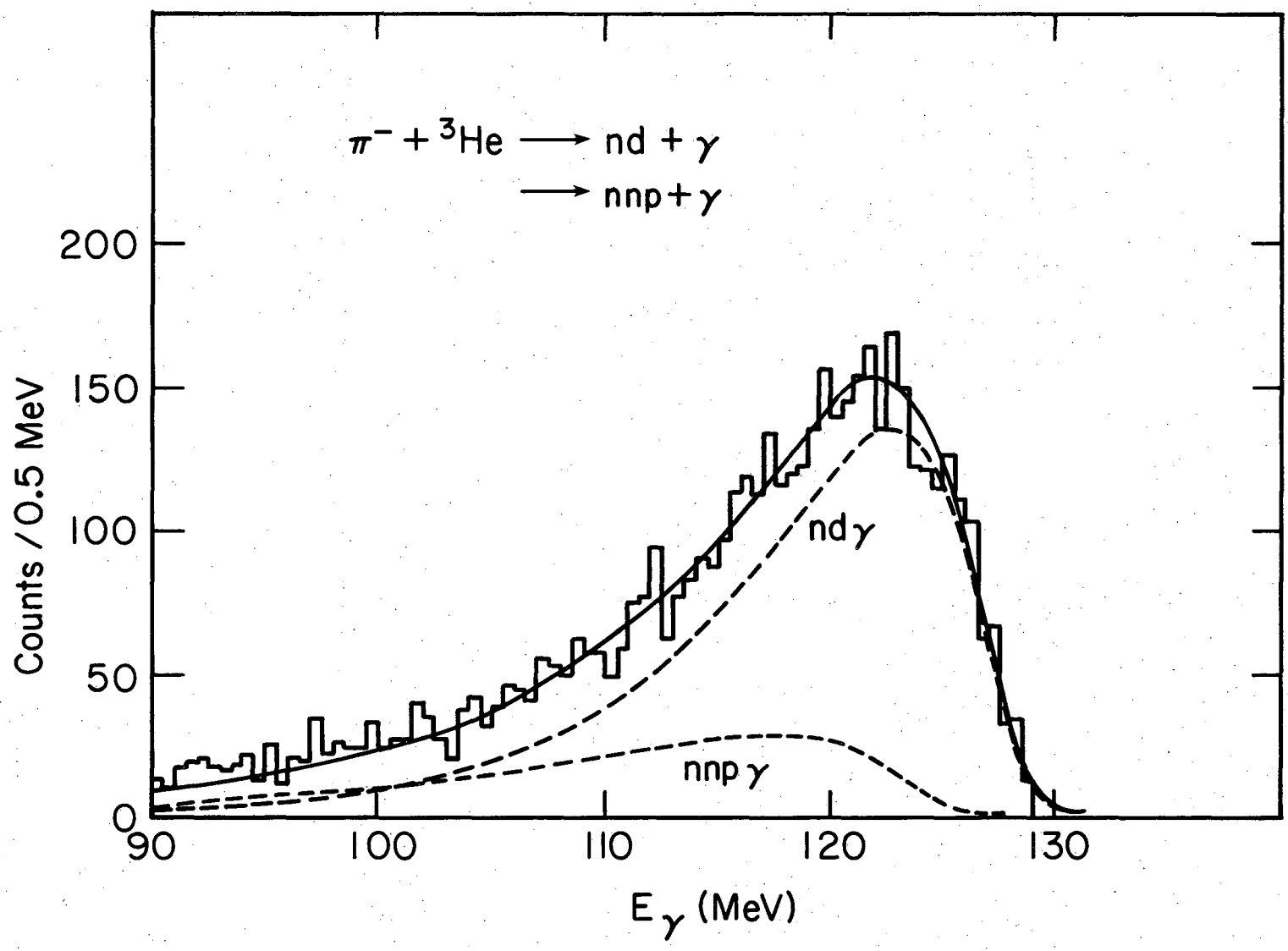

Fig. 9

XBL 763-2375

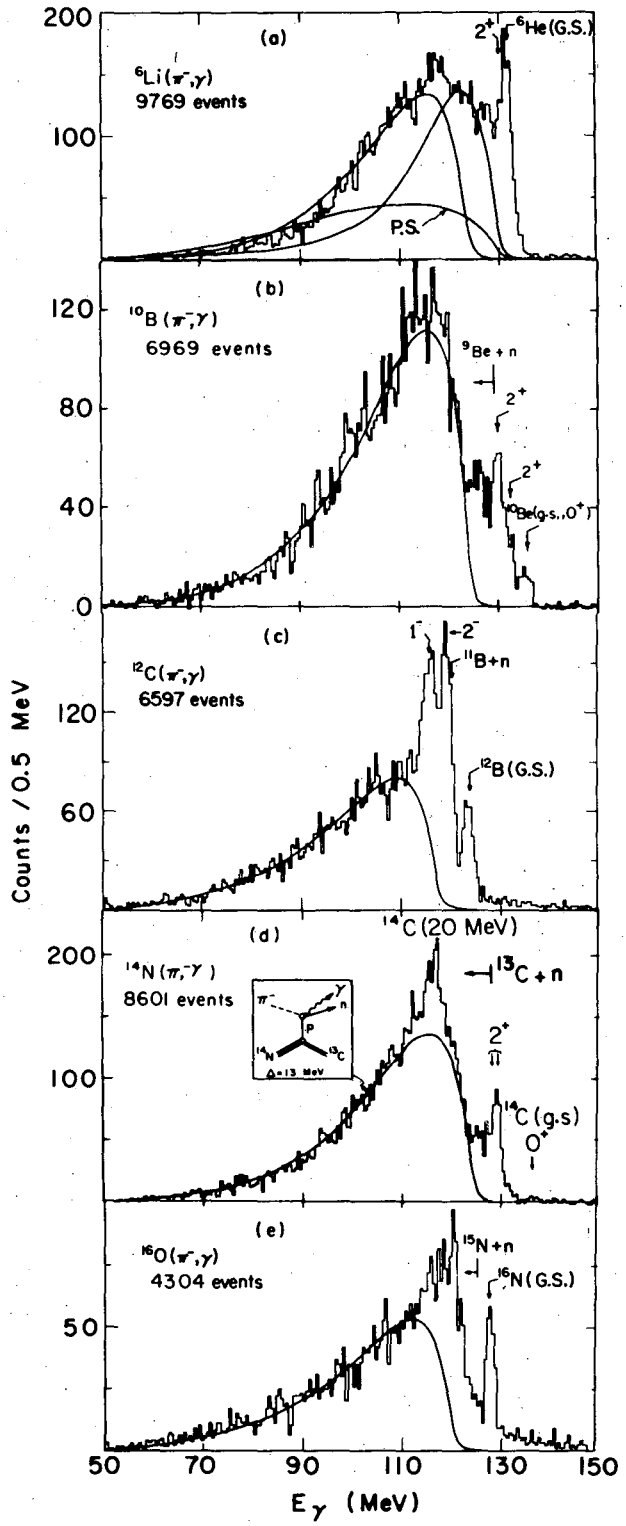
(a)
^{6}Li(π^-,γ)
9769 events
2$^+$
^{6}He(G.S.)
P.S.
(b)
^{10}B(π^-,γ)
6969 events
^{9}Be + n
2$^+$
2$^+$
^{10}Be(g.s.,0$^+$)
(c)
^{12}C(π^-,γ)
6597 events
1$^-$
2$^-$
^{11}B+n
^{12}B(G.S.)
(d)
^{14}N(π^-,γ)
8601 events
^{14}C (20 MeV)
^{13}C + n
2$^+$
^{14}C (g.s)
0$^+$
(e)
^{16}O(π^-,γ)
4304 events
^{15}N+n
^{16}N(G.S.)
Counts / 0.5 MeV
E$_\gamma$ (MeV)
XBL741-2240

Fig. 10

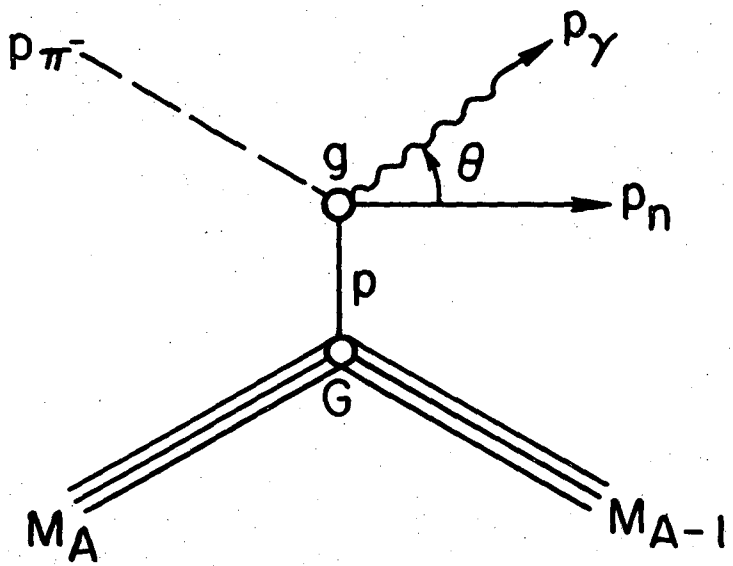

XBL 734-2600

Fig. 11

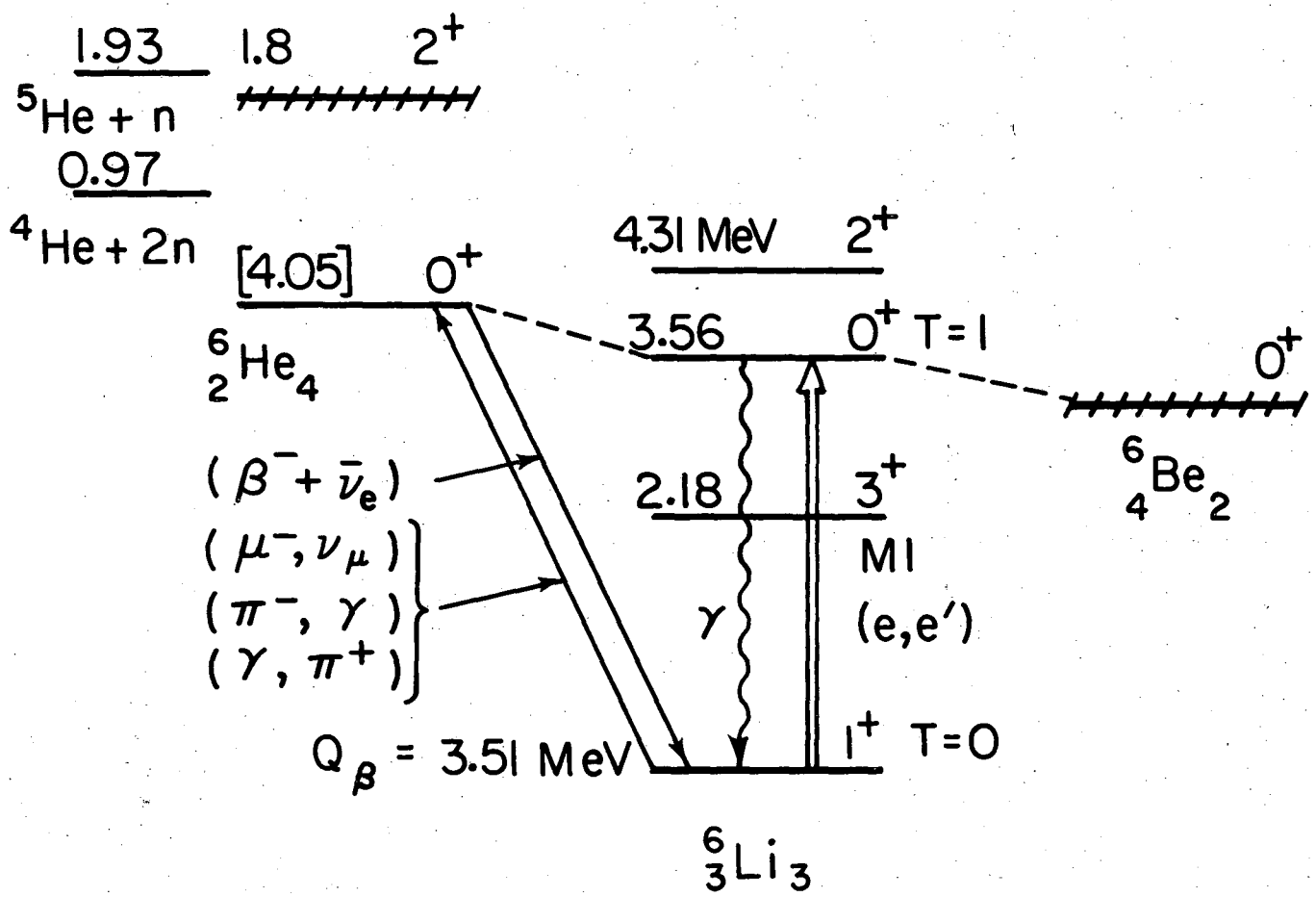

Fig. 12

XBL 757-3434

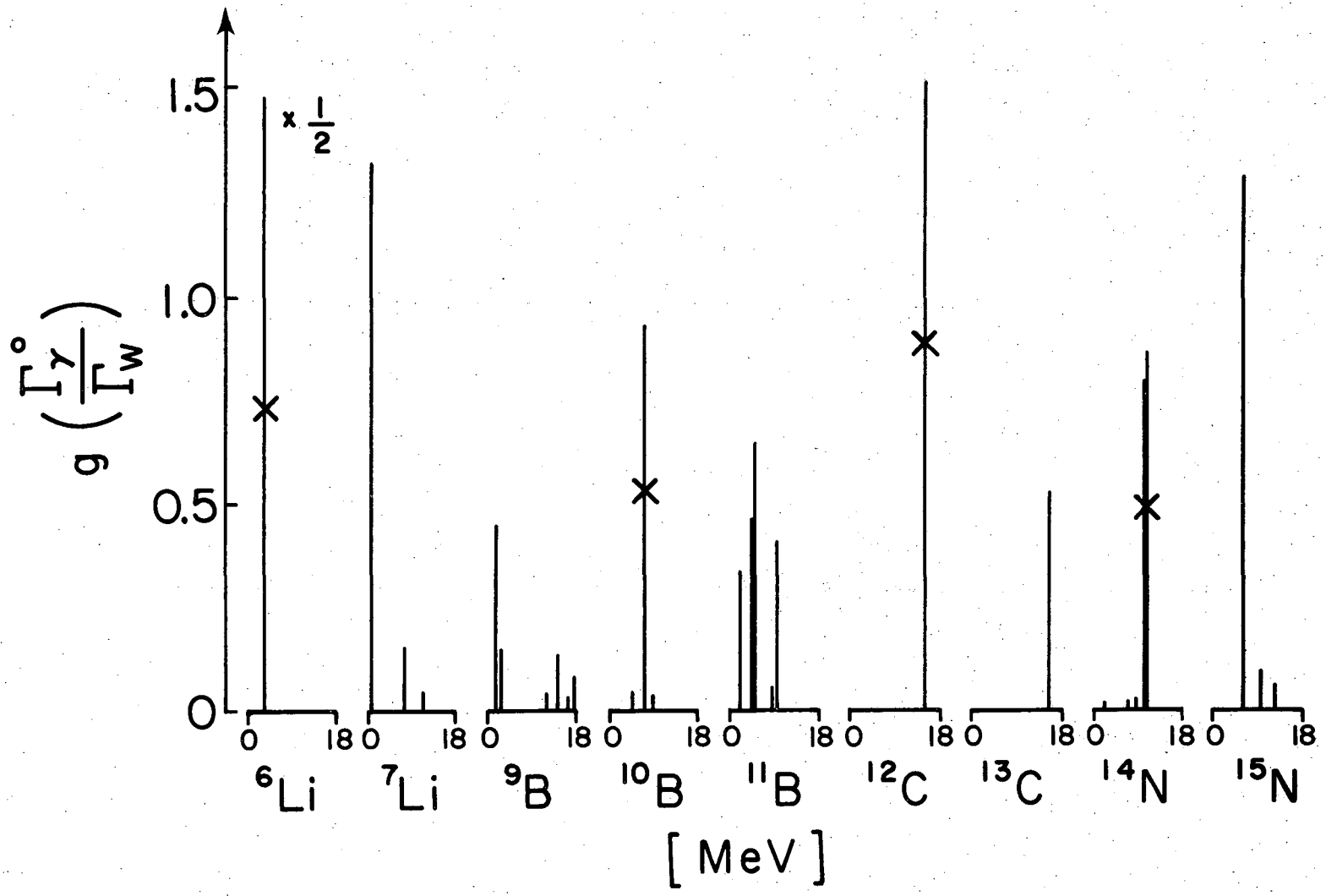

Fig. 13

XBL757-3592

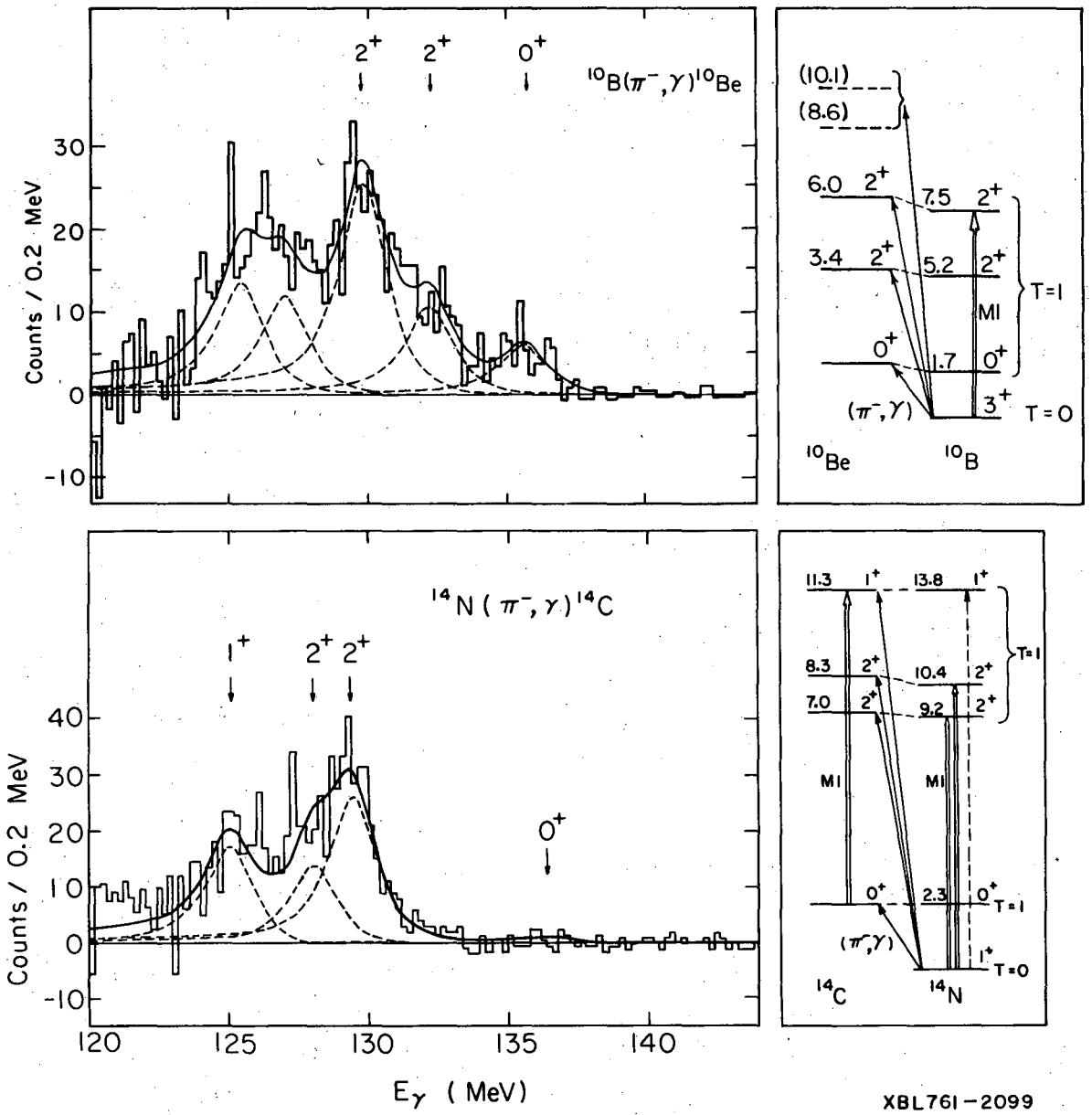

XBL761-2099

Fig. 14

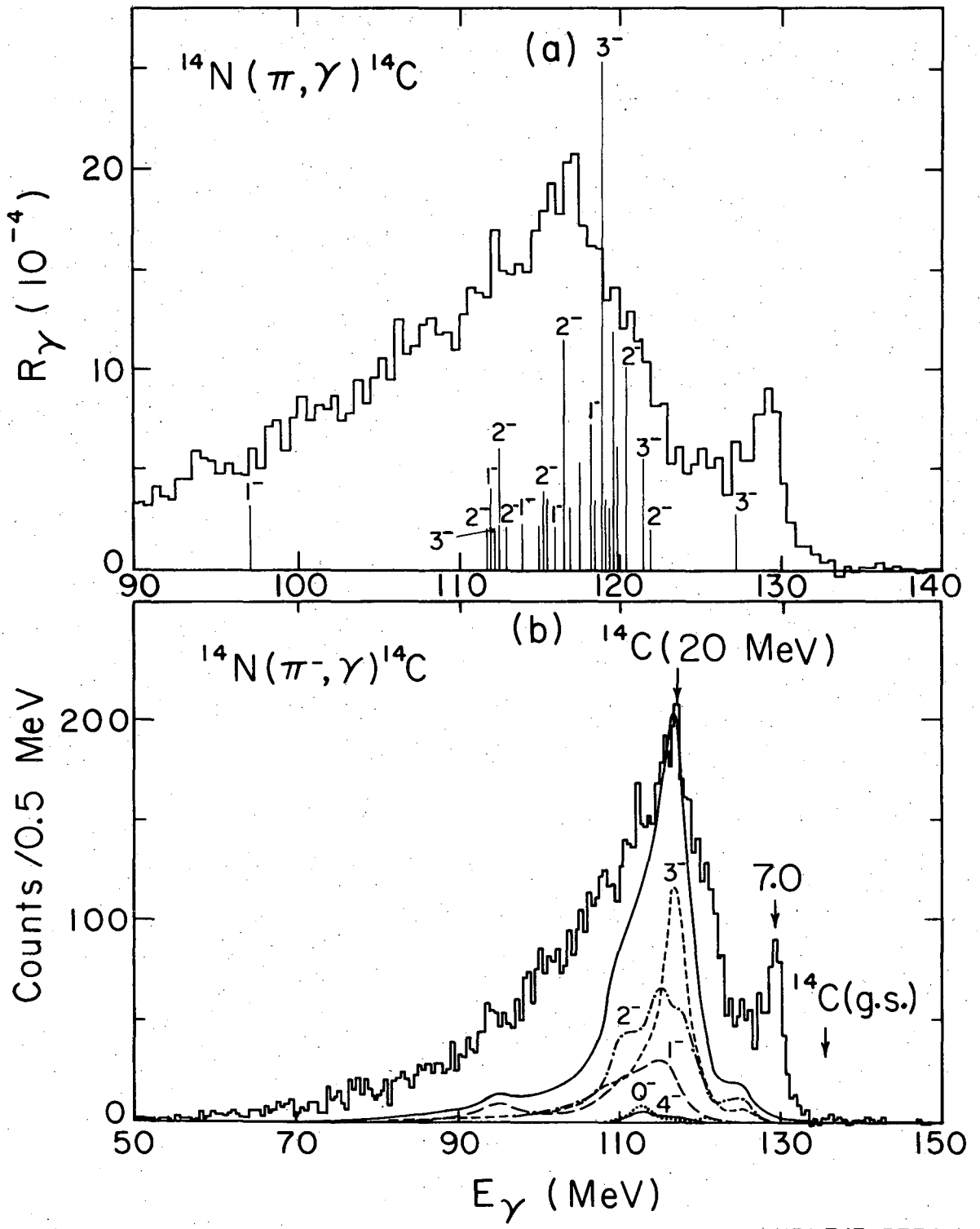

XBL747-3774

Fig. 15

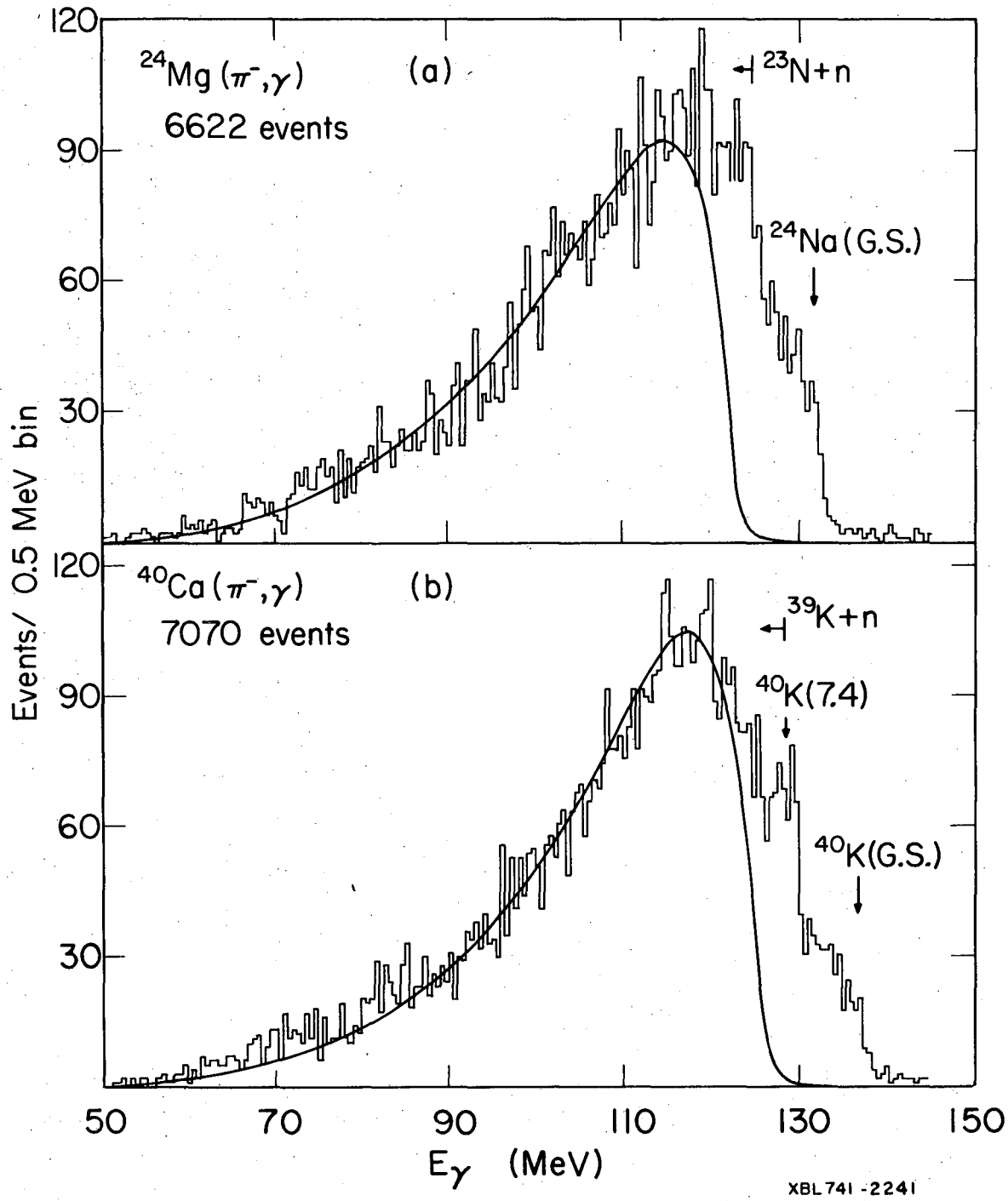
^{24}Mg (π^-,γ)
(a)
6622 events
^{23}N+n
^{24}Na(G.S.)
^{40}Ca (π^-,γ)
(b)
7070 events
^{39}K+n
^{40}K(7.4)
^{40}K(G.S.)
Events/ 0.5 MeV bin
120
90
60
30
50
70
90
110
130
150
E_γ (MeV)
XBL741-2241

Fig. 16

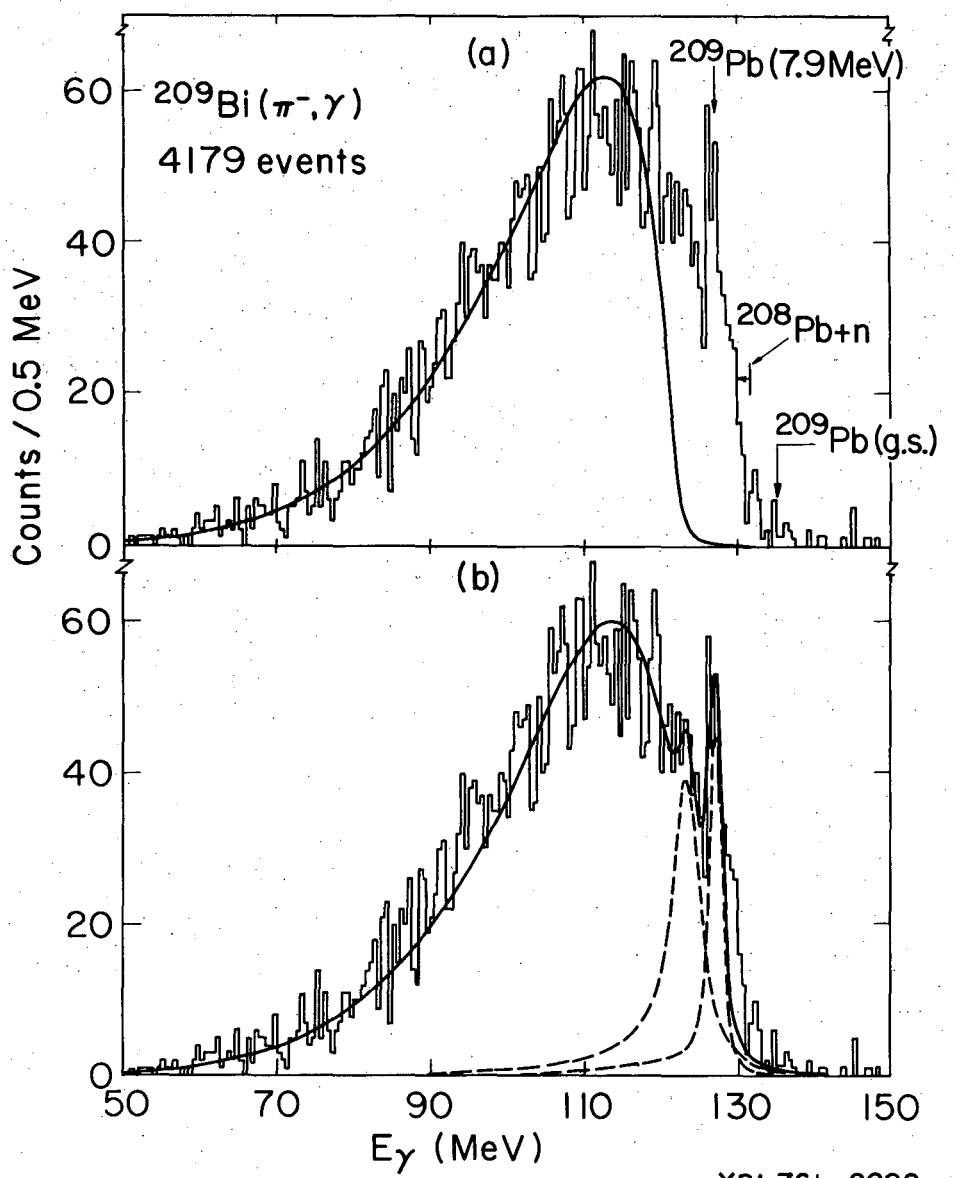
(a)
^{209}Bi(π^-,γ)
4179 events
^{209}Pb(7.9MeV)
^{208}Pb+n
^{209}Pb(g.s.)
(b)
Counts / 0.5 MeV
0
20
40
60
50
70
90
110
130
150
E_γ (MeV)
XBL761-2098

Fig. 17

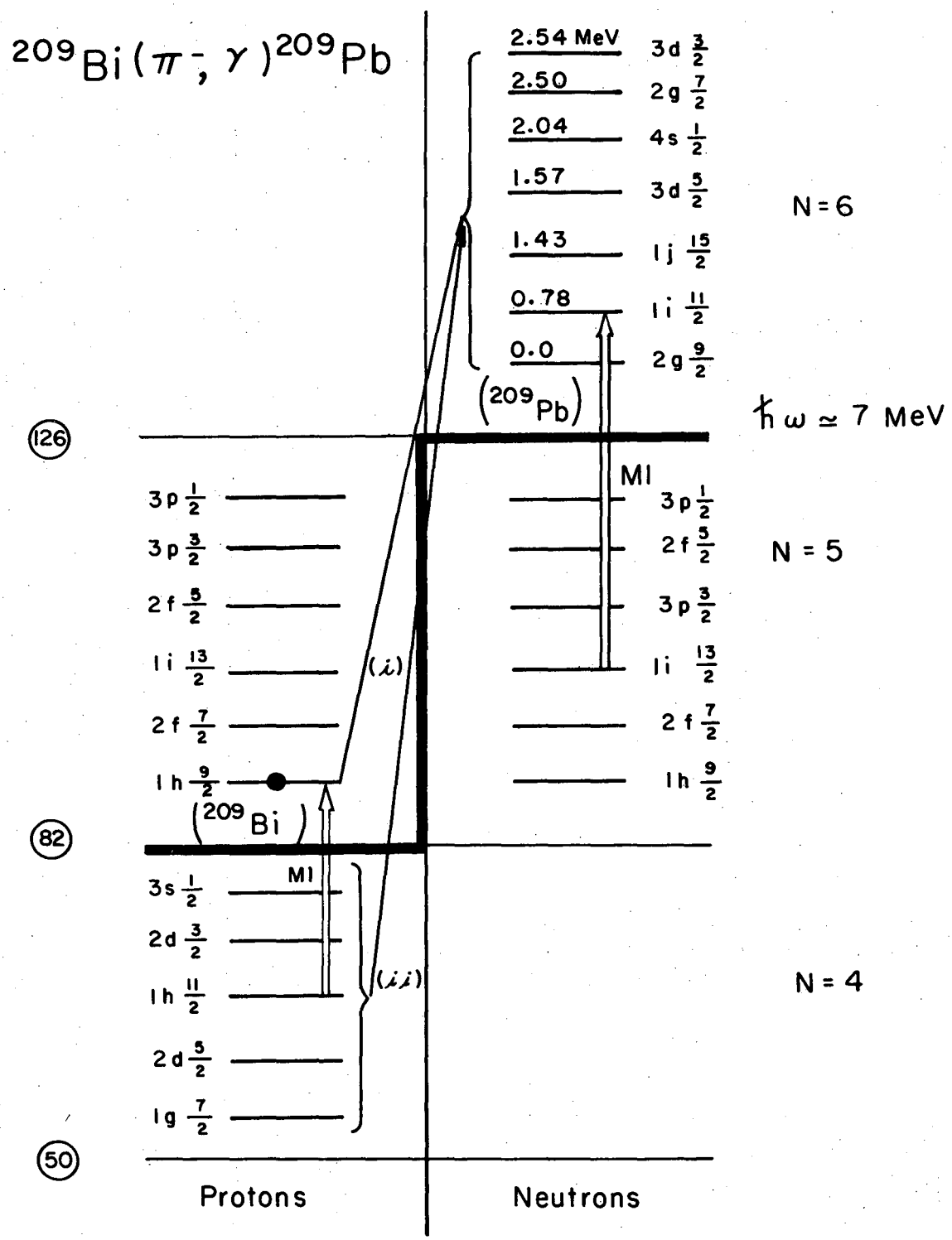

Fig. 13 XBL761-2097

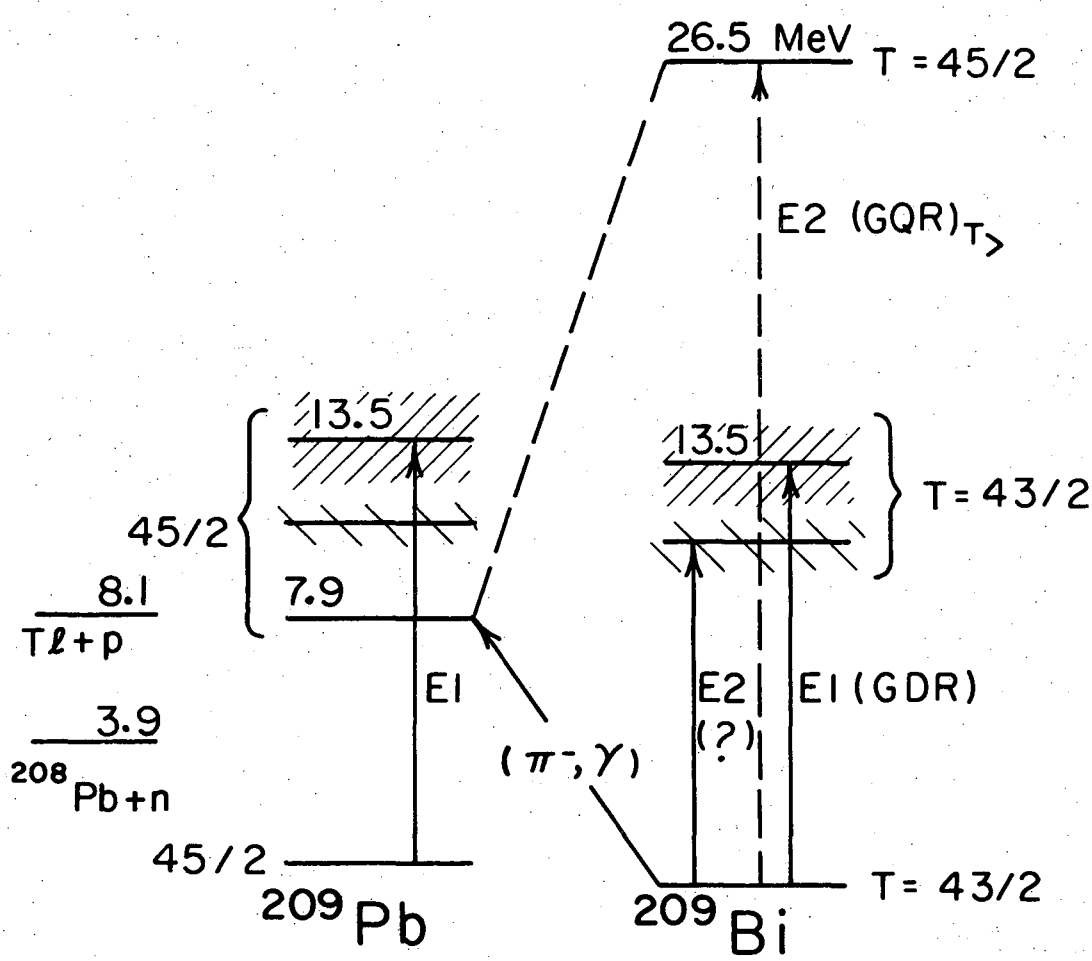

Fig. 19

XBL743-2629

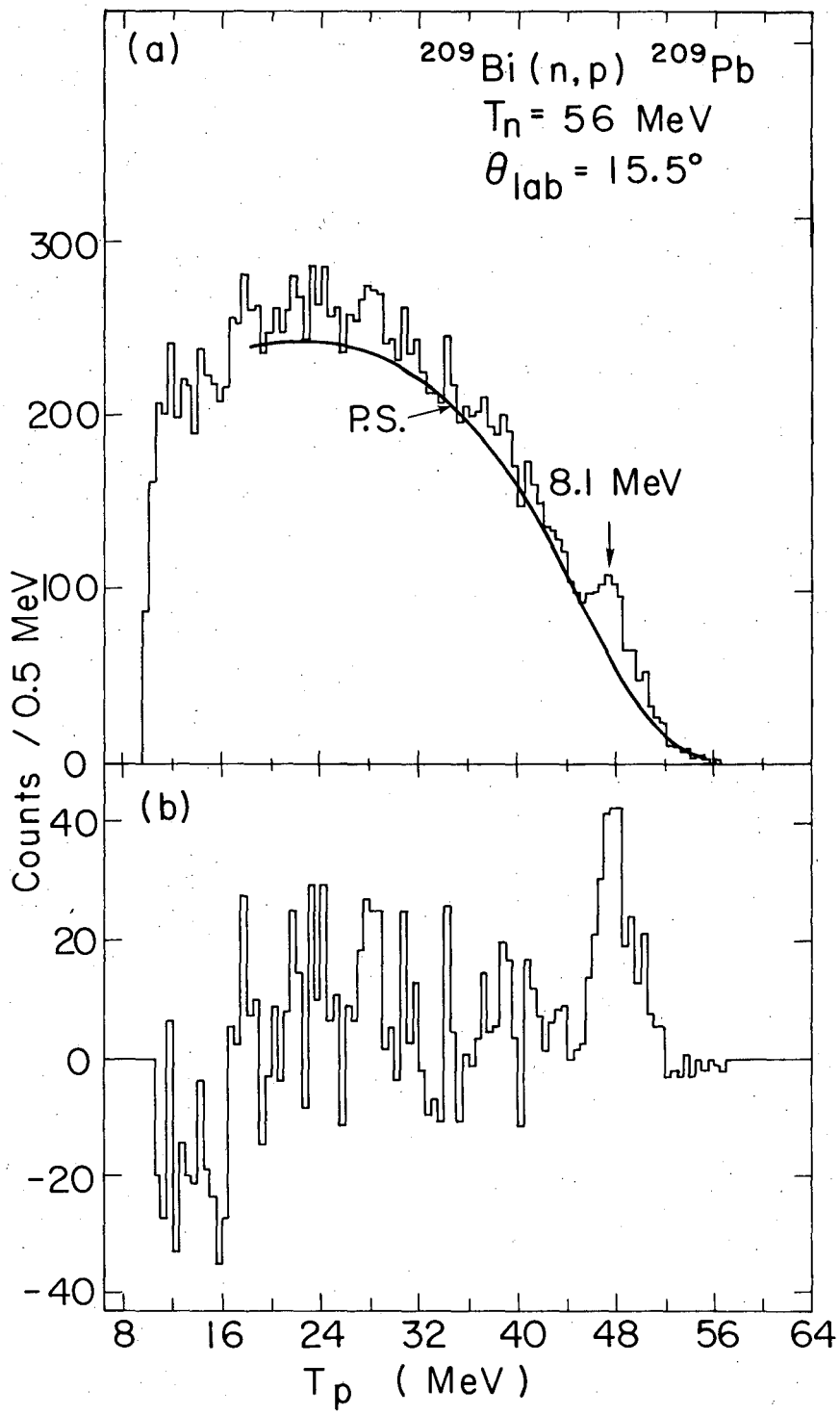

Fig. 20

XBL758-3771

0 0 0 0 4 4 0 0 5 1 6

LEGAL NOTICE

This report was prepared as an account of work sponsored by the United States Government. Neither the United States nor the United States Energy Research and Development Administration, nor any of their employees, nor any of their contractors, subcontractors, or their employees, makes any warranty, express or implied, or assumes any legal liability or responsibility for the accuracy, completeness or usefulness of any information, apparatus, product or process disclosed, or represents that its use would not infringe privately owned rights.

TECHNICAL INFORMATION DIVISION
LAWRENCE BERKELEY LABORATORY
UNIVERSITY OF CALIFORNIA
BERKELEY, CALIFORNIA 94720